Abstract

Due to the sensitivity of high latitude regions to global climate change, it is important to understand the role and response of the arctic environment to past climatic events. Lacustrine sediments can provide a useful archive of past environmental change preserved in structural, textural, and compositional variation. Linnévatnet, a large proglacial lake on Svalbard in the Norwegian High Arctic, contains a long record of annually laminated (varved) sediments. This study provides a high resolution sedimentation chronology from the lamination stratigraphy since 1963. Sediment cores were retrieved during fieldwork conducted in 2006 from sites along two transects. Using digital images of continuous thin sections, annual sediment couplets and intra-annual deposition laminae were identified. Laminae were visually correlated from proximal to distal coring sites and down to the depth of a 1963 ^{137}Cs age (~20cm). The data indicate a complex sedimentary environment across the basin affecting varve formation. Preliminary comparisons to temperature and precipitation records from Longyearbyen suggest a relationship between laminae thickness and precipitation. The sediment record in Linnévatnet may potentially contains a high resolution proxy for changing climatic and glacial conditions of Svalbard during the late Holocene.

Acknowledgements

I would like to thank my advisor, Prof. Mike Retelle, for his companionship and mentorship in the field and at Bates. Thank you, Al Werner, for your contagious excitement about Svalbard and glacial environments. I offer my thanks to Steve Roof for his work with the Svalbard REU and his helpful correspondence. Thanks to all of the Svalbard REU students for their help in the field, particularly Heidi Roop who continues to be a marvelous friend and is always ready to bounce ideas around about glaciolacustrine sediments and Svalbard.

I would also like to thank Anders Solheim and Tove Nielson who taught me a great depth of knowledge concerning arctic marine environments and led the geology cruise on R/V Jan Mayen in May 2006. Thank you, Hanne Christiansen and Ole Humlum for your teaching and help both at Kapp Linné and with data collection after returning home.

A special thanks goes to the faculty of the Bates College Department of Geology for their guidance and teaching throughout my Bates career. An especially warm thanks goes to my geology loving colleagues: Maria Jenness, Nate Eichelberger, Ben Lepesqueur, and John Reuter.

Foremost, I would like to thank my family for raising me to appreciate the natural world and fostering in me a love for the great outdoors. Friends and family, thank you for understanding my excitement about high latitudes, glaciers, cold weather, and geology. I am especially thankful for the unending friendship and support from Mária Dewees, who continues to amaze me with her thoughtfulness and keeps me on my creative toes.

The Bates College Barlow Grant, Bates College Student Research Grant, and the National Science Foundation (NSF) Svalbard Research Experience for Undergraduates (REU) contributed funding for fieldwork and laboratory work involved in this thesis.

Table of Contents

Abstract ii
Acknowledgements iii
Table of Contents iv
Table of Figures vi
Table of Tables vii

1. Introduction 1
Purpose and Overview 2
Site Description 3
Bathymetry 7
Climate of Svalbard 10
Bedrock Geology of Linnédalen 12
Glaciation and deglaciation history 13
Lacustrine Sediments 22
Lake stratification 22
Lake inflow 23
Deposits 27
Annually-laminated lake sediments: Varves 28
Previous Work 31

2. Methods 33
Field Methods 34
Site Selection 34
Sediment Coring 37
Laboratory Methods 39
Core cutting 39
Core logging 40
Bulk density 42
Thin section preparation 42
Sampling 43
Freeze drying 46
Embedding with epoxy 47
Thin section analysis 51

3. Results 53
Sediment Cores 54
Cores and Laminated Sediments 59
LV06-19 59
LV06-16 60
LV06-13 60
LV06-14 61
Varve Identification 66

Table of Contents (cont.)

4. Discussion **71**
Varve Character and Sedimentary Processes 72
Climatic variables 72
Depositional interpretations 73
Constructing a varve chronology 74
Varves and Climate—tentative correlations 76
Precipitation 77
Temperature 81
Statistical Analyses 81
Analysis of correlations 86
Future progress 87
5. Conclusions **90**
6. References **93**
7. Appendices **97**
Appendix A: Bulk Density measurements 98
Appendix B: Lamination thickness measurements 102

Table of Figures

1.1 Map of the Arctic. 4
1.2 Map of Svalbard. 5
1.3 Map of study area. 6
1.4 Bathymetric map of Linnévatnet. 8
1.5 Lacustrine sediment isopach map of Linnévatnet. 9
1.6 Temperature and precipitation plot for Longyearbyen. 11
1.7 Simplified bedrock geology map of the study area. 12
1.8 Map of Svalbard with furthest extent of Svalbard-Barents Sea Ice Sheet. 14
1.9 Side scan sonar and seismic profile from the northern Barents Sea. 15
1.10 Glaciation curve of west coast of Svalbard. 17
1.11 IRD, $\delta^{18}O$, and the terrestrial glaciation curve of the west coast of Svalbard. 19
1.12 Relative sea level curve of Spitsbergen. 20
1.13 Pre-isostatic rebound diagram of Linnédalen. 21
1.14 Thermal lake stratification diagram. 25
1.15 Inflow density currents diagram. 25
1.16 Fine grained sediment distribution in a glacier-fed lake diagram. 26
1.17 Underflow or turbidity current deposition in a glacier-fed lake diagram. 26
1.18 Lateral variation of rhythmites in a glacier-fed lake. 30
1.19 Comparison of "surge" rhythmites to varves. 30

2.1 Bathymetric map of the East Basin and diagram of core locations. 35
2.2 Photo of coring preparation in the field. 38
2.3 Photo of core logging LV06-19. 41
2.4 Photo of thin section sampling from LV06-19. 41
2.5 Schematic diagram of thin section sampling orientation and labeling system. 45
2.6 Photo of flash freezing setup for freeze-drying preparation. 50
2.7 Photo of thin section epoxy embedding. 50

3.1 Composite digital image of varve count and correlation. 56
3.2 Wet density plots. 57
3.3 Dry density plots. 58
3.4 Raw varve thickness plotted versus cumulative depth in the core. 64
3.5 Raw and normalized varve thicknesses plotted versus varve number. 65
3.6 Digital image of complex varves in thin section. 68
3.7 Digital image of simple varve couplets in thin section. 68
3.8 Digital image of massive lamination within a complex varve in thin section. 69
3.9 Digital image of diffuse varves in thin section. 69
3.10 Plot of summer to winter lamination ratio. 70

4.1 Varve thickness to precipitation comparisons. 79
4.2 Photomicrograph of rainfall unit in thin section. 80
4.3 Varve thickness to temperature, SSTA, and AMO comparisons. 83

Table of Figures (cont.)

4.4a Statistical tests between varve stratigraphy and precipitation. 84
4.4b Linear regression between varve stratigraphy without anomalies and precipitation. 84
4.5 Varve thickness comparison to temperature and precipitation, (anomalous laminae removed). 85

Table of Tables:

2.1 Masses and cumulative masses for epoxy ingredients for a 300g batch. 48
3.1 Core site information. 63

1. Introduction

Purpose and Overview:

The purpose of this study is to create an annual sedimentation chronology of Linnévatnet, a proglacial lake on Svalbard, and to identify corresponding patterns between the sediment record and weather data over the past four decades. Svalbard, located in the Norwegian High Arctic, is one of the highest latitude landmasses in the Northern Hemisphere. Where other studies of arctic and alpine lakes have focused on nival or glacial dominated inflow, this study of Linnévatnet represents a complex nival and glacial fed system. This system has been monitored by the Svalbard Research Experience for Undergraduates (REU), funded by the National Science Foundation (NSF) since 2004. These results show glacial sediment input to Linnévatnet is closely related to meteorological factors on diurnal time scales (Matell, 2006). Preliminary observations of the lamination stratigraphy suggest that annual sediment couplets exist in Linnévatnet (Pratt, 2006). Whether inter-annual fluctuations in meteorological factors can be observed from the lamination stratigraphy is critical to interpreting past environmental conditions.

This thesis has two goals. The first is to evaluate the sediment stratigraphy near the lake inlet and provide an accurate varve count. The second objective is to correlate the thickness of sediment layers with meteorological data that have been collected at the nearby settlement of Longyearbyen. A varve chronology is an interpreted sequence of annually deposited lacustrine sediments that has the potential to approximate past environmental conditions based on its textural, structural, and compositional variation.

Site Description:

The Svalbard archipelago lies between 74º and 81º north latitude, and between 10º and 35º east longitude, approximately half way between northern Norway and the North Pole (Figure 1.1). Linnévatnet is located in the Linné Valley (Linnédalen) on the west coast of Spitsbergen, the largest island in the Svalbard archipelago (Figure 1.2). Linnédalen merges with the southwest corner of Isfjorden (the "Ice fjord"), the largest fjord cutting into west Spitsbergen. Linnévatnet is a proglacial lake, six kilometers downstream from the Linné glacier (Linnébreen; Figure 1.3). The major meltwater stream flowing down Linnédalen connecting the glacier to the lake is known as Linnéelva. The Linnéelva inflow and delta are in the southeastern corner of the lake and can shift its primary channel east and west by about one to two hundred meters during the summer melt season. The outflow exits from the northeast corner of the lake and drains across a broad foreland into Isfjorden. The whole drainage basin for Linnévatnet is about 27 square kilometers, 6.3% of which is glaciated (Snyder et al., 2000).

Figure 1.1: Map of the Arctic region centered around the north pole. Note Svalbard at red arrow. (www.svalbard-images.com)

Figure 1.2: The Svalbard archipelago, and the field site, Linnédalen, marked by the arrow at the mouth of the Isfjord; and the Norwegian town, Longyearbyen (Norwegian Polar Institute, Svalbard 1:2,000,000).

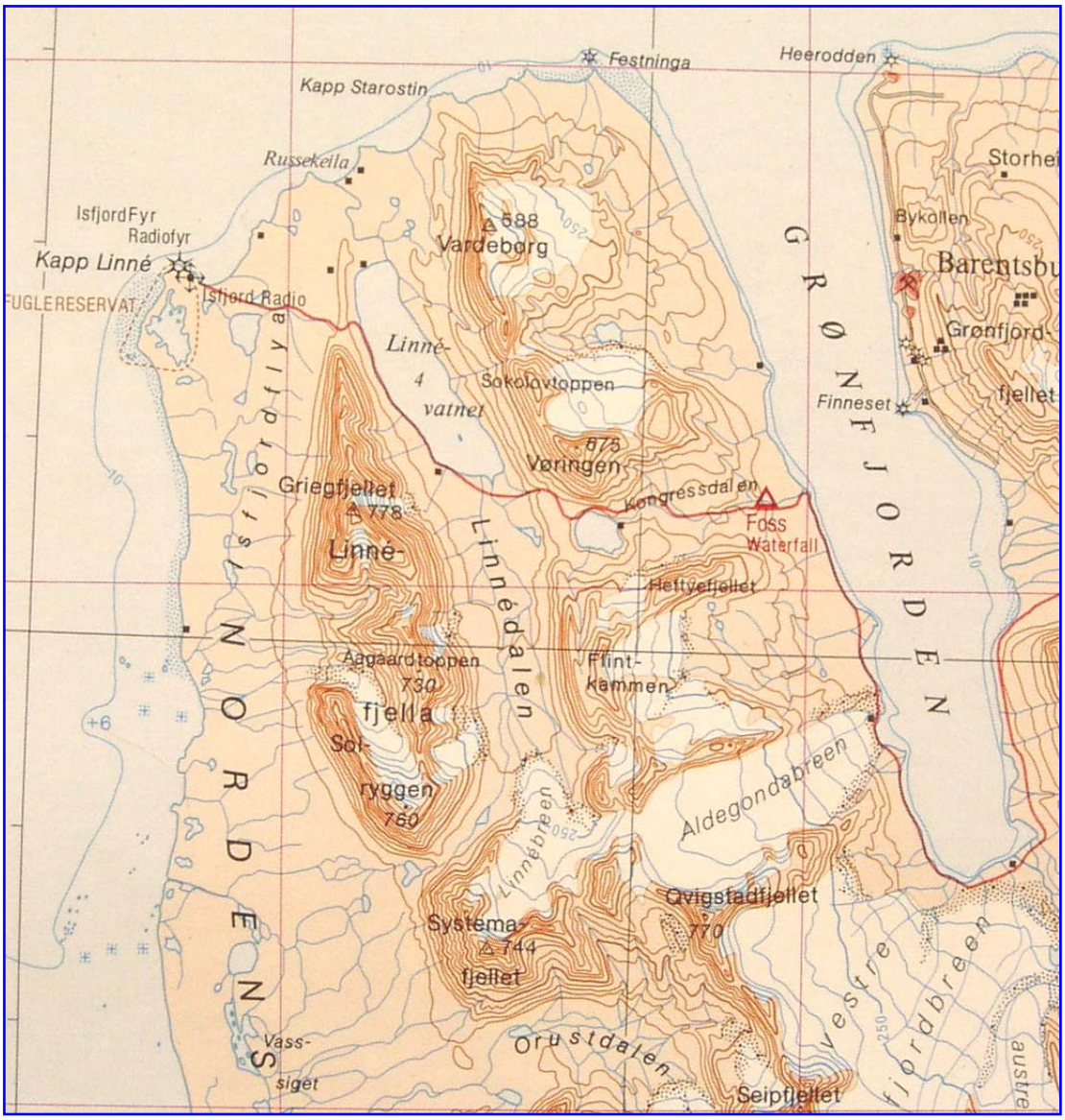

Figure 1.3: Topographic map of the study area, Linnédalen and Linnévatnet. Red line marks a snowmobile trail (Norwegian Polar Institute).

Bathymetry

The bathymetry of Linnévatnet reflects its glacial history and the structure of the bedrock. Linnévatnet is 5 km long, 1 km wide, and 35m deep at its deepest point in the main basin (Figure 1.4). The southern end of the lake consists of two basins divided by a bedrock ridge. These sub-basins are known as the East and West Sub-basins. An island created by a bedrock ridge is located approximately half a kilometer from the south end of the lake.

The sediment accumulation in Linnévatnet is thickest in the delta environment at the southeast corner of the lake (Figure 1.5). Lacustrine sediment accumulation is highest proximal to the inflow, east of the inflow, and declines gradually north along the eastern shore from 10m thickness down to 2m thickness over a distance of 1.8 km (Svendsen, et al., 1989). The sediment thickness gradually thins towards the north and west. There are also zones of thicker sediment in the main basin and north of the island that reach 2-6m (Svendsen, et al., 1989).

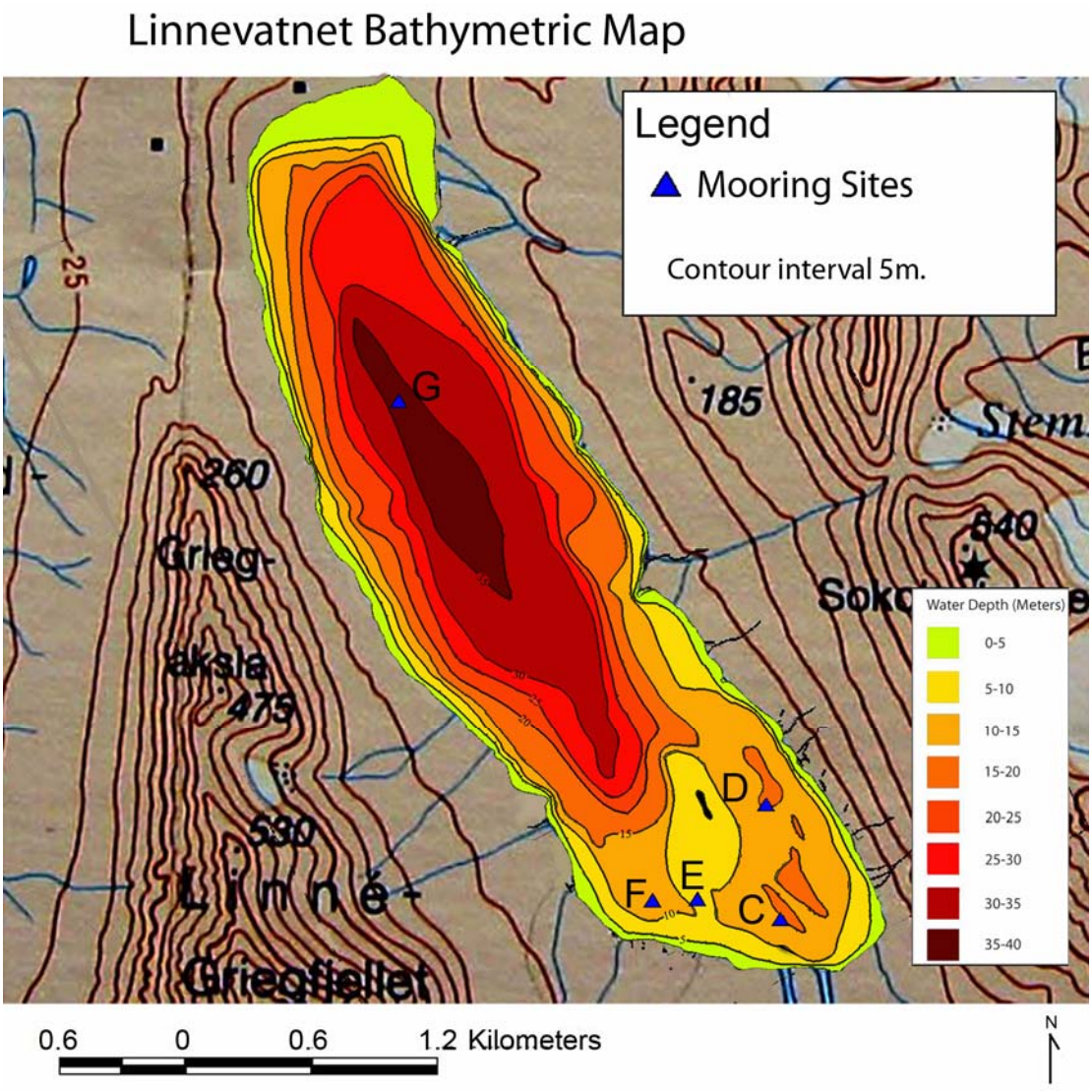

Figure 1.4: Bathymetric map of Linnévatnet. Contour interval is 5m, and north is oriented to the top of the map. Letters C through G are labels for the mooring sites where sediment traps and temperature loggers are deployed (Modified from Motley, 2006).

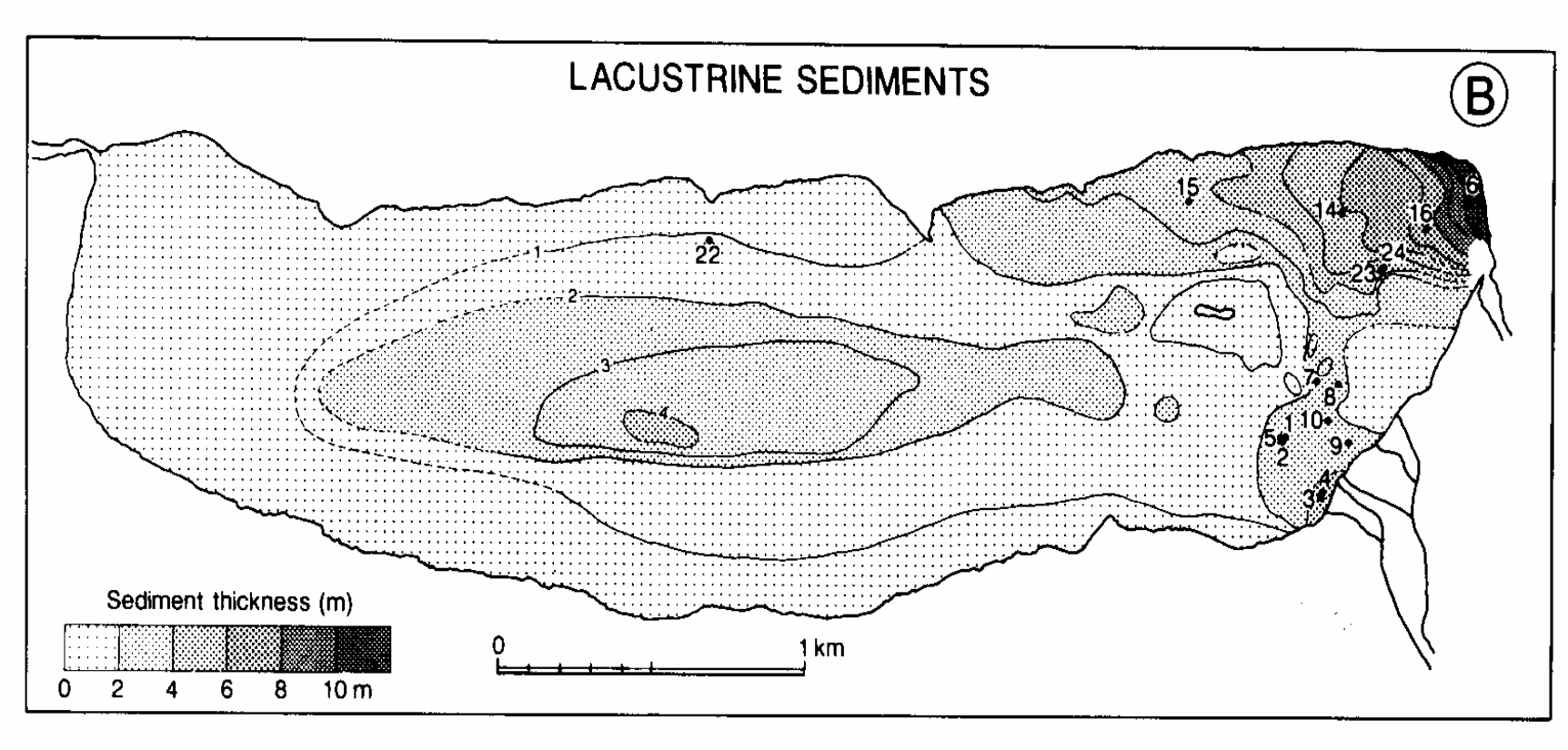

Figure 1.5: Isopach map of lacustrine sediments on the bottom of Linnévetnet, with north to the top-left corner. (Svendsen et al. 1989).

Climate of Svalbard:

The study of the earth's past and current climate is crucial to understanding its fluctuations and predicting future variability. The Arctic is acknowledged as being much more sensitive to climate change than lower latitude regions (ACIA, 2004). The sensitivity and high variability of climate in the Arctic makes it an important location in which to study proxies for past climate changes.

Svalbard has an arctic climate with mean annual temperatures of about -6 ºC near sea level and -15 ºC in the mountains (Humlum, unpublished data, 2006) (Figure 1.6). The coldest month is February which had an average temperature of -15.2 ºC from 1975 to 2000. The warmest month is July which had an average temperature of 6.2 ºC over the past thirty years. The majority of Svalbard is a polar desert with only 200mm water equivalency (w.e.) of precipitation each year. Western Spitsbergen and Kapp Linné receive 400mm w.e. on an average year.

Due to the addition of anthropogenic greenhouse gases, unprecedented changes are occurring in the arctic environment (ACIA, 2004). This is likely due to positive feedback factors such as melting snow and ice leading to decreasing surface albedo, which in turn leads to more heating of the surface (Overpeck et al., 1997). Monitoring the present climate of the Arctic is crucial to understanding these changes, what causes them, and how they may continue into the future. Monitoring modern sedimentary and glaciologic processes can aid in the interpretation of Svalbard's past environment.

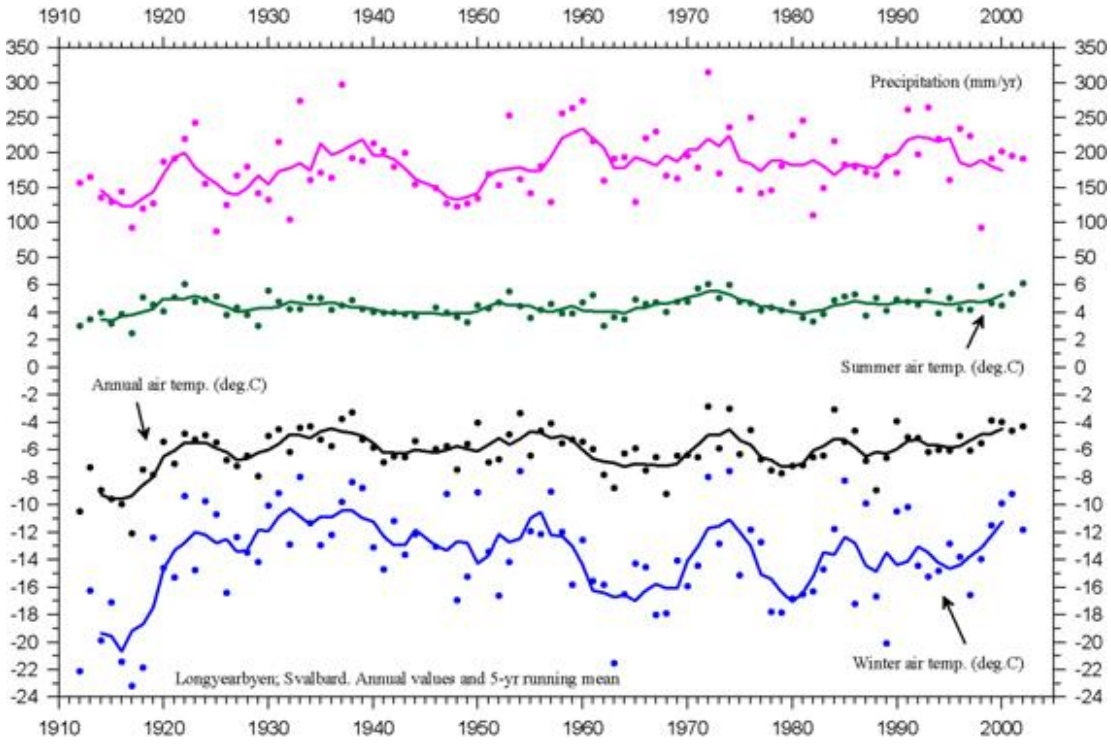

Figure 1.6: Temperature and precipitation over the 20th century at Longyearbyen, Svalbard. Dots are annual means, lines are 5yr running means. From top to bottom: Precipitation (mm/yr), Summer air temperature (°C), Annual air temperature (°C), and Winter air temperature (°C) (Courtesy of Ole Humlum).

Bedrock Geology of Linnédalen

The bedrock geology of Linnédalen is important as the source of superficial sediments that may ultimately become part of the lacustrine stratigraphy. The long axis of Linnévatnet lies along strike of the major bedding planes in the drainage. The lake is located over primarily Carboniferous sandstones bounded to the west by the Hecla Hoek formation of Precambrian metasediments (Figure 1.7; Hjelle, 1986). East of Linnévatnet is comprised of Carboniferous to Permian limestones and gypsum and Mesozoic shales, siltstones, and cherts.

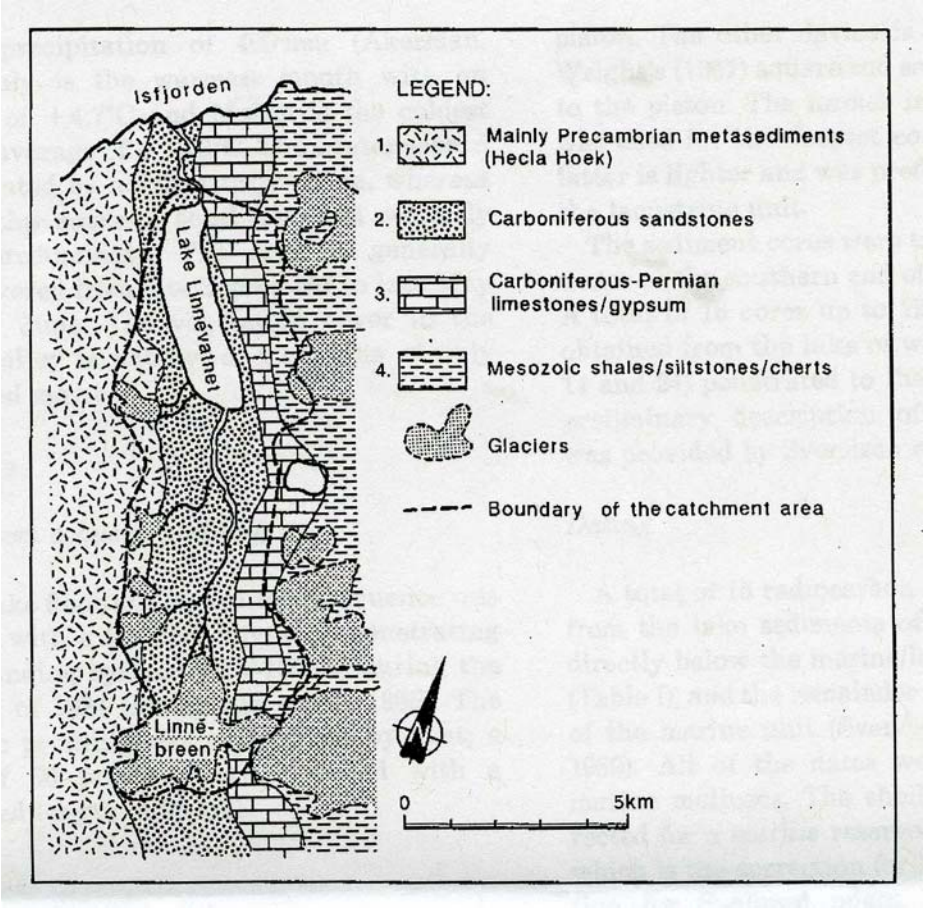

Figure 1.7: Simplified bedrock map of the study area (from Svendsen, 1989).

Glaciation and deglaciation history of Svalbard and the Svalbard-Barents Sea Ice Sheet

Svalbard has had numerous glaciations over the course of the Late Cenozoic. Raised marine terraces across Svalbard indicate that the arctic islands were covered by an ice sheet centered in the northern Barents Sea. Many studies have been undertaken to understand the feasibility of a grounded ice sheet on the continental Barents Sea (Solheim, et al., 1990). Mangerud et al. (1998) studied the Svalbard-Barents Sea Ice Sheet history over the course of the last 150,000 years through comparison and correlation of the terrestrial stratigraphic record to the marine record, which filled in the gaps of what could be found on land. Due to the highly erosive nature of glaciers, previous terrestrial evidence of glacial advances is often removed. Sections at Kapp Ekholm, Brøggerhalvøya, the 87 meter terrace in Linnédalen, Linnéelva, Skilvika, and Kongsøya (Figure 1.8) all have impressive terrestrial evidence of the Saalian and Weichselian glaciations as well as the Eemian interglacial period (Mangerud et al., 1998).

This summary covers the sedimentary and stratigraphic evidence of the past glaciations on Svalbard and focus on the last glacial maximum of the Late Weichselian and the patterns of deglaciation, followed by the Holocene conditions leading up to the state of glaciation on Svalbard today.

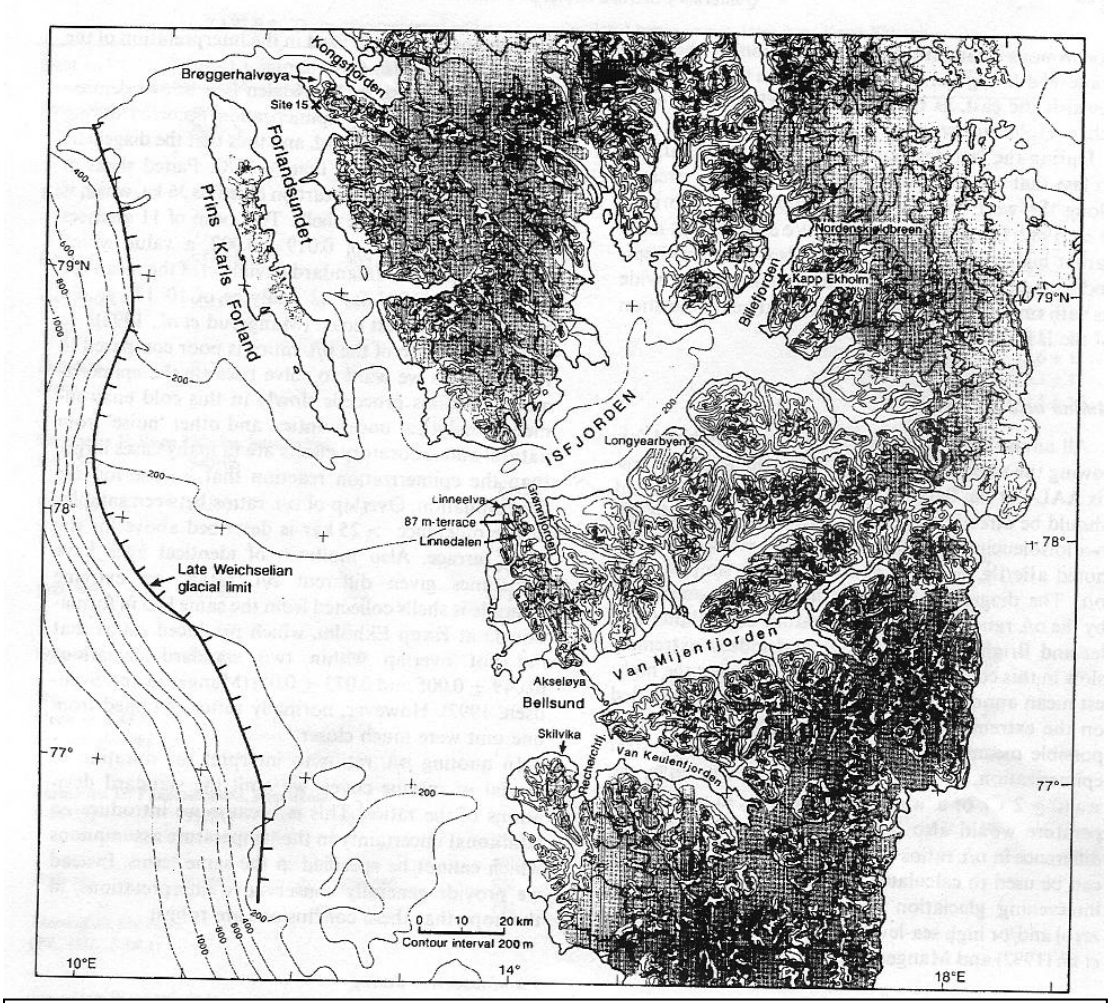

Figure 1.8: Svalbard and onshore stratigraphic section. (From Mangerud et al., 1998).

Pronounced alpine features of Svalbard indicate that valley and cirque glaciers played an important role in forming the landscape rather than an ice sheet. Late Pliocene and Early Pleistocene were probably the most favorable periods for glacial erosion above sea level (Svendsen et al., 1989). Lower amplitude temperature variations, with higher temperatures during glacial periods and lower temperatures during interglacial periods, would favor warm based ice conditions that would promote high erosional rates by valley glaciers and cirque glaciers (Jansen et al., 1987). However, erosion of the major fjords required an ice sheet with outlet glaciers

at pressure melting point. Core recovery from polar North Atlantic margins has shown a glacial history of the High Arctic over the course of the Late Cenozoic (Elverhøi et al., 1998). Sedimentological records of deep sea cores indicate that large ice sheets of the Northern Hemisphere originated at about 2.4-2.5 Ma (Shackleton et al., 1984; Jansen et al., 1987).

Evidence for an ice sheet centered on the Barents Sea is found through raised marine terraces that gradually rise from the western coast of Spitsbergen to the eastern coast, indicating significant isostatic loading further east (Solheim, et al., 1990). Glacial geomorphic features such as flutes and transverse ridges have been found also indicating a grounded ice sheet on the floor of the Barents Sea. High resolution seismic sections taken in the Barents Sea indicate cross sections of flutes while side scan sonar swaths show linear fluted features as well as iceberg plough marks on the seafloor (Figure 1.9). The presence of flutes indicates that the base of the Barents Sea Ice Sheet was at the pressure melting point and sat on a deformable till bed on what is now the seafloor (Solheim, et al., 1990).

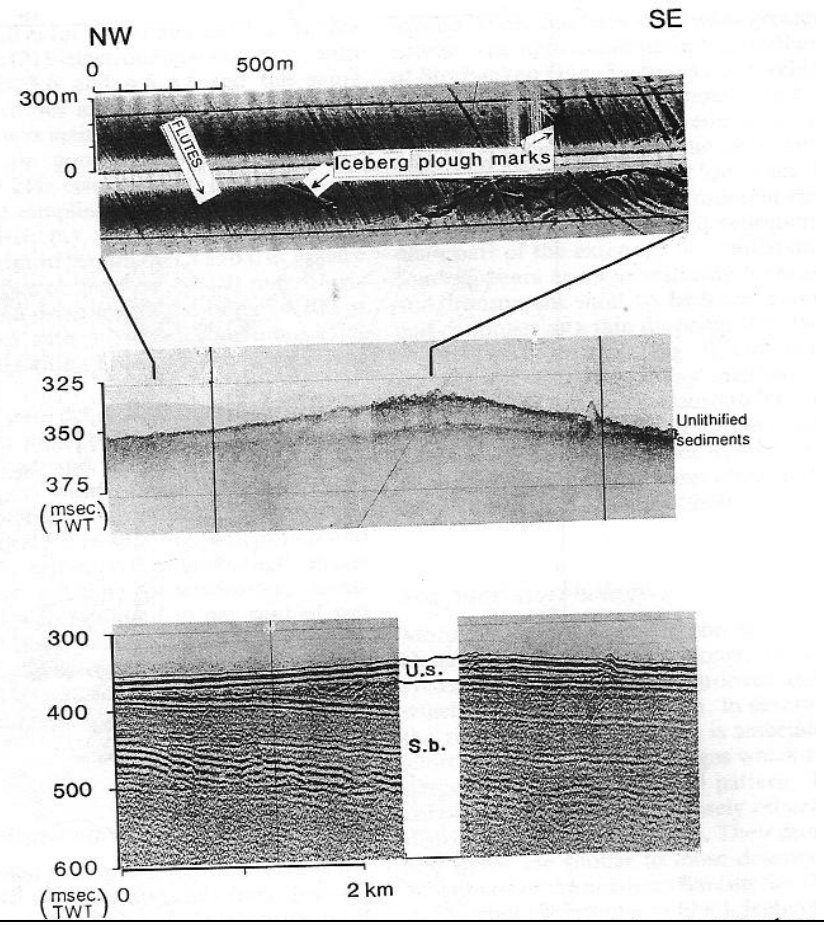

Figure 1.9: Side scan sonar, 3.5 kHz penetrating echosounder, and air gun (top to bottom respectively). Note the flutes in cross section from the 3.5 kHz and from above in the side scan sonar taken in the northern Barents Sea. (From Solheim et al., 1990).

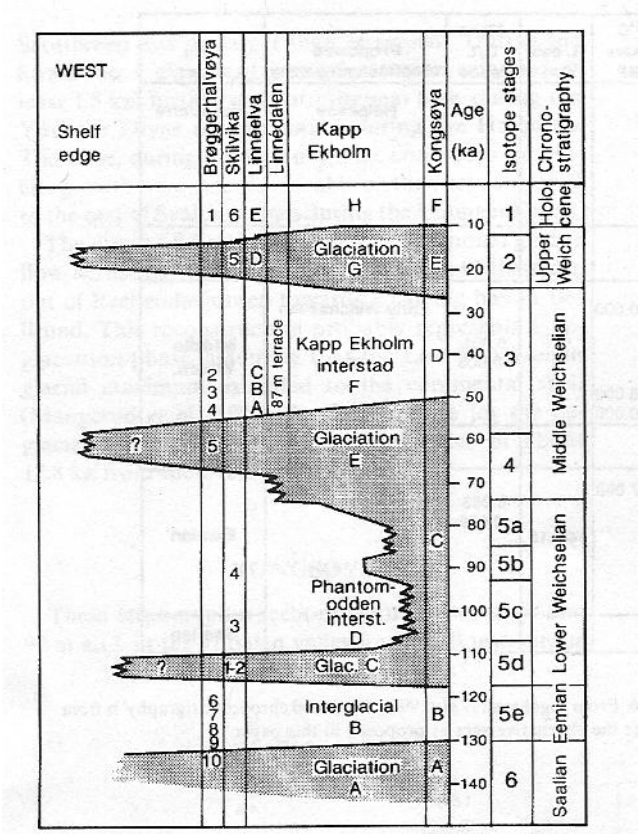

Figure 1.10: Glaciation curve of Svalbard and Barents Sea. (From Mangerud et al., 1998).

Figure 1.10 is a glaciation curve that indicates the extent of glaciation over time onshore and extending out to the continental shelf. Many shells of *Mytilus edulis* (common blue mussel) have been found in the middle of formation B, indicating warm ocean conditions or climate during deposition. The common blue mussel has only recently returned to the region. The common blue mussel was also present during the Holocene climatic optimum. It is therefore inferred that formation B is an interglacial deposit of Eemian age. The four marine formations indicate that the glacier extended less than 14 km beyond the present terminal position of the tidewater glacier, Nordenskjøldbreen, during the Eemian interglacial (120-130 ka), the Phantomodden interstadial (~100 ka), the Kapp Ekholm interstadial (40-60 ka),

and the Holocene (10ka-present). During these ice-free periods, it has been concluded that glaciers on western Svalbard were not significantly larger than today if at all. Brøggerhalvøya, the 87 meter terrace in Linnédalen, Linnéelva, Skilvika, and Kongsøya all have similar sections that only differ in so far as they may have missing portions within an unconformity, and contain evidence for an eastward retreat of the ice sheet. Kongsøya, the only site located east of Svalbard and in the Barents Sea was deglaciated last of all the sites, indicating that ice remained in the Barents Sea after it had retreated from Svalbard. The marine limit on Kongsøya is greater than 100m from 10,000 BP. Kongsøya was ice covered for the 56 ka duration between the Eemian interglacial and the Kapp Ekholm interstadial (Mangerud et al., 1998).

Figure 1.11 is a compilation of the Ice Rafted Debris (IRD) accumulation rate, $\delta^{18}O$ values from foraminifera, and the glacial curve for western Svalbard. These curves show periods of further glacial extent based on high IRD transportation events and during periods of low $\delta^{18}O$ ratios over time. As Figure 1.12 indicates, the on- and offshore stratigraphic records demonstrate a major Saalian glaciation, as well as three separate Weichselian glaciations. The Saalian and Weichselian glaciations are interrupted by the Eemian interglacial period, while the Weichselian glaciations are separated by interstadial periods (Mangerud et al., 1998).

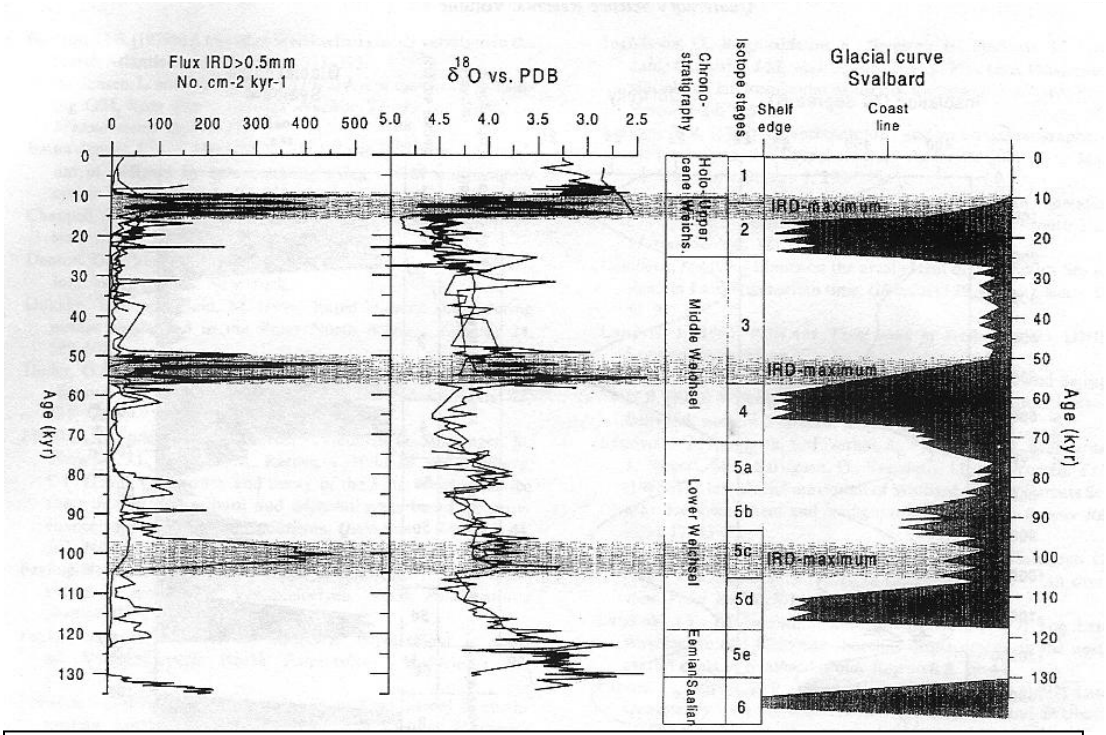

Figure 1.11: Comparison between IRD flux, $\delta^{18}O$ values, and the terrestrial glaciation curve (From Mangerud et al., 1998).

The deglaciation of the Svalbard-Barents Sea Ice Sheet occurred quite rapidly, leaving glacial flutes and transverse ridges in the northern Barents Sea. Two periods of stagnation when retreat was halted is evidenced by two accumulations of massive, homogeneous sediments in the seismic profiles. These formations indicate the rapid, though stepwise manner of deglaciation (Solheim et al., 1990). Relative sea level change and formation of raised marine terraces also indicates a two step retreat of the Barents Sea Ice Sheet from Brøggerhalvøya. The breadth of a raised beach is related to the rate of sea level fall with a slow rate making a wider beach terrace composed of numerous storm events. Initial unloading may have occurred prior to 13,000 yr BP when the marine based ice sheet on the eastern Spitsbergen Bank in the Barents Sea broke up and calved away. The second step occurred at about 10,000 yr BP and

resulted in deglaciation of the major fjords of Spitsbergen by 9000 yr BP (Figure 1.12) (Forman et al., 1987).

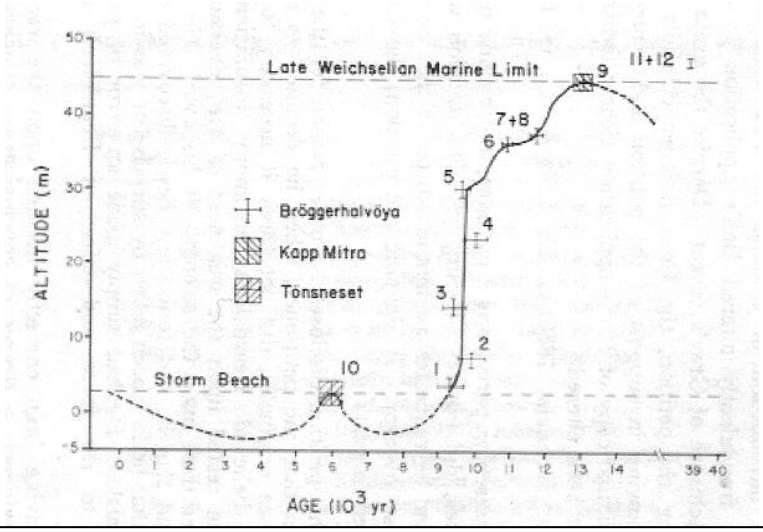

Figure 1.12: Relative sea level curve of Brøggerhalvøya, Spitsbergen during the Late Weichselian and Holocene (From Forman et al., 1987).

Deglaciation patterns have also been interpreted from marine sediments at Linnédalen where a bedrock ridge separated the overdeepened fjord from the sea after isostatic rebound (Figure 1.13). The lacustrine sediments of Linnévatnet are underlain by a unit of marine sediments with a basal till below, all on top of bedrock. The till was most likely deposited by the Late Weichselian glacial advance which eroded all preceding sedimentary units. Radiocarbon dates from shells found at the base of the marine sediments indicates glacial retreat from the lake basin began around 12,500 BP. Ice proximal lithofacies were not identified in cores from the lake indicating rapid glacial retreat. Evidence of other late glacial or early Holocene re-advances is lacking. Apparently Younger Dryas glaciers on Svalbard were much smaller than those of the Little Ice Age probably due to a very cold, dry climate (Mangerud and Svendsen, 1990).

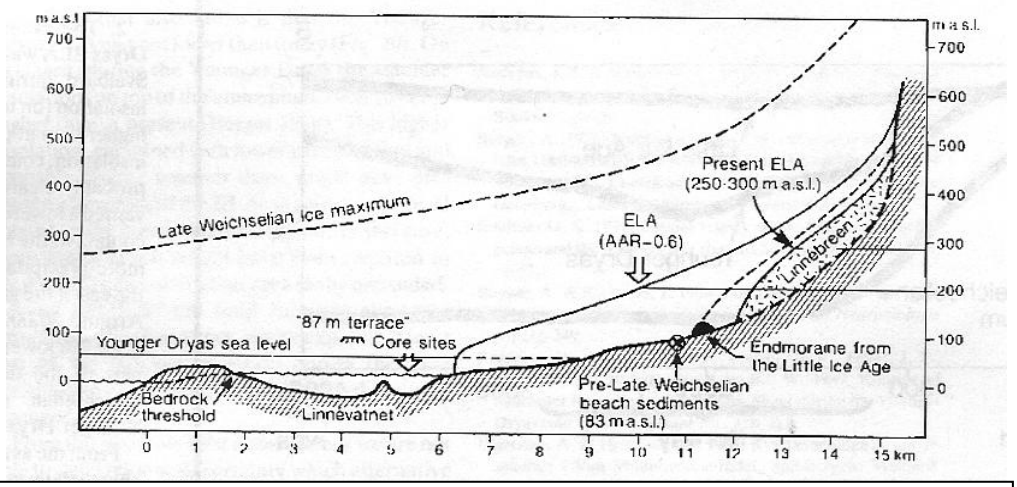

Figure 1.13: Profile of Linnédalen showing pre-isostatic rebound sea level and glacial conditions (From Mangerud & Svendsen, 1990).

The sediment stratigraphy from Linnévatnet reveals the Holocene glacial conditions on western Svalbard as well as the rapid deglaciation character of the Holocene warming. During the next 6000 years, glaciers were absent from the valley Linnédalen when there was no glacial signal recorded in the lacustrine stratigraphy. The current Linné glacier, Linnébreen, started to form 4000-5000 years ago during a late Holocene cooling and reached a maximum extent for the Holocene during the Little Ice Age (Svendsen & Mangerud 1996). Presently, Linnébreen has retreated approximately 2km from an ice-cored moraine that indicates the glacier's furthest Little Ice Age extent (Werner, 1993).

Svalbard has been subjected to numerous glaciations that have shaped the landscape that is seen today. 60% of Svalbard's landscape remains covered by ice. The Holocene climatic optimum saw a complete deglaciation of many of the western valley glaciers that regrew and advanced during the Little Ice Age (Snyder et al., 2000).

Today, western Svalbard is glaciated by many valley glaciers and cirque glaciers, while northeastern and eastern Spitsbergen, as well as Nordaustlandet, are covered by significant ice caps. The 20th century has seen significant glacial retreat that shows signs of continuing into the near future.

Lacustrine Sediments, Sedimentary Processes, and their use as a proxy for climate change:

Sediment deposition in a lake is a controlled by many factors including climate, glacial processes, and hydrology. Influx of sediment to a glacial lake is transported primarily by precipitation and meltwater runoff from snow and glacial ice. Annual sediment accumulation is dependent on many processes of transport. In order to obtain a reliable interpretation of lacustrine sediment cores, it is important to take into consideration the entire system in which different mechanisms provide sediments (Jansson et al., 2005).

Lake Stratification

The distribution of suspended sediment entering a lake is controlled by the relative density between the lake water and the inflow water, as well as the vertical temperature distribution of the water column (Smith & Ashley, 1985). Vertical temperature distribution of the water column is determined by solar heating and heat loss by conductive and convective transfer at the lake surface. Deep cold water and warmer surface water stratify a lake by temperature (Figure 1.14). The boundary between the upper water body known as the epilimnion and the cold lower water

body known as the hypolimnion is called the thermocline. The thermocline is marked by a layer of water with a large temperature gradient known as the metalimnion. Temperature is the dominant variable of density stratification in a glacial lake such as Linnévatnet.

Lake Inflow

The relative density between the lake water and the inflowing river water affects the pattern of mixing and the transport and deposition of sediment. Inflow density can be controlled by temperature, dissolved ion concentration, and suspended sediment concentration (Smith & Ashley, 1985). Suspended sediment and temperature are often the dominant variables in a glacial stream. Depending on the relative density, inflow will enter the water column as overflow, interflow, underflow, or homopycnal flow (Figure 1.15). If the inflow water is more dense than the lake water, the current will plunge down the delta front as an underflow. Underflows are more concentrated currents that are focused by the bathymetry of the lake bottom. If the inflow water is less dense, the current will flow along the surface as on overflow and will often appear as a distinct plume. Interflows can occur when the inflow density is greater than the epilimnion, but less dense than the hypolimnion (Smith & Ashley, 1985). Homopycnal flow results from even mixing of inflow when the two bodies of water are of relatively equal densities and the lake is weakly stratified. Aside from the coarsest bedload, density currents are responsible for the majority of sediment transport in a lake. Wind and gravity also play important roles in sediment distribution.

Suspended sediments flowing into a lake are also under the influence of currents created by wind, gravity, and waves (Smith & Ashley, 1985). Wind and wave action can greatly affect the range of silts and clays in an overflow plume. Transportation of suspended sediments is also influenced by the Coriolis effect which deflects moving water and suspended sediment to the right side of the inlet in the Northern Hemisphere (Figure 1.16). The coarse bedload is typically deposited on the delta front where sediments are affected by gravity driven down-slope processes such as sediment creep, slumps, and turbidity currents (Figure 1.17). Underflows or turbidity currents can scour previously deposited layers and resuspend sediment. Turbidity currents often occur during periods of high discharge, but can also be triggered by slumps and slides on the delta front. The flow dynamics into the lake greatly affect the structural nature of laminae deposited on the lake bottom.

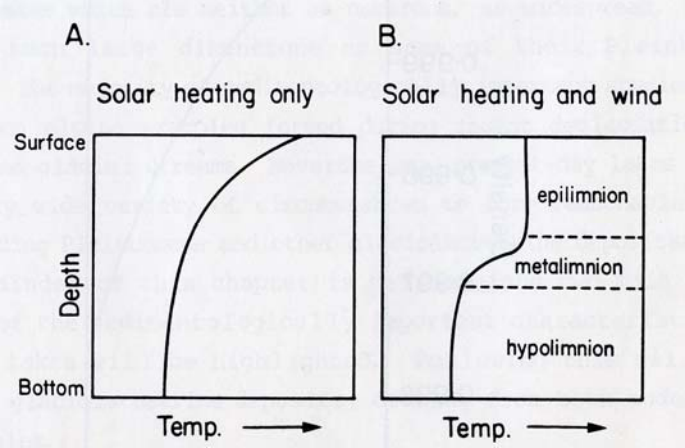

Figure 1.14: Hypothetical thermal stratification diagrams of a lake water column. A. Temperature curve of heating by solar radiation only. B. Stratified layers identified in a water column with the influence of wind mixing. (from Smith & Ashley, 1985).

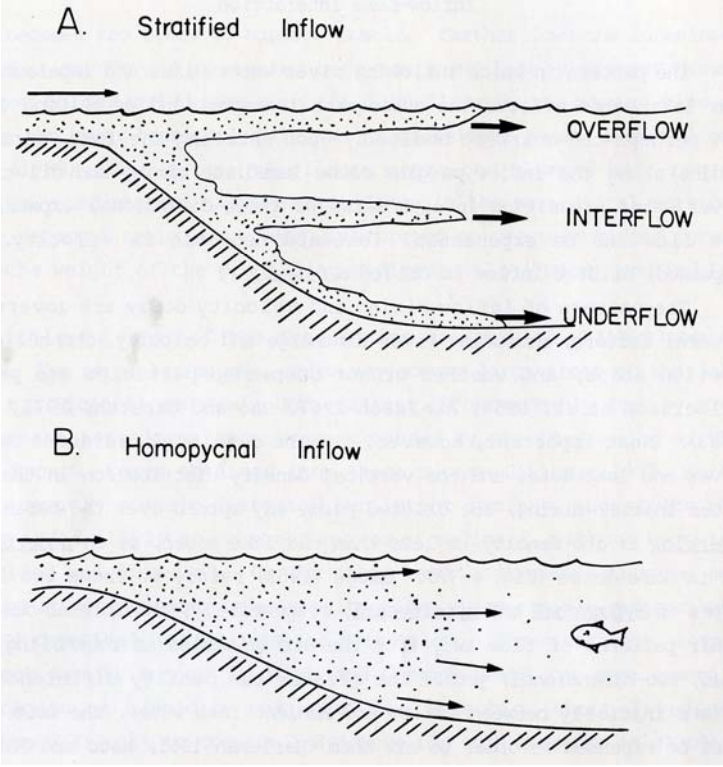

Figure 1.15: Four principle types of inflow mixing between the inflow stream (left) and the lake. Stippled area indicates area of flow with suspended sediment. (from Smith & Ashley, 1985).

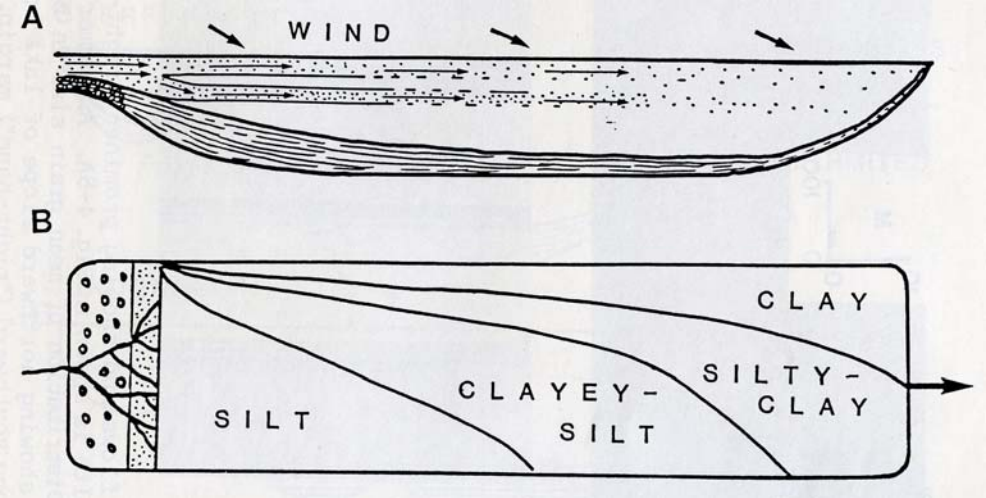

Figure 1.16: Distribution of fine grain sizes in a glacier-fed lake as a result of wind, particle inertia, and the Coriolis effect. A. Deposition thickness. B. Areal distribution. (from Smith & Ashley, 1985).

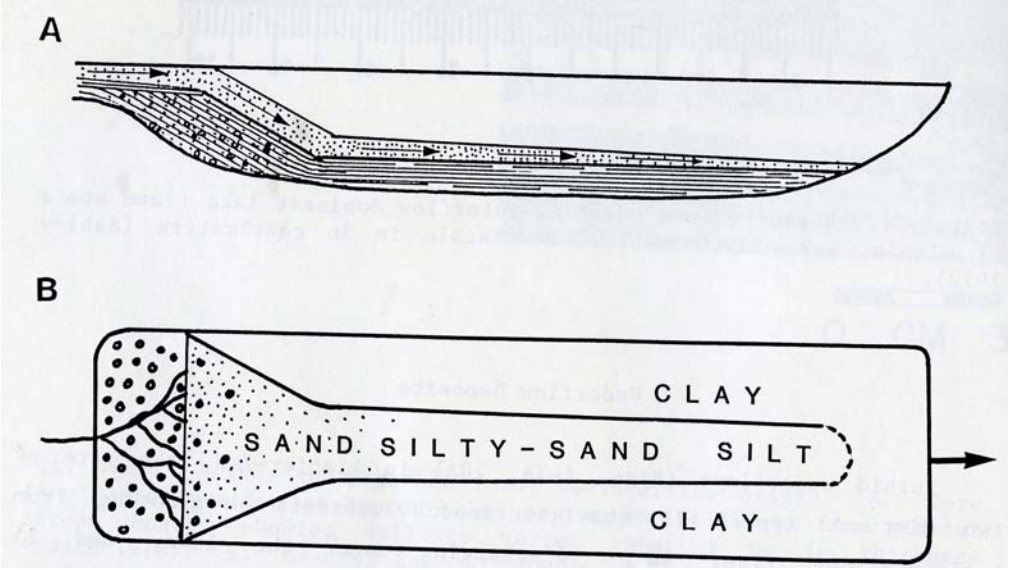

Figure 1.17: Distribution of underflow and turbidity current deposits. A. Deposits become thinner with distance from the inlet, and are restricted to low bathymetric areas. B. Fining grain size sequence away from the inlet (from Smith & Ashley, 1985).

Deposits

Sediment deposits change across the basin depending on their mode of transport. Laminae deposited by overflow and interflow currents are indistinguishable because they are both deposited through similar mechanisms (Smith & Ashley, 1985). These currents will drop coarser grains close to the inlet and carry fines further into the basin, where they are also influenced by wind, waves, and the deflection of the Coriois effect (Figure 1.16).

Underflow deposits can occur continuously or as a short surge. There is a continual controversy concerning the rhythmicity of surge-type versus seasonal sedimentary processes (Smith & Ashley, 1985). The deposits of these two underflow types can indicate their duration and cause. Surge-type underflows may occur on the order of minutes and deposit a gradual fining upwards sequence because all of the grain sizes were transported together. Sediment load and grain size decrease into the basin (Figure 1.18). On the other hand, continuous underflow currents may make a more distinct boundary between silt and clay laminae that reflects changing transport conditions. The deposit from an underflow lacks the gradually fining upwards sequence due to the steady flow regime depositing similar sized particles over a period of time, and is ultimately capped by a clay layer settled from suspension. Continuous underflows are considered a part of regular seasonal deposition that create annual couplets, or varves, although surge deposits are not generally considered with regular annual sedimentation due to the relatively random nature of the frequency of events. Continuous interflows can occur when the inflow sinks to the thermocline and meets a more dense hypolimnion (Smith & Ashley, 1985).

Annually-laminated lake sediments: Varves

Regularly deposited lake sediments in a glacial environment have been interpreted as annual accumulations, known as varves, as early as DeGeer (1912). A varve is generally represented as a pair of light and dark laminae that have been deposited in the summer and winter respectively (Sturm, 1979). Suspended sediments and stratification of the water column are the dominant driving features of varve formation. As these conditions change, so do varve structures; a varve is created by numerous depositional mechanisms throughout the year (Figure 1.19) (Smith & Ashley, 1985). In theory, varves can provide a precise chronology based on years of sedimentation whereas other dating techniques such as radiometric dating can have wide margins of error (Saarnisto, 1986). It is often difficult, for example, to find reliable organic material in the clastic varves from Linnévatnet for radiocarbon dating (Svendsen & Mangerud, 1996).

Lacustrine sediments with rhythmic laminae have been shown to reflect climatic, hydrologic, and suspended sediment fluctuations in arctic lakes (Lamoureux et al., 2001; Lamoureux 1999; Retelle & Child, 1996). Differences in laminae thickness and grain size have been related to precipitation events and runoff rates, which are also partly controlled by temperature (Lewis et al., 2001; Leeman & Niessen 1994).

Seasonal changes in weather, density differences in the lake stratification, and variations in rates of glacial erosion are three major factors to consider for the formation of varves in a proglacial lake (Leeman & Niessen, 1994). Simple varve

couplets are often complicated by intra-annual events of high sediment influx and calm periods of fine sediment settling, caused by changes in temperature and precipitation. Although sediments from Linnévatnet are rhythmically deposited and interpreted to be varves (Pratt, 2006), the relationship between climatological, hydrological, or glaciological factors affecting sedimentation remains unclear.

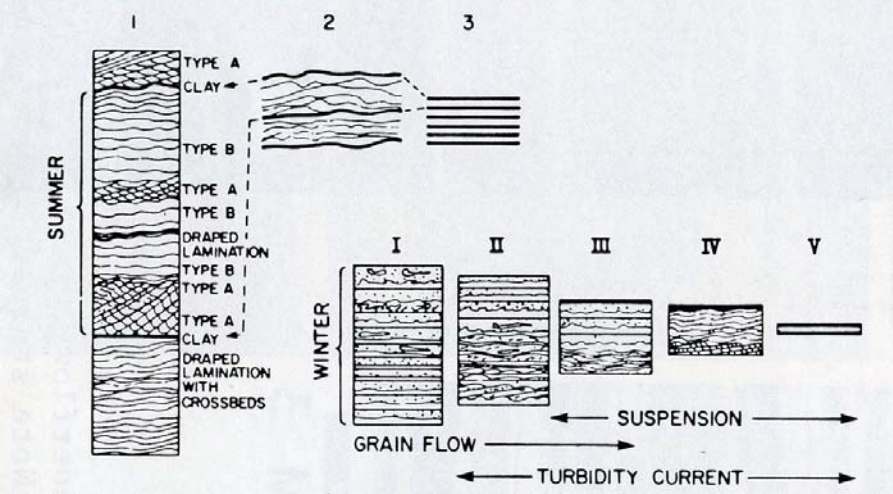

Figure 1.18: Lateral variation (delta proximal to distal, 1-3) variation of rhymites in a glacier-fed lake. Note distal fining and thinning; I to V indicate variation within the winter layer due to slumping. (from Smith & Ashley, 1985).

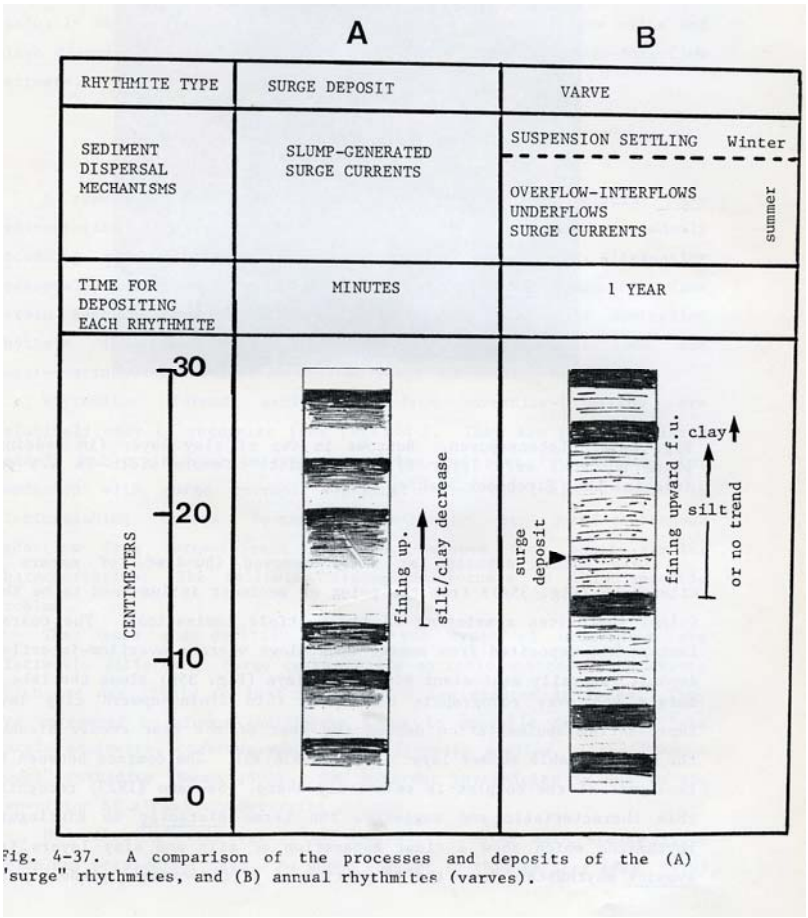

Fig. 4-37. A comparison of the processes and deposits of the (A) "surge" rhythmites, and (B) annual rhythmites (varves).

Figure 1.19: A temporal, depositional, and structural comparison between "surge-type" rhymites and annually deposited varves.

Previous Work:

Linnévatnet is the most thoroughly studied and well understood lake on Svalbard (Ingólfsson, 2006). Seismic profiles and core logs from the lake show till overlain by marine sediments, topped by lacustrine sediments (Svendsen et al., 1989; Mangerud & Svendsen, 1990). Linnévatnet is interpreted as a glacial isolation basin that was isolated from the sea around 9600 yr B.P. (Svendsen et al., 1989). During the Late Weichselian retreat from the glacial maximum, Linnédalen was occupied by a glacier flowing north into Isfjorden, the largest fjord on Svalbard. Before the crust rebounded from the removed weight of the Barents Ice Sheet, the Linné glacier was a calving tidewater glacier and Linnédalen was a fjord with marine sediments accumulating at the glacier's margin. As the ice retreated further and the crust rebounded, the fjord sill cut off the ocean from the overdeepened fjord basin to create the lake (Mangerud & Svendsen, 1990).

The National Science Foundation (NSF) Svalbard Research Experience for Undergraduates (REU) has been measuring modern processes of the glacier-river-lake system since 2004. Sediment cores taken from proximal, intermediate, and distal sites from the inlet delta of Linnévatnet have been analyzed for lamination continuity and relationship to temperature and precipitation records from Longyearbyen (Pratt, 2006). Linnévatnet laminations can be defined as varves based on Cesium 137 dates and sediment trap results (Pratt, 2006; Motley, 2006). It is difficult to positively correlate a single variable of glaciological or meteorological influence due to changing environmental influences on sediment transport (Pratt 2006). For each year

that modern processes are monitored, a better understanding will arise of the variability in the glacier-river-lake drainage.

There is a significant amount of background information that has contributed to the ability to observe and interpret the Linnévatnet stratigraphy. Intimate knowledge of the site area through field work was integral to this process as was the work by many other REU students which can be found at, or requested through, the Svalbard REU website: http://www.mtholyoke.edu/proj/svalbard/. Meltwater discharge and suspended sediment concentrations from below the glacier and at the river inflow to Linnévatnet have shown fluctuation through the summer field season (Matell, 2006). Sediment traps in particular have shown in detail the nature of sedimentation over the course of a year. Linnévatnet has been found to have a large influx of sediment during the nival runoff and probably during large precipitation events (Motley, 2006). Although Motley (2006) represents only the 2004-2005 year's sediment accumulation, further sediment trap results will contribute to the background information concerning sedimentation processes affecting lake bottom deposition.

Monitoring modern processes in Linnédalen provides glaciological, meteorological, and limnological understanding of the catchment that can aid in the interpretation of past sediment deposition. This study includes an interpretation of the varve stratigraphy back to approximately 1963 and a preliminary analysis of varve thicknesses and the weather data recorded in Longyearbyen during this period.

2. Methods

Methods Overview

Ten sediment cores from the bottom of Linnévatnet were collected in summer 2006 ranging from 18 to 40 cm each. Thin sections were manufactured to analyze sub-millimeter scale laminae variations. Using digital images of thin sections, laminae were visually correlated across core sites. In addition, the laminae at the depth of the 1963 ^{137}Cs age was correlated to corresponding laminae in these cores. Annual laminations were interpreted to the depth of the sediments inferred as being deposited in 1963. From the varve count, laminae thicknesses were measured and compared to temperature and precipitation records back to 1963.

The following methods include procedures from the field and from the laboratory. In particular, some of the laboratory procedures were described in detail in order to minimize the chance for omitted information that may be found useful by a later party.

Field Methods

Site Selection

Coring sites were located in the East Basin of Linnévatnet along two intersecting transects (Figure 2.1). Coring sites were selected to recover a basin wide representation of the sediment deposition. The East Basin contains four areas of slightly deeper water, below the 15m contour. Mooring site C is located in the southwesternmost of these holes and mooring site D is located in the northern most of these holes. The delta proximal east-west transect that intersects site C and the proximal to distal north-south transect that intersects site D each intersect at coring

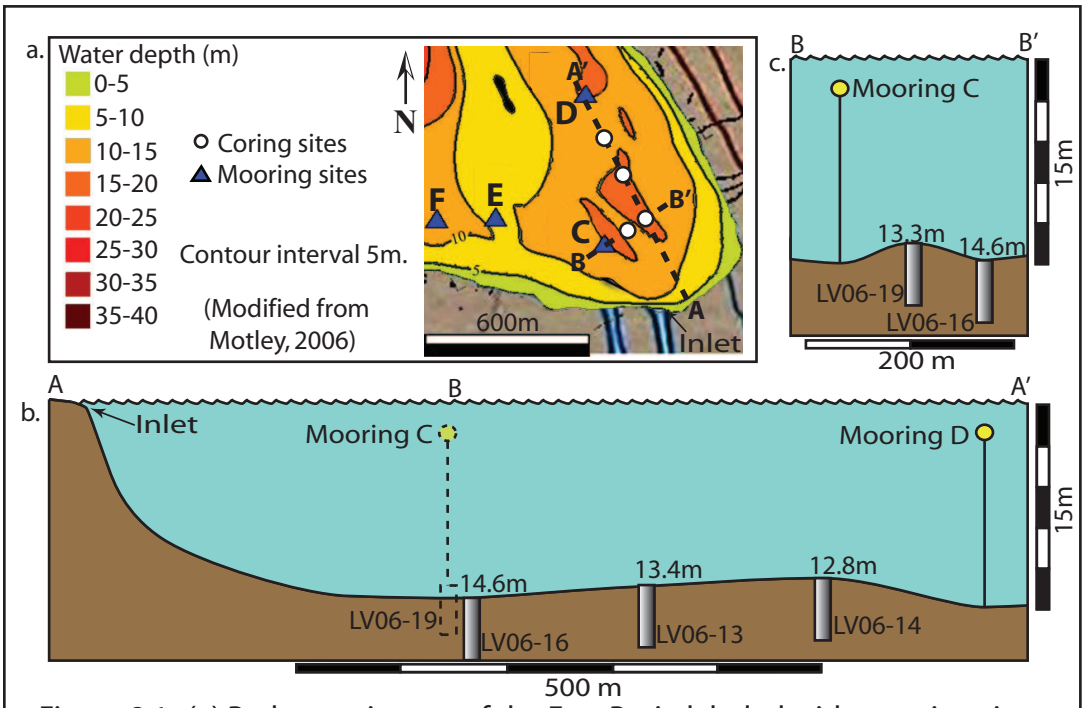

Figure 2.1: (a) Bathymetric map of the East Basin labeled with mooring sites, core sites, and transects. (b) Delta proximal to distal transect (A to A′) from the inlet to Mooring D. (c) Delta lateral transect (B to B′) from Mooring C across the East Basin to core LV06-16. Transect cross sections (a) and (b) are at the same scale, exaggerated vertically. Water depth is labeled by each core.

site 16. Mooring sites C and D were selected previously in the deepest portion of their particular areas of interest. Cores retrieved in the summer of 2006 were given numbers based on arbitrary waypoint numbers that were recorded from the Garmin GPS. For example, core LV06-19 is from Linnévatnet (LV), retrieved in 2006 (06), at waypoint 19.

Two coring sites were selected on the transect propagating east from C. The Loran GPS and echosounder provided the location and depth for each site. LV06-19 was retrieved from the minor bathymetric ridge between site C and the southeasternmost hole. The ridge has a rise of approximately one meter relative to the adjacent depressions to the east and west. LV06-16 was retrieved from the southeasternmost depression. This transect was selected to compare sedimentation across the East Basin equidistant from the Linnéelva inlet, and to compare differences between deposition on the bathymetric ridge and in the deeper holes.

Another transect was selected to retrieve cores from proximal to distal sites relative to the inlet delta. This roughly north-south transect connects mooring site D and LV06-16. Using the Loran GPS in the Zodiac, two core sites were selected that divided the distance into rough thirds. A sequence of cores at regular intervals from the delta proximity of mooring site C out to mooring site D was desired for later laminae correlation. Site C, being the most proximal sediment trap location to the inlet, was found to contain the highest resolution record (Motley, 2006). Lamina or patterns of laminae are more difficult to correlate from site to site with increasing distance or difference in environment, leading to the selection of core sites within 200 m of one another.

Four core sites were analyzed, including two core sites along the east-west transect and three core sites along the north-south transect (where LV06-16 was located on both transects). The potential changes from site to site as well as how many cores could be returned to the lab were considerations when choosing sites.

Sediment Coring

A Universal Surface Corer with a percussion hammer was lowered from the side of the Zodiac as another crew member operated the outboard to maintain the position on the water (Figure 2.2). A calm day was required for best operation. Once the coring device touched the lake bottom, the sliding brass percussion hammer was operated to penetrate the compact sediments. Once the coring tube was thought to have penetrated to approximately length of the core tube, the device was slowly extracted from the lake bottom until the vacuum released as the coring tube left the lake bottom. Once the coring device was hauled to the water surface, a plastic cap was placed over the bottom of the core tube before it was lifted out of the water.

The coring tube was removed from the device and capped with the lake water remaining. The cores were returned to the Isfjord Radio station with plastic caps taped securely to the tubes. The sediment-water interface remained intact during this transport. At Isfjord Radio the water was siphoned from on top of the core and the tube was left open for the core to lose some of its moisture. Water was also removed by siphon as it later accumulated on the surface. The core tubes were then cut to within 7 to 10cm of the core top in preparation for packaging. A plug of absorbent florist's foam was inserted into the core tube with a thin plastic barrier to protect the

Figure 2.2: The author prepares to core during a calm day on Linnévatnet using the Universal Surface Corer.

sediments from being incorporated into the foam. Once the space in the core tube was filled with the foam, it was recapped, taped securely, and ready for transport to the laboratory.

Laboratory Methods

Core cutting

Cores were cut lengthwise on two opposing sides on a table saw with the blade set to cut only partially through the thickness of the core tube wall. In order to contain the sediments, the core tube was cut with the plastic caps in place. Due to the plastic caps having a wider diameter than the core tube, as they rode over the saw table the distance between the core tube wall and the saw table was changed. This created an undesirable variability of the kerf depth that occasionally cut all of the way through the plastic wall. Where the saw cut all of the way through the core tube, the blade did not penetrate deep enough to remove or significantly disrupt the sediments. Once scored by the table saw, the remaining tube wall and the caps were cut through with a utility knife. A monofilament fishing line was then pulled through the cuts and a few drops of deionized water were squirted on the cut through the sediments so that the two halves would easily separate. One half was chosen as an archive, wrapped in plastic, labeled with its core identification and top arrow, and stored in the refrigerator. The remaining half was labeled as the working half and was logged and sampled for thin section fabrication before being stored with the archive. Some sediment deformation had occurred particularly near the core tops where it slumped

during transportation. Once opened and split, the internal structure of the sediments appeared intact. This deformation may have some consequences in lamination thickness measurements.

Core logging

Each core half was described with a range of Munsell Soil Color values and overall length (Figure 2.3). Photographs were taken of the core with a scale and Munsell Soil Color chart. Photographs were also taken after sheet metal cutters were pressed into the sediment for thin section preparation (Figure 2.4).

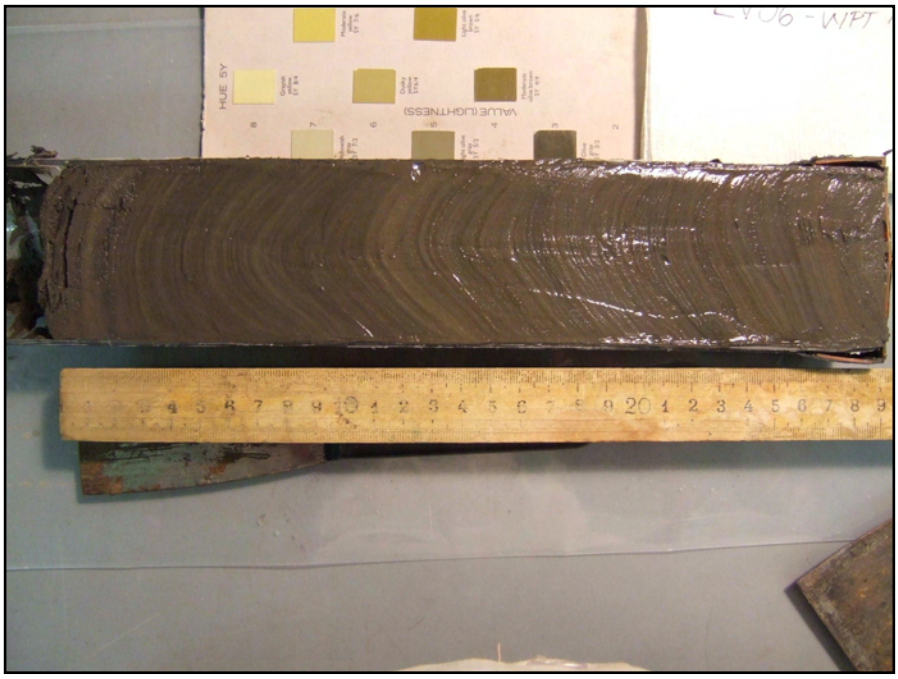

Figure 2.3: Core logging LV06-19; note top interface (core top to the left) and dragged laminae by core tube walls.

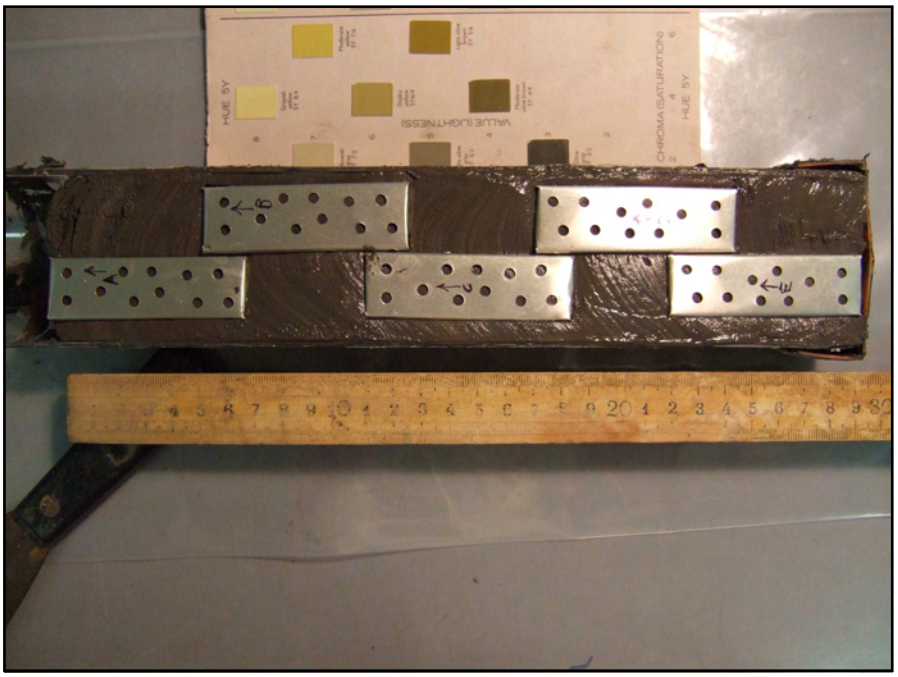

Figure 2.4: Thin section sampling LV06-19 with metal containers. Core top to the left.

Bulk Density

Each core was sampled for bulk density in order to correct varve thickness if a significant variability existed from top to bottom of the cores. Wet and dry densities of the sediments were calculated. One cubic centimeter (cm^3) was sampled at every centimeter along each core. First, ceramic crucibles were weighed on an analytical balance and placed into racks. Schematic diagrams of each rack were drawn so that crucibles would not be misplaced. A core half was laid out with the sediment surface covered by plastic wrap to prevent moisture loss. The plastic wrap was peeled back enough to sample two $1cm^3$ samples which were transferred to two separate, previously weighed crucibles and then weighed again immediately. This procedure was repeated for two samples at a time until the whole core was sampled.

After wet samples were weighed, the racks were placed into the drying oven. The samples were dried for 24 hours at 100 ºC. As the racks were removed from the oven, they were placed into a desiccator to cool. Once the samples cooled to room temperature, they were weighed again on the analytical balance. Wet and dry densities were then calculated as mass divided by sample volume ($1cm^3$) and plotted by depth (Figures 3.2-3,3).

Thin Section Preparation

Creating thin sections requires taking samples from the core in an orientation that is best for viewing particular areas of interest, or in this case the overall stratigraphy. In order to mount sediments on a slide with little to no deformation from their appearance in-situ, the interstitial pore water must be removed and

replaced with epoxy that will harden and essentially "lithify" the sediments. At this point the stratigraphy cannot be disturbed and a cross section sliver of the sample is cut and mounted to a slide, then polished to an appropriate thickness for either viewing under a microscope, or in this case, scanning into a computer for analysis on-screen.

Two different methods were considered for removing the water from the thin section samples. The first method uses acetone exchange baths to replace the interstitial water (Lamoureux, 1994; Lotter & Lemcke, 1999). The second method involves freeze drying samples with a vacuum freeze-drier (Lotter and Lemcke, 1999; Pratt, 2006). Both methods were attempted with core LV06-C.

The freeze drying method was chosen over the acetone exchanges. Freeze drying does not require using hazardous solvents and has a faster processing time because it generally requires less labor, although care must be taken in freezing to not crack the samples. The acetone exchange method may be better for other types of sediments that are higher in organic matter or fine grain sizes. A more in depth comparison of the methods appears in Lotter & Lemcke (1999).

Sampling

In order to manufacture thin sections to fit on a slide of 8x5cm, sediment samples were cut from the core using a metal container or tray of 7x2x1cm. The metal containers were made from cutouts of aluminum flashing. Multiple 1/8in holes were drilled into the flat pieces of flashing before they were folded into shape. The containers were pressed open side down into the sediment. The containers were

oriented in a pattern designed to maximize coverage of the sediment in the center of the core where there was minimal drawdown from the friction between the sediment and the core tube during penetration. The cutters alternated sides across a centerline down the core, and overlapped vertically by at least one centimeter (Figure 2.5).

An orientation straight down the middle of the core with overlap created by an angle in the cutter was considered, but was discounted due to the past occurrence of thin section corners occasionally having been ground too thin. Furthermore, previously made thin sections have an unknown gap between adjacent thin sections where no overlap was taken at all due to the butting of two square-ended metal cutters. These factors decrease the ability to visualize the laminations near thin section boundaries and therefore more overlap was preferred.

With all of the cutters in place in the core, each was labeled with a top arrow and a letter to designate its place in the core. The containers were then delicately cut out using a sampling spatula with a ninety degree bend in it to slip under and cut the sediments out.

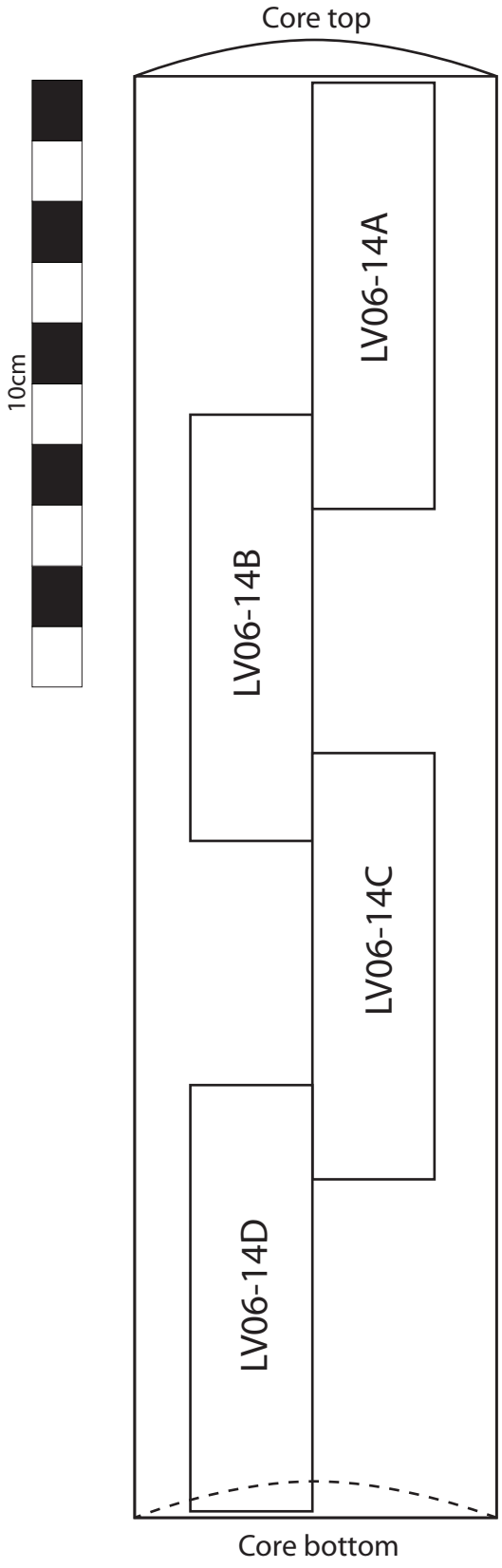

Core: LV06-14

Figure 2.5: Thin section sampling orientation from a split core. Note the core labeling system: Linnévatnet (LV), 2006 (06), waypoint 14 (14). Thin sections are labeled with an extra letter starting with "A" at the core top.

Freeze drying

All of the sediment-filled containers were then placed in a plastic dish labeled by core, and placed on the table ready for freeze-drying preparation. The process of freeze-drying first requires samples to be pre-frozen (Labconco®, 1998). The freeze drier then removes the frozen water in the sample by sublimation.

To freeze the samples in preparation for placement in the freeze-drying vacuum chamber, they were frozen by submersion in liquid nitrogen. Liquid nitrogen was graciously provided by the Bates College Chemistry Department. In order to prevent serious cracks in the sediments during freezing, the samples were slowly pushed down the floor of an inclined Styrofoam fish shipping box in which the liquid nitrogen formed a shallow end to deep end (Figure 2.6). Over five minutes, the samples were moved into the deep end where they remained for another minute. Samples were then transferred to another Styrofoam box with sufficient liquid nitrogen to keep the sediments submerged. Samples were left submerged in the liquid nitrogen for another ten minutes during which the Labconco® freeze drier was prepared by cooling the collector coil to around -50 to -80º C (Labconco®, 1998). The samples were returned to their original plastic dishes which were then stacked within the vacuum chamber of the freeze-drier maintaining that air could freely flow around them. The vacuum in the freeze drier was slowly applied to prevent the sediments from exploding. The samples were left in the freeze-drier for 48 hours and were then removed after reversing the procedure by very slowly opening one valve to allow the pressure to equilibrate so as not to destroy them.

After freeze-drying, the sediment samples were returned to their plastic dishes labeled by core and oriented with tops toward one side. Due to the characteristic of the epoxy erasing the permanent marker from the sediment containers, the outside walls of the plastic dish were carefully labeled so that the samples could later be identified after epoxy submersion.

Embedding with epoxy

Spurr low viscosity epoxy, obtained from Polysciences, Inc., was used to embed the sediments. Epoxy was mixed in manageable 300g batches. An epoxy mixture of Vinylcyclohexene dioxide (VCD), Diglycidyl ether of polypropyleneglycol (DER 36), Nonenyl succinic anhydride (NSA), and Dimethylaminoethanol (DMAE) was combined in a plastic deli cup and stirred for a full minute. These components were mixed in the following ratio by mass (after Lamoureux, 1994):

VCD : DER : NSA : DMAE :: 10 : 4 : 26 : 0.4

Table 2.1 contains the mass of each component and the cumulative mass for a 300g batch as they were combined on the balance:

Component	Mass (g)	Cumulative mass (g)
VCD	74.26	74.26
DER	29.70	103.96
NSA	193.07	297.03
DMAE	2.97	300.00

Table 2.1: Mass and cumulative mass for weighing components of Spurr low viscosity epoxy for a 300g batch. VCD= Vinylcyclohexene dioxide, DER= Diglycidyl ether of polypropyleneglycol, NSA= Nonenyl succinic anhydride, and DMAE= Dimethylaminoethanol.

The epoxy was then gradually and stepwise poured into a plastic dish containing four to five of the freeze-dried samples. Just enough epoxy was added to reach one third of the height of the samples' side walls to allow pore space to be infiltrated as air escaped through the top of the sample (Figure 2.7). For this reason, it was important to carefully seep the epoxy in the side without dripping any on the tops of the sediment. The plastic dish was laid inside a vacuum chamber to ensure that the epoxy was adequately soaked in. The vacuum, created by a hose to a valve on a faucet, was slowly increased to 25-30inHg. The sediment samples would generally draw up the epoxy within 30 minutes to a few hours so that they looked entirely wet on their surface. If they did not become entirely wet on their surfaces after three hours, epoxy was added to the plastic dish to a point about half of the way up the sides of the metal sample containers. Once the sediments appeared entirely soaked through, enough epoxy was added to completely submerge the samples.

Labels were submerged in the epoxy over each sample with an up-arrow for identification purposes later after the epoxy set. Pencil was used to write the labels as

some pigments that would otherwise be permanent were found to dissolve in the epoxy.

After complete submersion, the plastic trays were carefully moved to the oven for curing. The samples were left in the oven at 50ºC for 48 hours or until the epoxy could not be scratched by a fingernail.

The samples were then cut from the larger epoxy block and from their metal trays using a diamond rock trimming saw. Care was taken to cut away the metal trays while removing a minimal amount of sediment. In addition to the embedded labels in the epoxy, labels were scratched into the surface of the epoxy as a backup.

The small bricks of epoxy impregnated sediments were carefully packed and shipped to the Mt. Holyoke College Earth and Environment Department where they were mounted to slides, ground, and polished. Thin sections showed minimal cracking, if any, from the freeze-drying process.

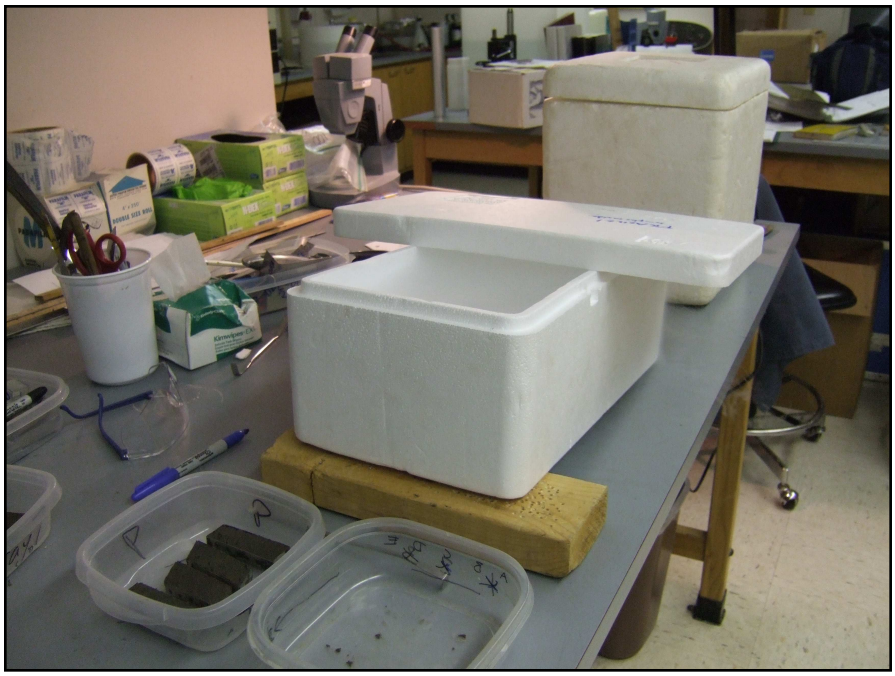

Figure 2.6: Setup for freeze drying thin section samples. Note trays of thin sections, inclined styrofoam box for initial freezing, and second box for longer submersion.

Figure 2.7: Freeze dried samples in epoxy impregnation stage. Tray on the left has overtopped thin sections after saturation in the vacuum chamber; tray on the right is ready to go into the vacuum chamber.

Thin section analysis

Thin sections were analyzed using high resolution digital scans that could be observed, moved, and zoomed in and out on a computer screen. Thin sections were scanned using an Epson Scanner at 1600 dots per inch (dpi). A metric ruler with millimeter graduations was scanned with each thin section to maintain the scale. Using Adobe Photoshop CS2, thin section scans were compiled in a mosaic for each core in the orientation in which they were extracted (Figure 3.1). A mosaic image file for each core was imported into Adobe Illustrator CS2 and lined up across the workspace from the proximal transect straight into the cores from the second transect with the most distal core on the right.

The scanned thin section image from core C2 by Pratt (2006) with the accompanying indicator at the 18.5cm depth of the cesium 137 spike was correlated to the laminae in cores LV06-19 and LV06-16, each having been retrieved at an equal distance to the inlet. For each core, initial boundaries of potential annual laminae were marked in red to become familiar with the stratigraphy. Correlations were first made between cores LV06-16 and LV06-13 by matching particularly recognizable patterns of laminae. Indistinct laminae would then be correlated relative to their position with those already correlated. Green lines were drawn to link matching couplets from one core to the other. All of the couplet-linking lines between two cores were set in a unique layer that could then be turned off to make them invisible. Once the lines from the first series of correlations were hidden, new correlations were interpreted to another core. This method was utilized to make independent

interpretations between each core by minimizing the influence from the interpretation of annual or intra-annual events from the one comparison to the next.

After correlations of laminae between the cores were completed from the 1963 cesium spike to the most recent deposition, a simplified stratigraphic column was drawn. The simplified stratigraphy included the interpreted summer layer, winter layer, and the date of deposition of the couplet. The simplified stratigraphy was imported to Sigma Scan, an image measuring software program, with an accompanying scale bar. Using Sigma Scan, the thickness of the summer layer, winter layer, and complete couplet was measured. The laminae thicknesses were then plotted against the inferred date of deposition. The results of these plots are included in the following section (Figures 3.4-3.5).

3. Results

Sediment cores

Four short cores from the East sub-basin of Linnévatnet were analyzed for this study. The analyzed cores from proximal to distal were: LV06-19, LV06-16, LV06-13, and LV06-14 (Figure 2.1). Core characteristics will be discussed for each core separately in the following sections. A number of other cores were also recovered from the lake, but were not opened because they were either duplicates from the same site, were from sites previously cored, or were from sites considered unnecessary to the goals of this project. The site locations and water depth of the unopened cores are included in Table 3.1

, also with the information for the cores that were analyzed.

The visual character of the sediments was generally consistent among the four cores opened for analysis. Laminae were visible in all cores as soon as they were split. Layers differed slightly in visible grain size differences and slightly by color. All cores had some deformation by friction with the core tube side wall, ranging from little to none at the core tops to 2-3cm of displacement from the flat crest of the layers in the core's center to the side walls.

The varve count extends from the surface to the lamination correlated from the depth of the 1963 ^{137}Cs age location in a core from Mooring Site C by Pratt (2006). Varves were interpreted downcore and across all core sites (Figure 3.1). Lamination thickness decreases from the proximal LV06-16 basin to the proximal LV06-19 bathymetric high, as well as with greater distance from the inlet to sites LV06-13 and 14. Particularly massive marker beds were correlated at varve numbers 3 and 26 (2002 and 1979, or "02" and "79" on Figure 3.1). The raw thickness

measurements for each annual lamination are plotted by cumulative core depth in Figure 3.4. Varve thicknesses were normalized for the period 1963-2004 after Hardy et al. (1996) using the following calculation, where Z_n is the normalized annual thickness:

$$Z_n = \frac{(\text{annual thickness} - (1963 - 2004 \text{ mean}))}{1963 - 2004 \text{ standard deviation}}$$

Raw varve thicknesses and normalized varve thicknesses were plotted versus varve number (or interpreted year) in Figure 3.5.

Bulk density was measured in order to test whether varves were compacted with greater depth in the core. Varve thicknesses would be corrected with respect to bulk density if a significant change was observed. The results for all cores show little change in density downcore. Wet density was found primarily to average between 1.8-2.0g/cm^3 (Figure 3.2). Dry density plots generally follow the same pattern as wet density, though values are generally reduced to 1.3-1.6g/cm^3 (Figure 3.3). The error involved in sampling with a 1cm^3 cutter may limit accuracy to 0.1g/cm^3. Due to the little difference in bulk density downcore, the results indicate that the sediments are not significantly compacted 30cm below the lake bottom in comparison the sediments at the sediment-water interface. Assuming that organic matter and variation in mineralogical composition remained constant, varve thicknesses were not corrected with respect to density. Organic matter composes approximately 6% of the sediment and is therefore insignificant for adjusting lamination thickness (Pratt, 2006).

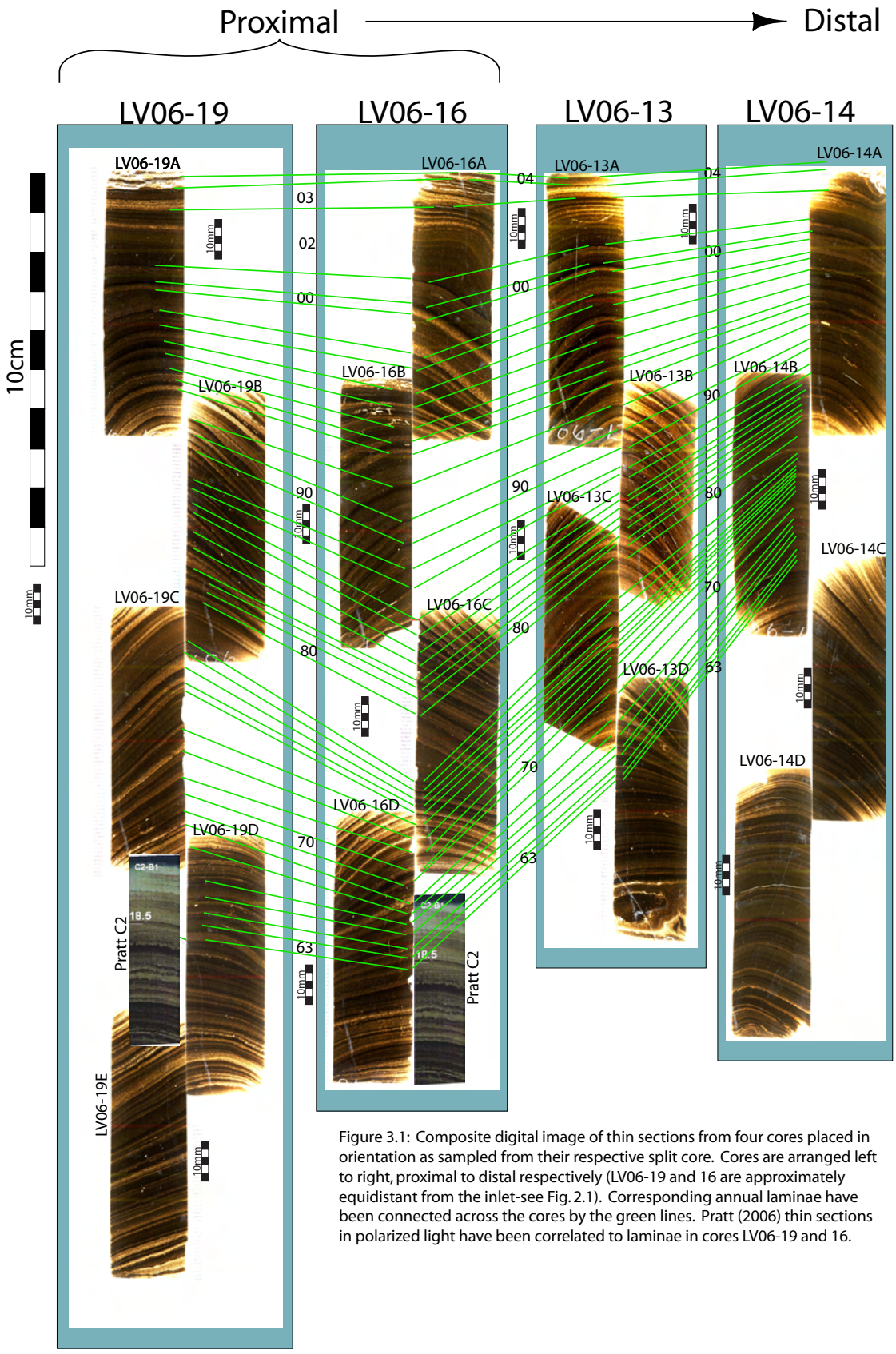

Figure 3.1: Composite digital image of thin sections from four cores placed in orientation as sampled from their respective split core. Cores are arranged left to right, proximal to distal respectively (LV06-19 and 16 are approximately equidistant from the inlet-see Fig. 2.1). Corresponding annual laminae have been connected across the cores by the green lines. Pratt (2006) thin sections in polarized light have been correlated to laminae in cores LV06-19 and 16.

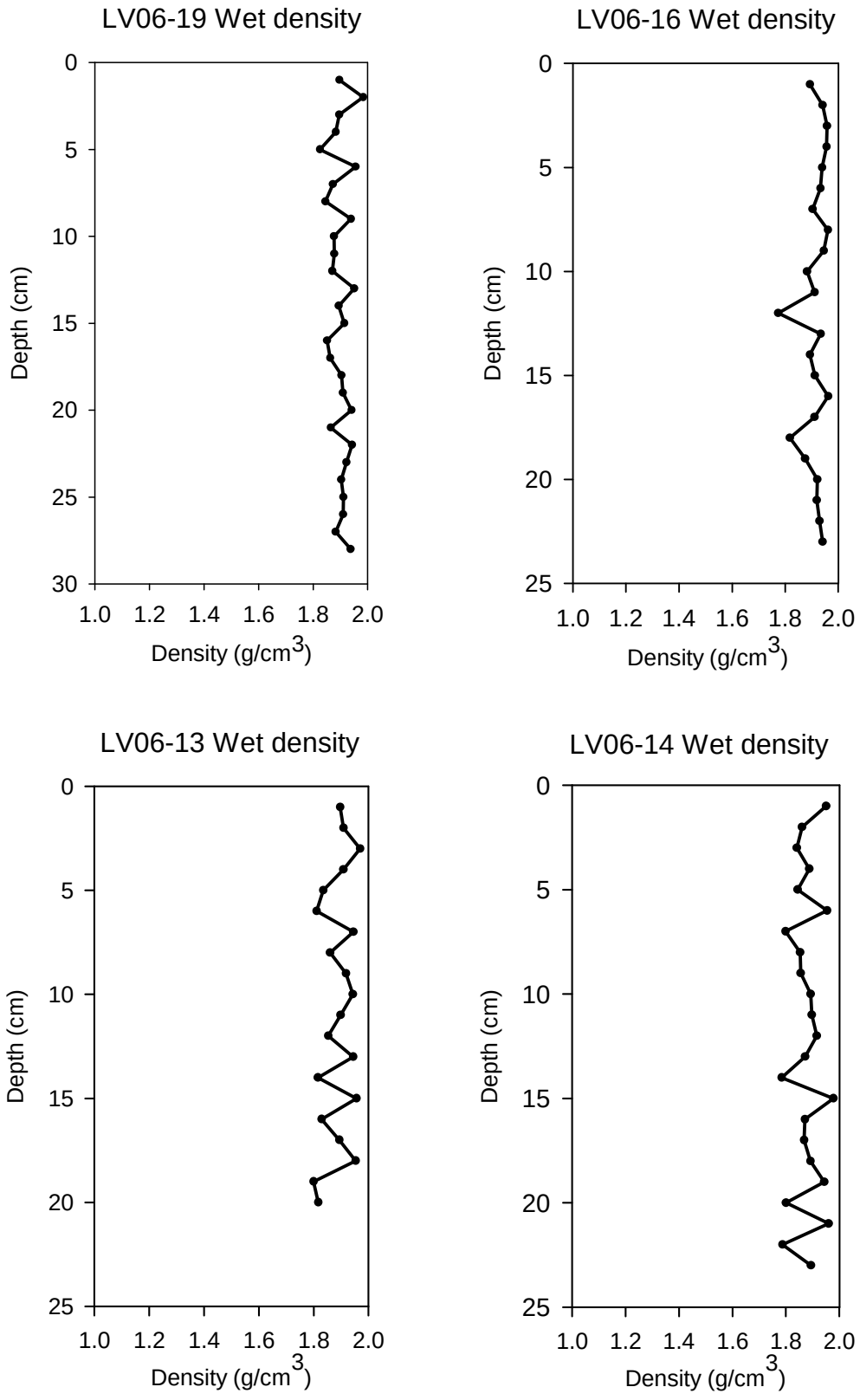

Figure 3.2: Wet density plots by depth in cores LV06-19, 16, 13,and 14.

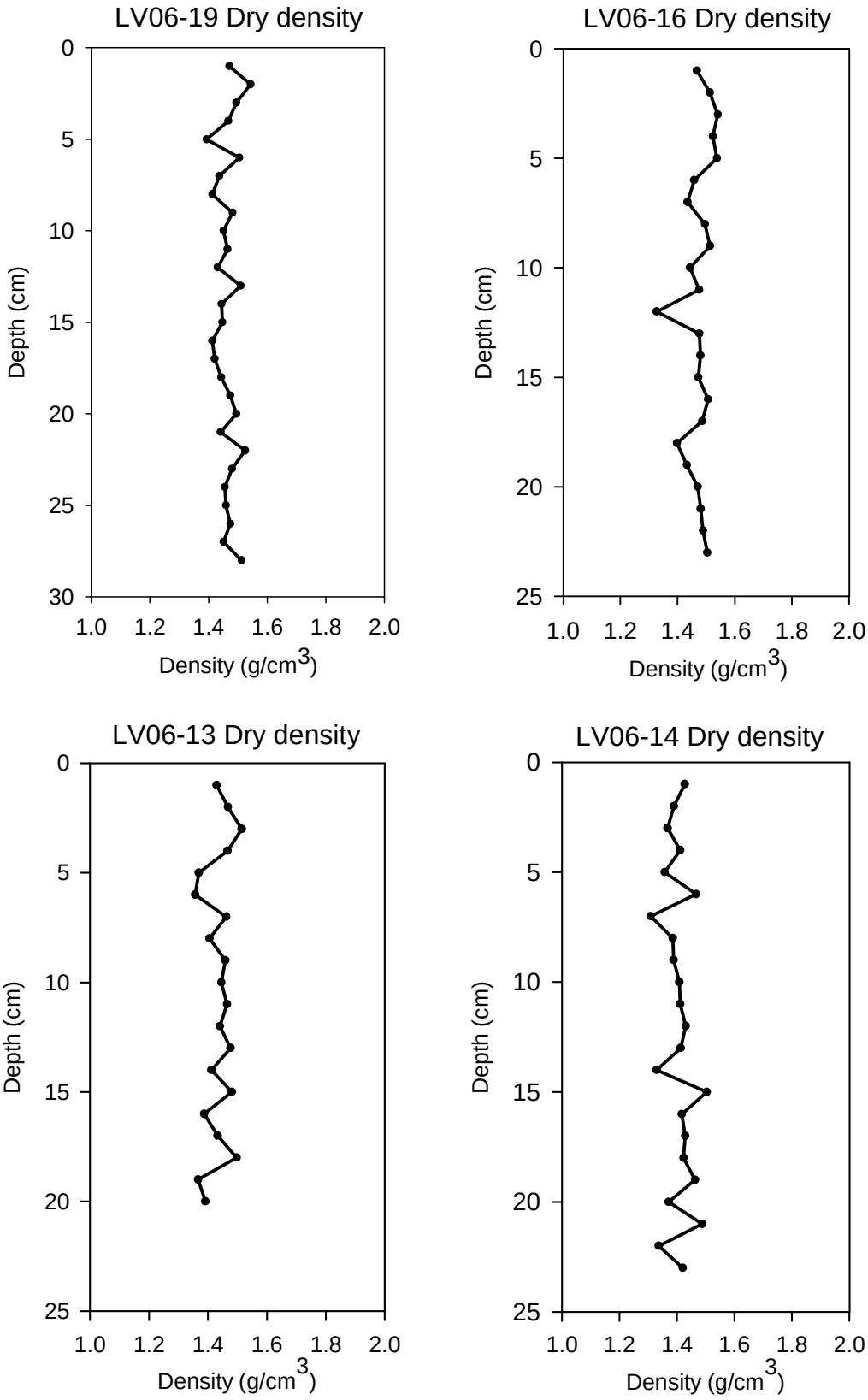

Figure 3.3: Dry density plots by depth in cores LV06-19, 16, 13,and 14.

Cores and Laminated sediments

LV06-19

The proximal core, LV06-19 retrieved from the bathymetric high between sub-basins, is 28.6cm long and has alternating laminae of light olive brown (Munsell 5Y 5/6) to olive gray (Munsell 5Y 3/2). Five thin section samples were extracted from LV06-19 with the following depths: A, 0-7.0cm; B, 5.6-12.6cm; C, 11.2-18.3cm; D, 17.0-24.0cm; and E, 21.5-28.6cm.

Varves interpreted at LV06-19 were complex with intra-annual deposition events. Varve thicknesses fluctuate significantly with depth. The range of varve thickness is 2.1-13.4mm (Figure 3.4 & 3.5). Mean varve thickness was 4.5mm with a 2.4mm standard deviation for all varve thicknesses from the mean. The most anomalous varves were 13.4mm and 11.2mm thick at 2.2mm and 11.6mm respectfully. The top 2mm of sediment of thin section LV06-19A was not included in the varve count because the winter cap layer was obscured.

Wet density in LV06-19 is consistently between 1.8 and 2.0g/cm^3 (Figure 3.2). Greater fluctuation occurs in the top 15cm of the core. The average wet density is 1.90g/cm^3. The dry density average is 1.46g/cm^3. The dry density curve follows a similar pattern to the wet density curve, though at lower values. Dry density fluctuates between 1.39 and 1.54g/cm^3 (Figure 3.3).

LV06-16

The second proximal core, LV06-16 taken from the sub-basin, is 23.6cm long and has a color range of moderate olive brown (Munsell 5Y 4/4) to olive gray (Munsell 5Y 3/2). Four thin section samples were extracted at the following depths: A, 0-6.9cm; B, 5.2-12.1cm; C, 10.9-18.0cm; and D, 16.0-23.2cm.

The full range of varve thicknesses in LV06-16 is 1.6mm to 17.9mm (Figure 3.4 & 3.5). The mean varve thickness is 4.8mm with a 3.5mm standard deviation of all varve thicknesses from the mean. The range of varve thicknesses in the top 15.2cm of the core is 1.8-17.9mm. There are two anomalous varves of 17.9mm and 16.7mm at 26.5cm and 15.2cm respectfully. Varve thickness fluctuates significantly between these anomalies. Below 15.2cm to the last interpreted varve at 20.0cm, varve thickness remains between 1.6-5.4mm. The varve count includes all laminations up to the top of thin section LV06-16A.

Wet density remains between 1.8 and 2.0g/cm^3 except for one sample at 12cm depth that is 1.7g/cm^3 (Figure 3.2). The core has another relatively low density sample of 1.91g/cm^3 at 18cm depth. The average wet density is 1.91g/cm^3. The dry density average is 1.48g/cm^3. Dry density ranges from 1.33-1.54g/cm^3 (Figure 3.3).

LV06-13

Core LV06-13 was retrieved roughly a third of the distance from LV06-16 to Mooring site D. This core is 20.5cm long and ranges in color from light olive brown (Munsell 5Y 5/6) to moderate olive brown (Munsell 5Y 5/6). Four thin section

samples were extracted from LV06-13 at the following depths: A, 0-7.0cm; B, 5.2-12.1cm; C, 8.7-15.6cm; and D, 13.5-20.5cm.

LV06-13 has less varve thickness variability than the more proximal cores. Varve thickness ranges from 1.4-11.9mm (Figure 3.4 & 3.5). The mean varve thickness is 3.6mm with a 2.2mm standard deviation of all varve thicknesses from the mean. The two most anomalous, thickest varves are 11.9mm and 10.3mm at depths of 1.7cm and 10.6cm respectfully. Varve thickness fluctuates between 1.7cm and 8.0cm and then remains constant between 8.0cm and 9.5cm with seven varves all between 2.0 and 3.4mm. Again, from 11.4cm and 12.2cm, thickness remains constant with five varves ranging from 1.8-2.0mm. Below 12.2cm varve thickness is more variable with a peak thickness of 6.6mm. A layer of 1mm at the core surface was not included in the varve count.

Wet density fluctuates widely between 1.8 and 2.0g/cm^3 through the length of the core (Figure 3.2). The average wet density is 1.89g/cm^3. The dry density average is 1.44g/cm^3. The curve for dry density fluctuates from 1.36-1.51g/cm^3 (Figure 3.3).

LV06-14

Core LV06-14 is the most distal core site in this study and was retrieved approximately two-thirds of the distance from LV06-16 to Mooring site D. LV06-14 is 23.1cm long and has color variation from moderate olive brown (Munsell 5Y 5/6) to olive gray (Munsell 5Y 3/2). Four thin section samples were extracted from this core at the following depths: A, 0-7.0cm; B, 5.3-12.4cm; C, 10.5-17.5cm; and D, 16.0-23.1cm.

Varve thickness in LV06-14 is less than that of the preceding (more proximal) cores. Thickness varies the least of the cores between 0.6mm and 7.2mm (Figure 3.4 & 3.5). The mean varve thickness is 2.3mm with a 1.3mm standard deviation for all varve thicknesses. The most anomalous varve thickness is 7.2mm thick near the surface of the core. Unrecognizable sediment in the top 5mm of the core was not included in the varve count due to possible disturbance at the sediment-water interface.

Wet density fluctuates back and forth between 1.8 and 2.0g/cm^3 (Figure 3.2). The average wet density is 1.88g/cm^3. The dry density average is 1.41g/cm^3. Dry density ranges from 1.33-1.50g/cm^3 (Figure 3.3).

Core	UTM Coordinates East (33X)	UTM Coordinates North	Descriptive location	Core length (cm)	Water depth (m)	Analyzed?	Date of recovery
LV06-C			Mooring C	16.7	~15	No	8/6/06
LV06-D			Mooring D	40	~15	No	8/6/06
LV06-11	473749	8662215	Proximal	27.2	14	No	8/9/06
LV06-12	473741	8662220	Proximal	18.2	14.3	No	8/9/06
LV06-13	473750	8662416	On C-D transect	20.5	13.4	Yes	8/9/06
LV06-14	473653	8662611	On C-D transect	23.1	12.8	Yes	8/9/06
LV06-15	473617	8662232	Proximal	32.2	14.8	No	8/9/06
LV06-16	473743	8662228	Proximal	23.6	14.3	Yes	8/9/06
LV06-17	473842	8662024	On the delta	38.2	9.55	No	8/9/06
LV06-19	473697	8662215	Proximal	28.6	13.3	Yes	8/11/06

Table 3.1: Core site information.

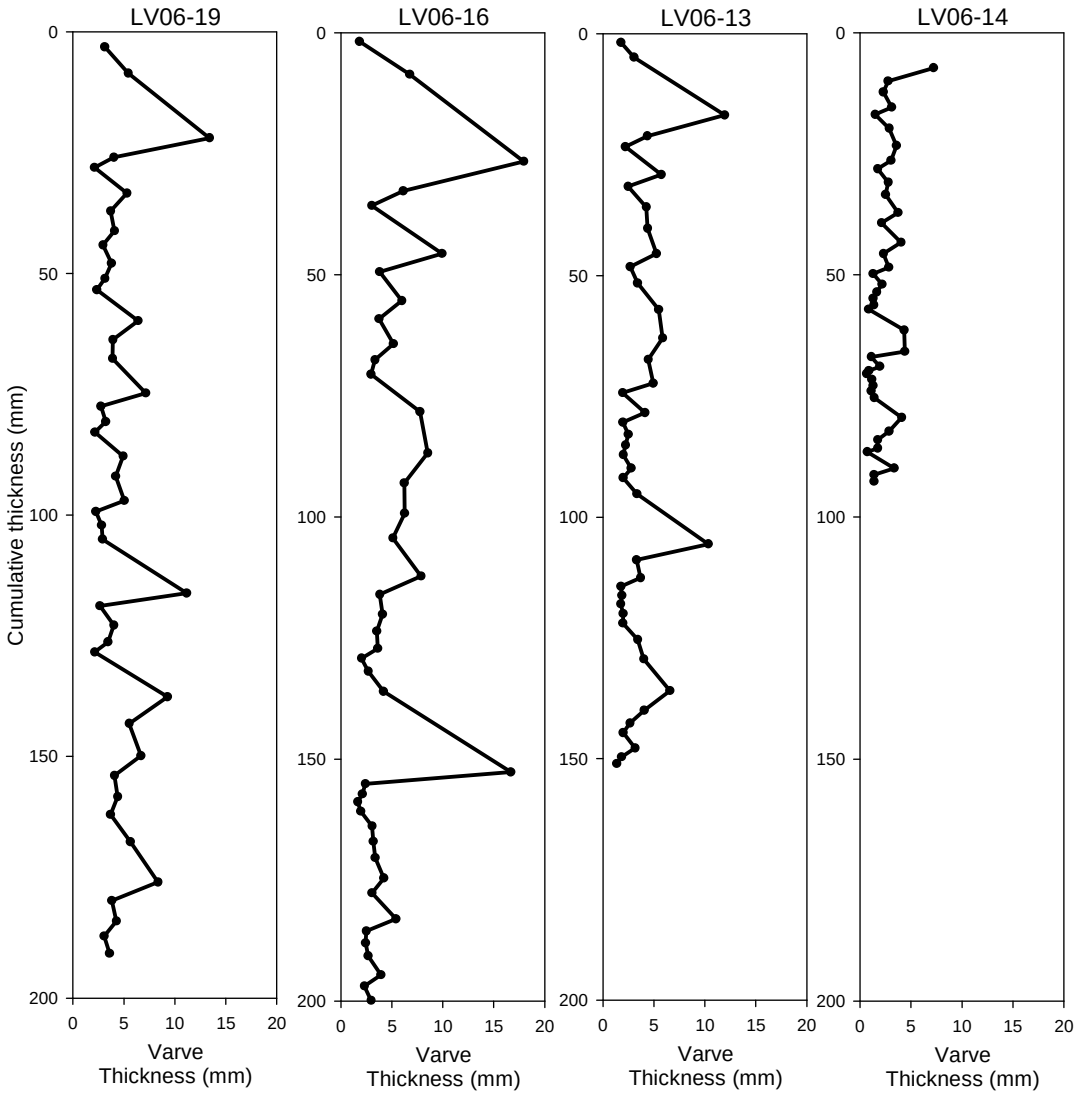

Figure 3.4: Plots for each core of raw varve thickness (horizontal) by cumulative varve thickness (i.e. depth) down the core (vertical). Note thinnning and shallower depth from proximal (left) to distal (right) and with deeper core location (LV06-16 equidistant from the inflow, though in a deeper basin than LV06-19).

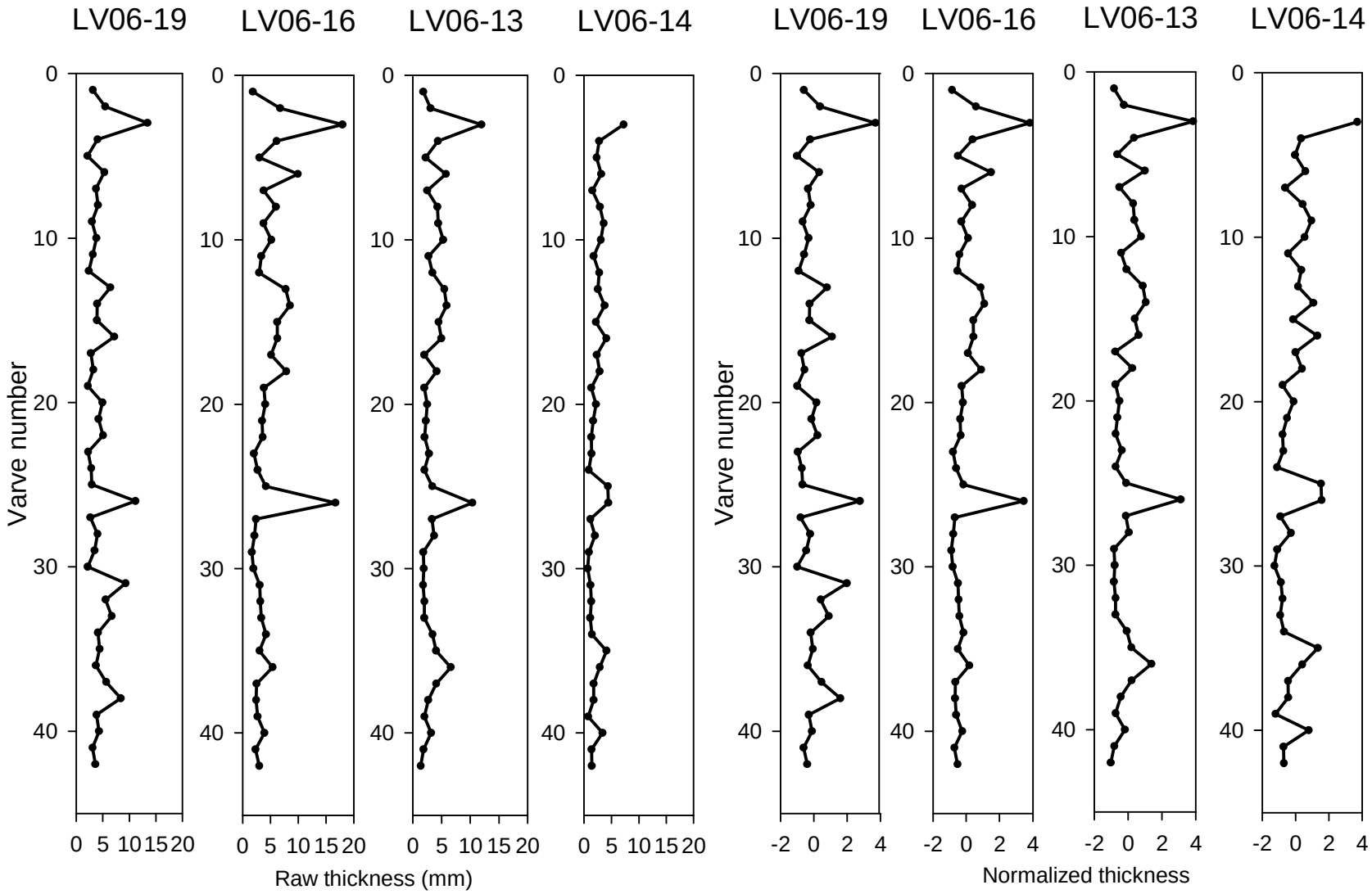

Figure 3.5: Raw and normalized thicknesses for all cores by varve number. Note thinning of raw varve thickness from proximal to distal cores (left to right).

Varve Identification

The varve stratigraphy changes with spatial relationship to the inflow source and bathymetry. Higher volumes of sediment are deposited in proximity to the inlet delta that can produce high resolution records of sediment pulses into the lake. Less sediment and finer textures are suspended to greater distances from the inlet. The distal varve record is has more regular varve couplets without the complexity of the intra-annual sediment deposits. At locations distal to the inlet, however, couplets also become diffuse so that they are difficult to differentiate. Varves were categorized into four designations: complex varves, simple varve couplets, massive laminae, and diffuse varves (Figures 3.6-3.9 respectively) modified after Lamoureux & Bradley (1996).

The varve count involved designating a winter and summer lamination for each year. The stratigraphy of proximal cores LV06-19 and LV06-16 was found to be highly variable. Varves that were found to contain many intra-annual sedimentation events were designated as complex varves (Figure 3.6). Winter boundaries between couplets were not always clear, dark clay caps, but were often intermediate in color tone and visually appeared to be composed of mixed grain sizes. Summer layers often included multiple laminae.

The most distal core in this study, LV06-14 contained sequences of distinct varve couplets of a consistent summer layer with little variation, distinctly capped by a dark winter clay layer (Figure 3.7). Regions of diffuse laminations were also counted (Figure 3.9). Diffuse laminations consisted of a layer of intermediate tone with little evidence for a winter cap to separate it from the next varve. This may be

due to low and relatively constant sedimentation that transports a small range of grain sizes.

Massive laminae were identified as thick, homogenous layers modified after "homogenites" (Figure 3.8) (Sturm et al., 1995). Massive laminae also varied with multiple homogenous layers, particularly in varve number three (also labeled as 2002 or "02" in Figure 3.1) in LV06-19 and 16. This distinction may include turbidites or other surge-type flows that may or may not be triggered by weather events. See discussion for a more in depth interpretation of these sediments.

Winter layers were consistently thinner than summer layers, although some winter layers were interpreted as thicker. The ratio of summer laminae thickness to winter laminae thickness was irregular (Figure 3.10). The winter to summer thickness ratio was skewed most in years during which there was particularly high summer sedimentation, or in which there was a massive lamination or possible turbidite.

Many processes and environmental conditions are responsible for the structure and composition of this varve stratigraphy and will be addressed further in the discussion.

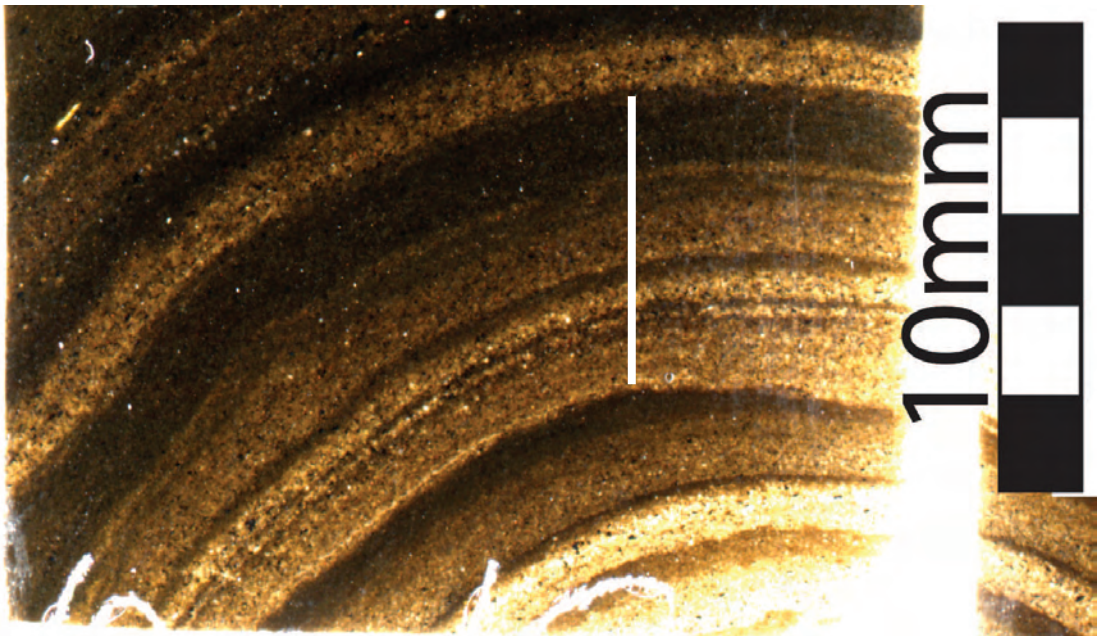

Figure 3.6: Digital scan of a complex varve from core LV06-19 at 5.6-7.0cm depth (thin section LV06-19A). Note complete year (white line) with five or six seasonal laminae capped by dark winter clay layer. Image resolution 1600dpi, enlarged with Adobe Illustrator CS2.

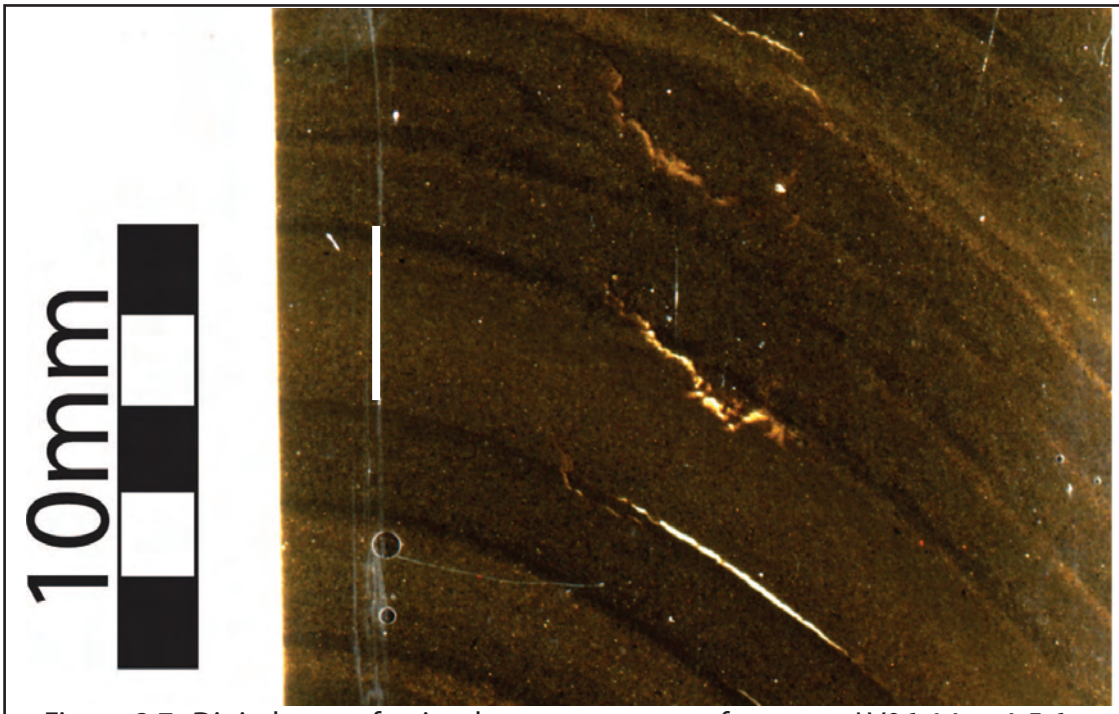

Figure 3.7: Digital scan of a simple varve sequence from core LV06-14 at 4-5.6cm depth. Note fining upwards sorting and dark winter clay layer within one year (white line). Image resolution 1600dpi, enlarged with Adobe Illustrator CS2.

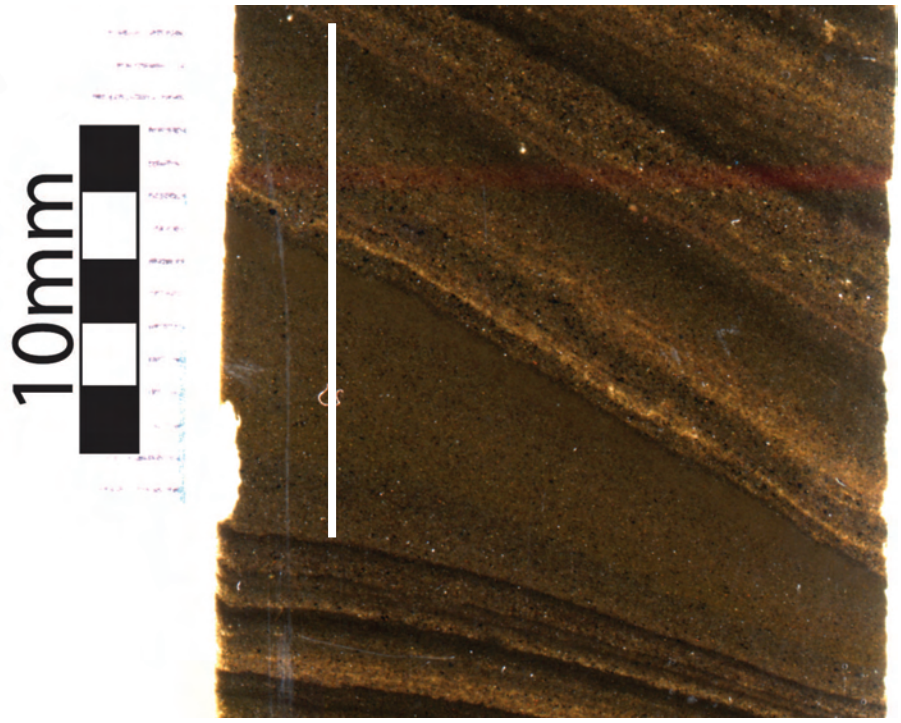

Figure 3.8: Digital scan of a massive lamination within a complex varve from core LV06-16 at 13.5-15.5cm depth (thin section LV06-16C). Note homogenous layer, with fining at its top 1-2mm. Further sedimentation above is interpreted as deposited during the same year and capped by dark fines (white line signifies entire year). Image resolution 1600dpi, enlarged with Adobe Illustrator CS2.

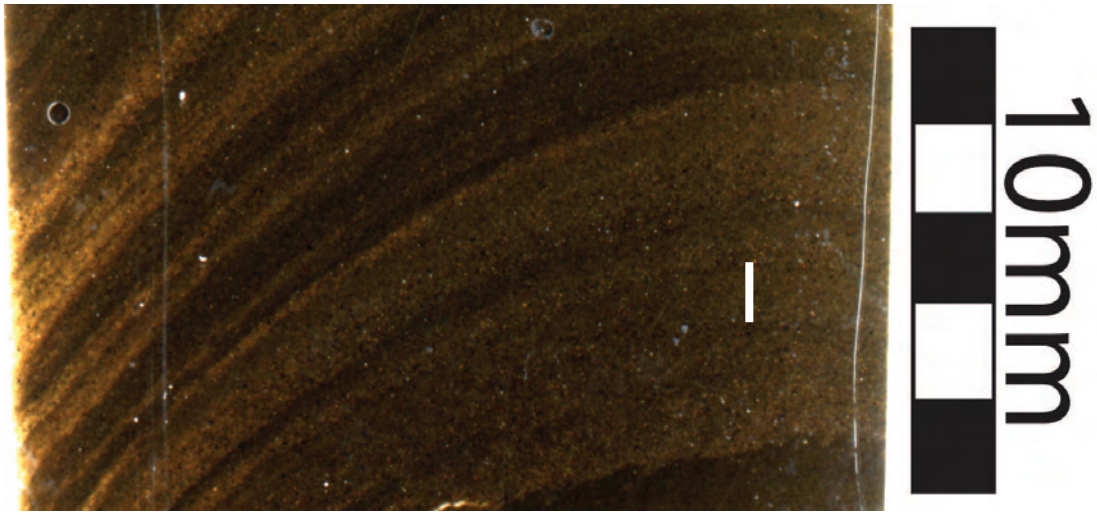

Figure 3.9: Digital scan of a sequence of diffuse varves from core LV06-14 at 9.9-11cm depth (thin section LV06-14B). Note low grain size variability and thin winter layer within one varve year (white line). Image resolution 1600dpi, enlarged with Adobe Illustrator CS2.

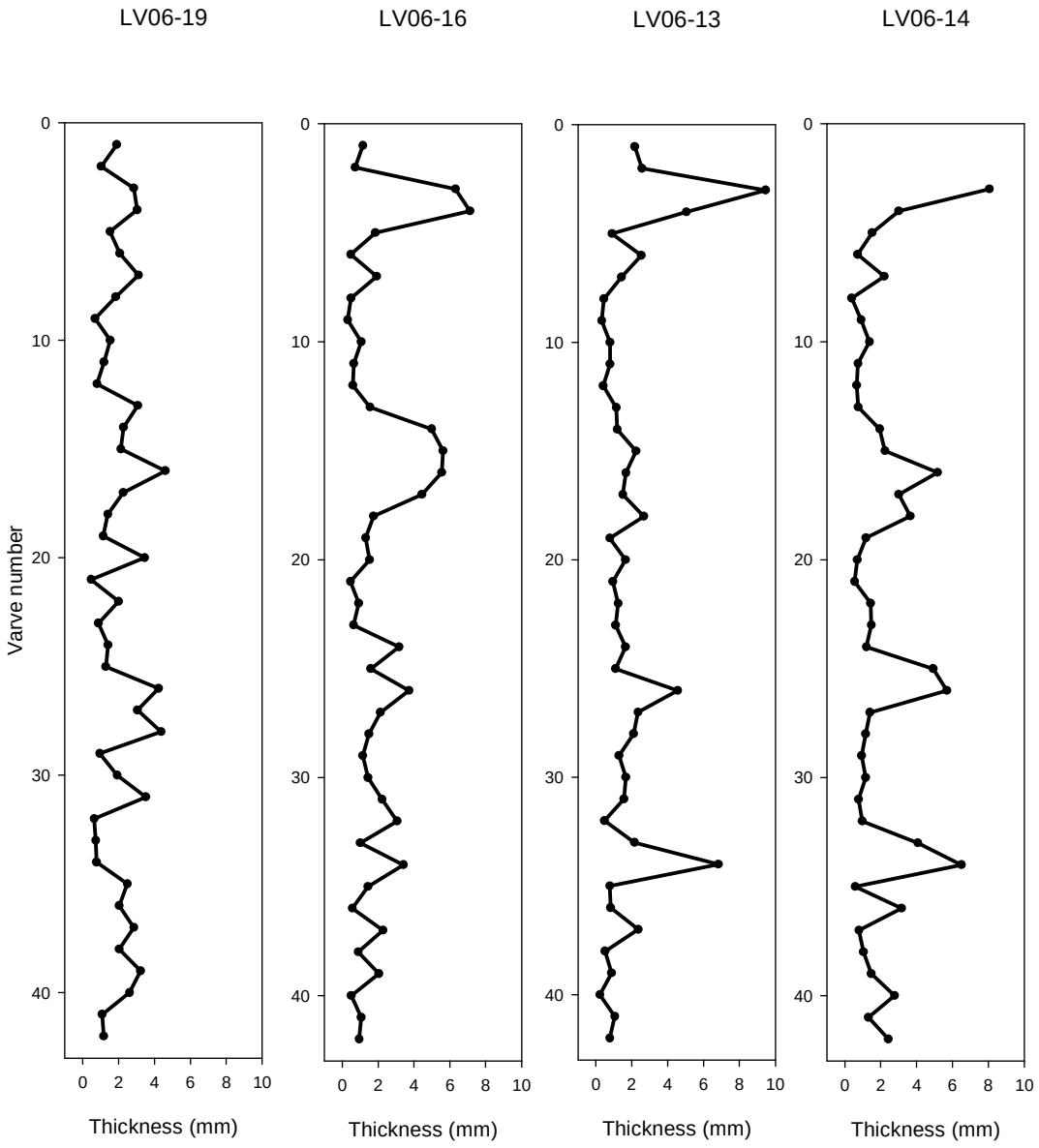

Figure 3.10: Ratio of summer to winter lamination thickness versus varve number.

4. Discussion

Varve Character and Sedimentary Processes

The character of an annual layer of sediment in a lake basin depends primarily on sediment sources and depositional processes. The texture, structure, and composition of varves and intra-annual laminae can be analyzed to understand the conditions under which they were deposited.

Climatic variables

Based on isopach maps of Linnévatnet, the stream Linnéelva that runs between the glacier and the lake transports more sediment to the lake than other sources (Svendsen, 1989). It has been shown that suspended sediment discharge to the lake is closely related to the discharge of Linnéelva on a diurnal scale (Matell, 2006). Discharge rates are closely linked to the climatic factors in the valley. Higher temperatures cause the snow pack and the glacial ice to melt, thereby increasing discharge. The onset of warm temperatures in May or June often creates a high rate of melting of the winter snowpack that greatly increases the intensity of discharge over a short period, the nival freshet (Woo, 1983; Hardy et al., 1996). The intensity of glacial meltwater also increases with higher temperature and insolation (Jansson et al., 2005).

Precipitation increases runoff and suspended sediment discharge. Runoff from the watershed during and after periods of high precipitation can dramatically increase the discharge and the suspended sediment concentration (Lewis et al., 2005). Rain will also increase melting rates on the glacier. Large precipitation events are known to cause debris flows that contribute to readily entrainable sediment and have

been recorded in Longyearbyen (Larsson, 1982). Large precipitation events can cause debris flows that flush large quantities of sediment from where it has previously been deposited and stored along banks or in the mudflats of Linnéelva (Humlum, pers. comm., 2005). In the Canadian Arctic on Lake C2, Lewis et al. (2005) monitored 32% of the season's monitored suspended sediment discharge in a four hour period. Due to the climatic influences on the discharge and suspended sediment concentration of Linnéelva, sediment influx to Linnévatnet is determined to be closely related to short term climate changes.

Depositional interpretations

Varves deposited during different flow regimes will have different characteristics (Smith & Ashley, 1985). Interpretation of depositional mechanism is more accurately determined through cross-core correlation (Hardy et al., 1996). Sediment plumes such as overflows and interflows may produce more widely distributed laminae than underflows that may concentrate the flow of suspended sediment according to bathymetric contours, producing a relatively localized, thicker bed (Smith & Ashley, 1985). Grain size distribution and sorting may also indicate past flow regime. Fining upward sequences may be produced by overflows and interflows due to the relative rates of settling of different grain sizes through the water column. Homogenous layers are more likely to have been deposited quickly during an underflow or turbidite.

The massive laminae, or homogenites (Sturm et al., 1995), of the East Basin are characterized by an unsorted grain size distribution similar in character to surge-

type sediments described by Zolitchska (1996) that are transported by underflows or turbidites triggered by high discharge events or slumps on the delta front. These homogenites occur far enough into the basin to be recorded at the more distal coring site, although thickness decreases rapidly from the inlet. Evidence has not been observed for disruption to underlying laminae. Evidence may include an unconformity where there is an erosional surface. These layers are interpreted to have been deposited by more constant underflows triggered by seasonal changes or high discharge events with more inertia than random slump-triggered turbidites off the delta front. The bathymetry of the East Basin is such that slumps are probably frequent occurrences on the delta front, although it is probably too flat to sustain momentum between Mooring sites C and D. This may explain the homogenous laminae from 17.9mm at proximal LV06-16 to 7.2mm at distal core LV06-14. The underflows must overcome a bathymetric rise as they approach LV06-14. Zolitchska (1996) found that turbidity currents were responsible for transport of large grained sediment to distal environments in cores at a similar distance to the inlet as LV06-14 from the Linnéelva inlet. Although Lake C2 is 80m deep and the East Basin is 15m deep, these underflow currents in Linnévatnet appear to have only enough energy to reach moderately distal sites.

Constructing a Varve Chronology

Varves have been interpreted and correlated across all four core sites in this study. The complexity of intra-annual events recorded in the varves of the East Basin contributes to the high resolution of this chronology. Despite the possibility of higher

inaccuracy in counting these varves, there are multiple methods that make this process significantly more precise. Using a dating method such as the ^{137}Cs to accurately find the age of a particular depth in the core and maintaining the present sediment-water interface of the core top were invaluable in constructing the varve count.

The sediment water interface was determined to be maintained in three out of four cores (LV06-19,16, and 13) due to consistency of the top laminae in thin sections from all three cores. Core LV06-14 was not missing a significant amount of sediment from the core top relative to the other three cores, but the first two varves interpreted from the other three cores were disturbed in the top layers of LV06-14. The first complete varve was interpreted to be 2004 based on the presence of some sediment over the winter clay layer that could represent 2005, and the assumption that the sedimentation that had occurred during 2006 up to the coring date in August was probably lost in transport from the Arctic. The assumption that 2004 is the first complete varve is supported by the visual analysis of the integrity of the core tops when the core was split open. Accordingly, it is judged that an uncertainty of plus or minus two years for the interpreted 2004 varve year is reasonable.

The lamination corresponding to the 1963 ^{137}Cs age found at 18.5cm depth in a core from Mooring site C was visually correlated to the proximal cores LV06-19 and LV06-16 that are approximately equidistant from the inlet (Figure 3.1). The year associated with the increase of this radiotracer may be either 1963 or 1964 (Robbins, 2006) which contributes a small source of error to the varve count, along with the determination of the lamination corresponding to the sample that was tested

(performed by Pratt, 2006). The laminations assigned to year 1963 are considered to have a small uncertainty due to the precision concerning the ^{137}Cs age.

Given the above assumptions that varves for 2004 and 1963 are known within a small uncertainty, it was determined that forty two years of sedimentation should be present in this stratigraphic interval. The complexity of delta proximal cores tended to result in over counting varves, whereas, the indistinct varves in the most distal core resulted in under counting. Visual correlations between proximal and distal cores helped determine the boundaries between years. Taking into account the uncertainty, there may be intra-annual events interpreted as varves or varves interpreted as intra-annual events, though the total number of misrepresented laminae appears to be low. The increased accuracy achieved through varve correlation across multiple cores as has been done in this thesis has been established in Lake C2, Ellesmere in the Canadian Arctic (Hardy et al., 1996; Lamoureux & Bradley, 1996; Zolitchska , 1996). It is unlikely that the varve chronology has significant errors.

Varves and Climate—tentative correlations

The annual layer thicknesses of the varve count from each core correlate well among the other cores (Figure 3.5); where one year of more sedimentation in one core corresponds to a year of high sedimentation in another core. Periods of low varve thickness are also found across all cores with corresponding varve number. The following analysis of the varve thickness variation to the Longyearbyen weather record will use the varve thicknesses of core LV06-13 which was judged to contain

the most representative stratigraphy for the basin based on the above discussion of proximal to distal parameters.

Precipitation

Using the interpreted varve chronology from LV06-13, measured varve thickness was compared to precipitation data from Longyearbyen from 1963 through 2005 (Figure 4.1). June-July-August (JJA) summer precipitation was used for comparison because it is the period of the melt season and most sediment deposition as shown by Motley (2006) and by the summer to winter laminae ratios presented in this study (Figure 3.10). The varve year interpretation was shifted in the positive direction by two years in order to bring the most anomalous varve thicknesses in phase with the summers of anomalous precipitation. This adjustment of the varve count data is justified in small increments such as two years given the uncertainty of the varve count (after Hardy et al., 1996). The years 2004, 1997, 1994, 1989, 1981, 1972, and 1967 have anomalously high mean precipitation (>1 standard deviation from the mean) for the summer months. These years appear to correspond to peaks in the varve thickness results and have been illustrated in Figure 4.1.

Average precipitation by month shows particularly anomalous precipitation events that may occur over a short time span more clearly because they are not muted by the mean over a three month period. Looking at short rain fall events is important in order to explain surge-type deposition such as annual laminae interpreted at varve number 3, 26, and 36 (at LV06-13). Lewis et al. (2005) has shown that during a high discharge event for four hours, caused by high rainfall over two days, can account for

32% of the season's total sediment discharge. Major summer rainfall events have also been recorded in sediments of Nicolay Lake, Canadian High Arctic (Lamoureux et al., 2001). Precipitation induced runoff events are significant contributors to the lamination stratigraphy (Figure 4.2). Using high resolution meteorological data, or discharge data if available, is important for analyzing the complex varve stratigraphy of a proglacial lake.

The year of highest recorded precipitation is 1972, during which there was a record rainfall in Longyearbyen for July that caused significant debris flows and significantly increased suspended sediment discharge in the Longyear valley (Larsson, 1982). This precipitation anomaly can be seen in the mean July precipitation graph. Varve number 36 was found to correspond with this event. The period of low varve thickness between varve number 29 and 34 corresponds to a period of low mean summer precipitation from 1974 to 1979 except for a relatively high precipitation year at 1976. This may be accounted for by the varve count where two interpreted annual laminae may in reality be one thicker unit, or the pulse of sediment during this year was not recorded at the core site. Varve number 31 in the LV06-19 varve stratigraphy may be reflective of the high precipitation during 1976.

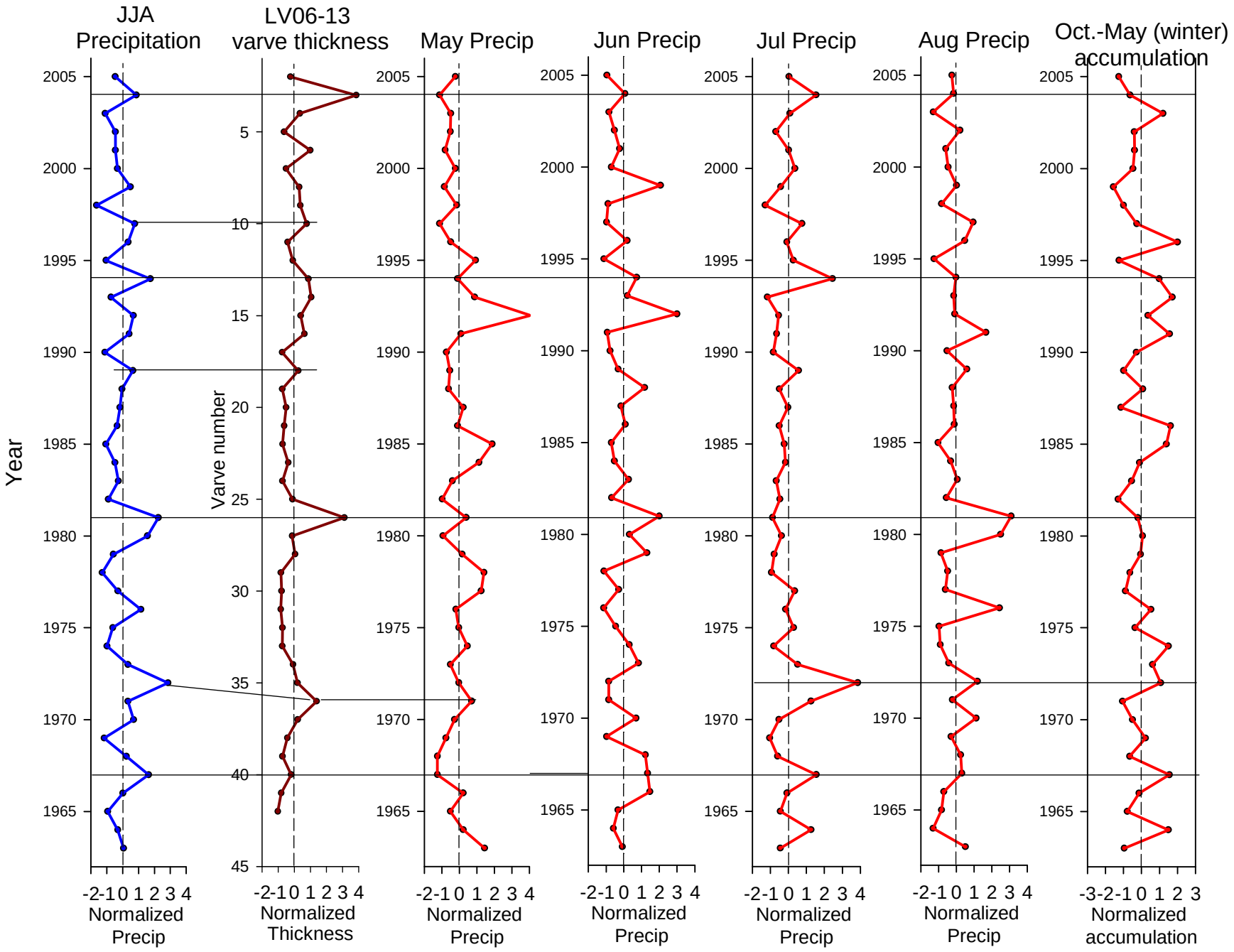

Figure 4.1: Comparison of precipitation and varve thickness plots for the period of the varve count. Varve count has been shifted +2 years to put it in phase with precipitation anomalies. Precipitation and thickness values are normalized, except for the Oct.-May accumulation plot which is the sum of monthy averages from October through May. Plot on the left is June-July-August (JJA) average precipitation. Horizontal lines highlight some corresponding years of thick varves and high precipitation. Weather records provided by Ole Humlum.

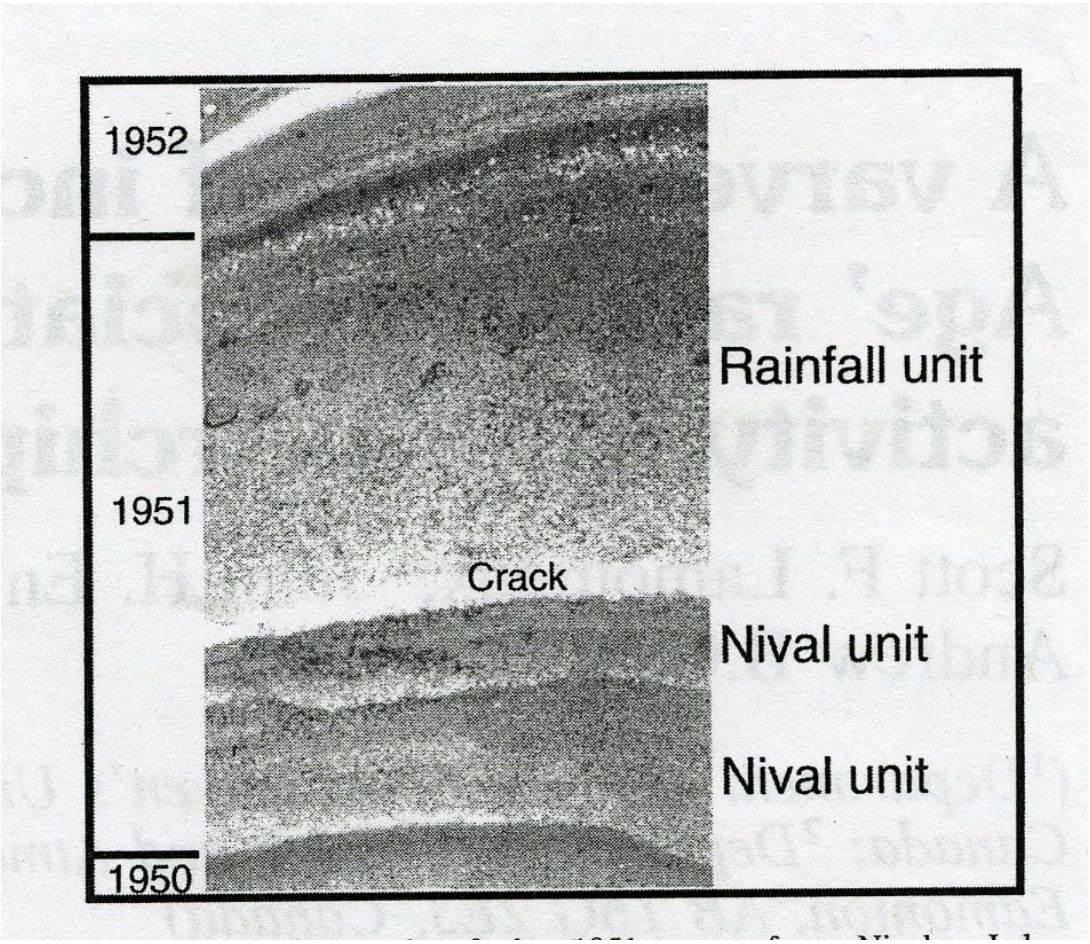

Figure 4.2: Photomicrograph of a varve from Nicolay Lake illustrating the magnitude of deposition by rainfall. The two lower units are interpreted as deposits resulting from periods of snowmelt (from Lamoureux et al., 2001).

Temperature

The average summer temperature graph does not appear to have any clearly corresponding anomalies (Figure 4.3). However, a general trend of increasing summer temperature is apparent as is a general varve thickening over the period of study. Direct correlations were not drawn between the summer temperature and varve thickness plots because the relationship is unclear. Although in some instances high temperature appears to correspond to high sediment thickness, sequences of low varve thickness also correspond to higher temperature.

Statistical Analyses

As a preliminary statistical test, a linear regression was performed between summer precipitation and the varve thickness where the thickness curve was adjusted by two years in order to put the anomalies mentioned above in phase with one another (Figure 4.4a). The result of the regression was weak with r^2=0.18. Although this is a weak correlation, the regression indicates some relationship and is promising for further work that may ultimately discover a stronger correspondence to climatic factors.

Although it can be argued that the anomalously thick varves may not be turbidites deposited independently of weather or lake inflow conditions, those greater than two standard deviations from the mean were removed and replaced with the new mean thickness for each of the cores (Figure 4.5) (modified after Lamoureux & Bradley, 1996). This was done to see whether the non-anomalous record is in agreement with precipitation and temperature records. The varve record was

compared to weather data with anomalies removed because surge-type deposition is not necessarily triggered by high discharge or precipitation events, but can also be caused by non-climatic factors such as a slump triggered by gradual oversteepening of the delta front or by a tectonic disturbance. A regression was performed on this new set of lamination thickness values versus precipitation (Figure 4.4b). No linear correlation was found with the anomalous varves removed, although the two plots have some trends that can be seen visually

The laminae interpreted to be associated with the high 1972 precipitation was included in the second comparison between varve thickness and weather data because it was within two standard deviations of the mean. This lamination has been correlated to the precipitation peak at 1972 (Figure 4.1) despite the varve chronology being slightly out of phase. Likewise, the same series of low lamination thickness has been linked to the generally low precipitation from 1974 to 1978, despite that there does not appear to be a corresponding rise in sediment accumulation with the high 1976 summer precipitation.

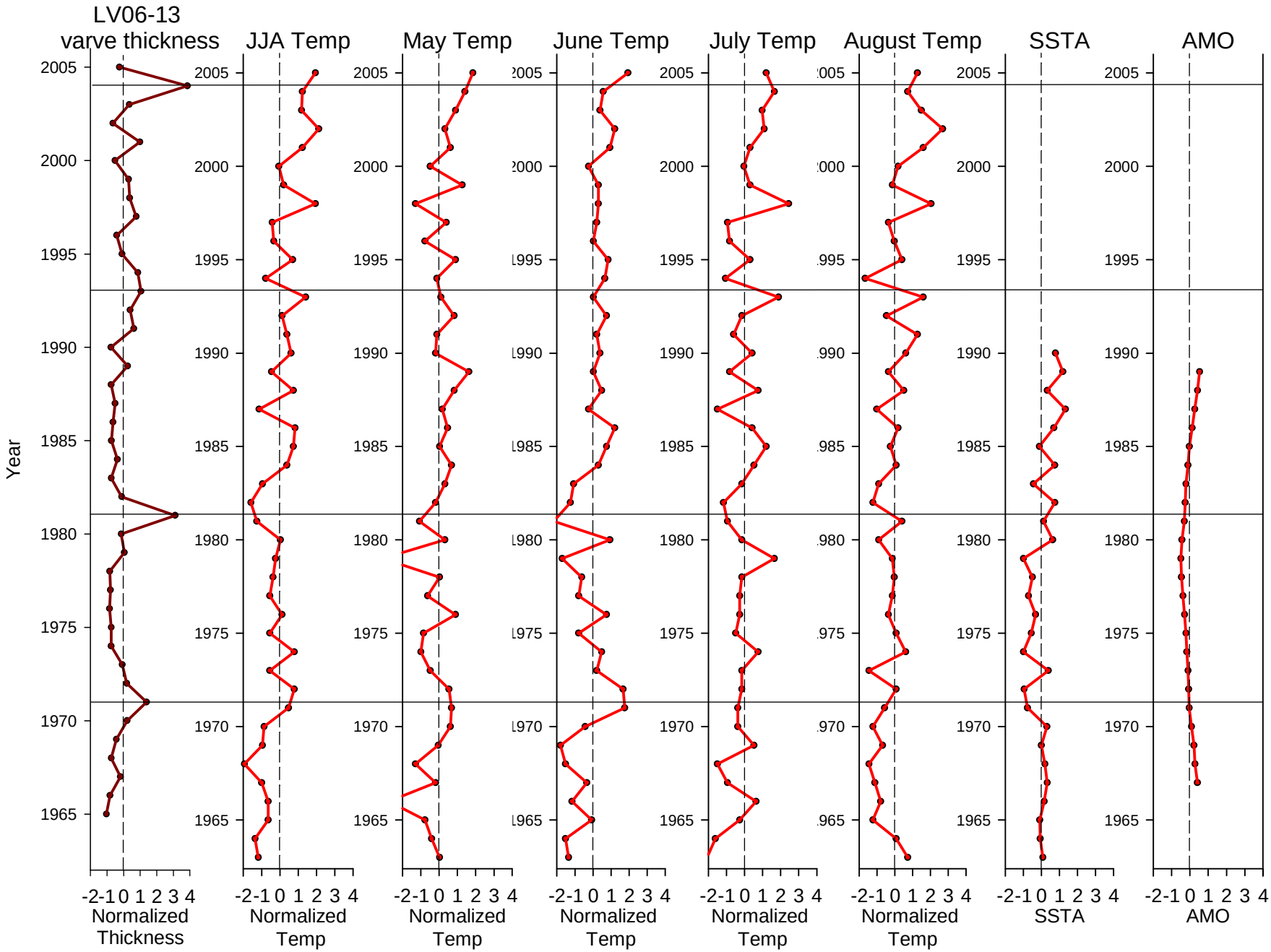

Figure 4.3: Normalized varve thickness compared to Longyearbyen temperature data (courtesy of Ole Humlum). June-July-August (JJA) mean temperature and monthly averages from May though August are noramlized for anomaly comparison. Normalized sea surface temperature anomalies (SSTA), and the Atlantic Multidecadal Oscillation(AMO) calculated for a ten year running mean from annual SSTA (data from Gray et al., 2004).

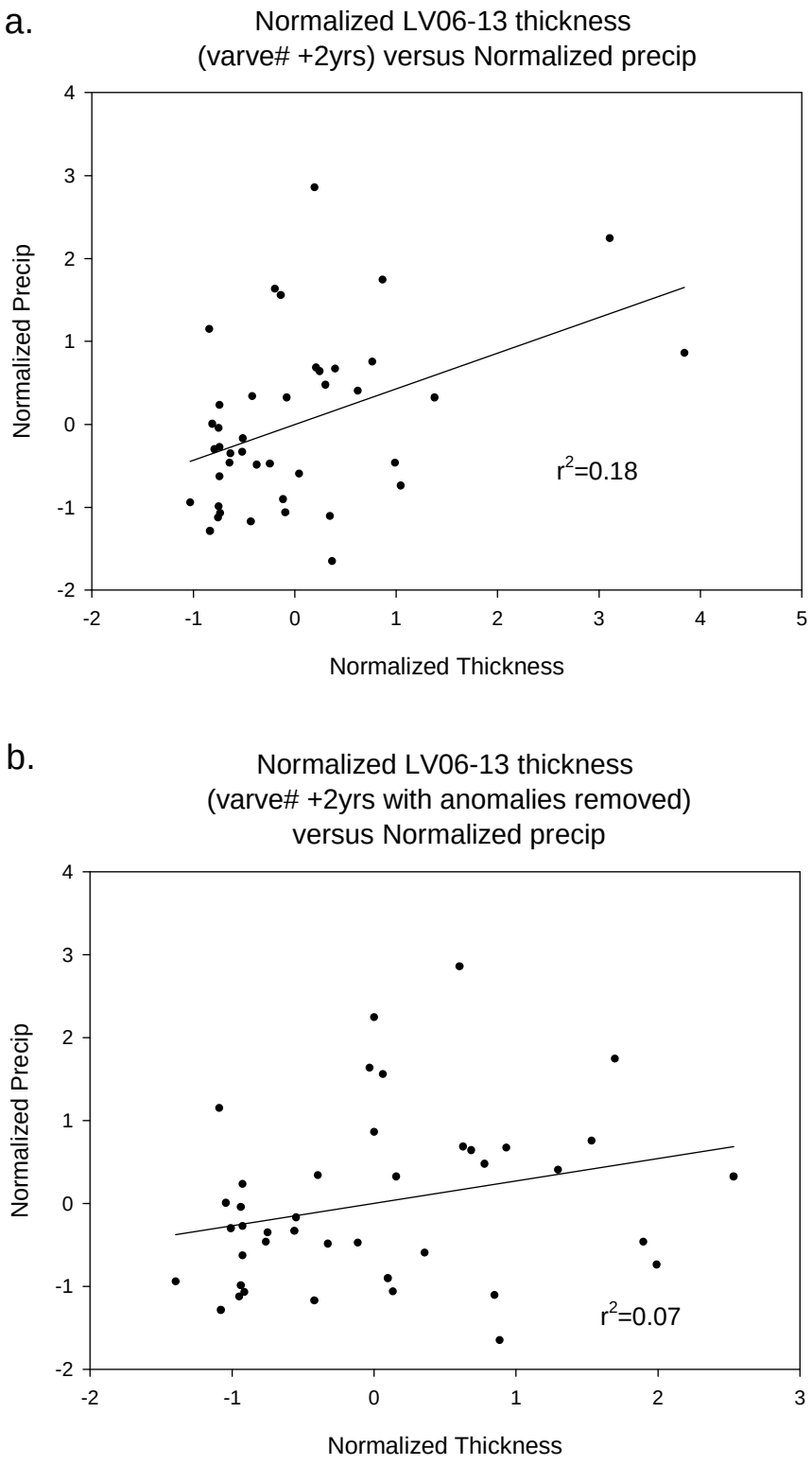

Figure 4.4: Linear regression between June-July-August (JJA) precipitation and thickness. (a.) is varve thickness including anomalies, while (b.) has anomalies removed. Both include varve thickness shifted in phase by plus two years.

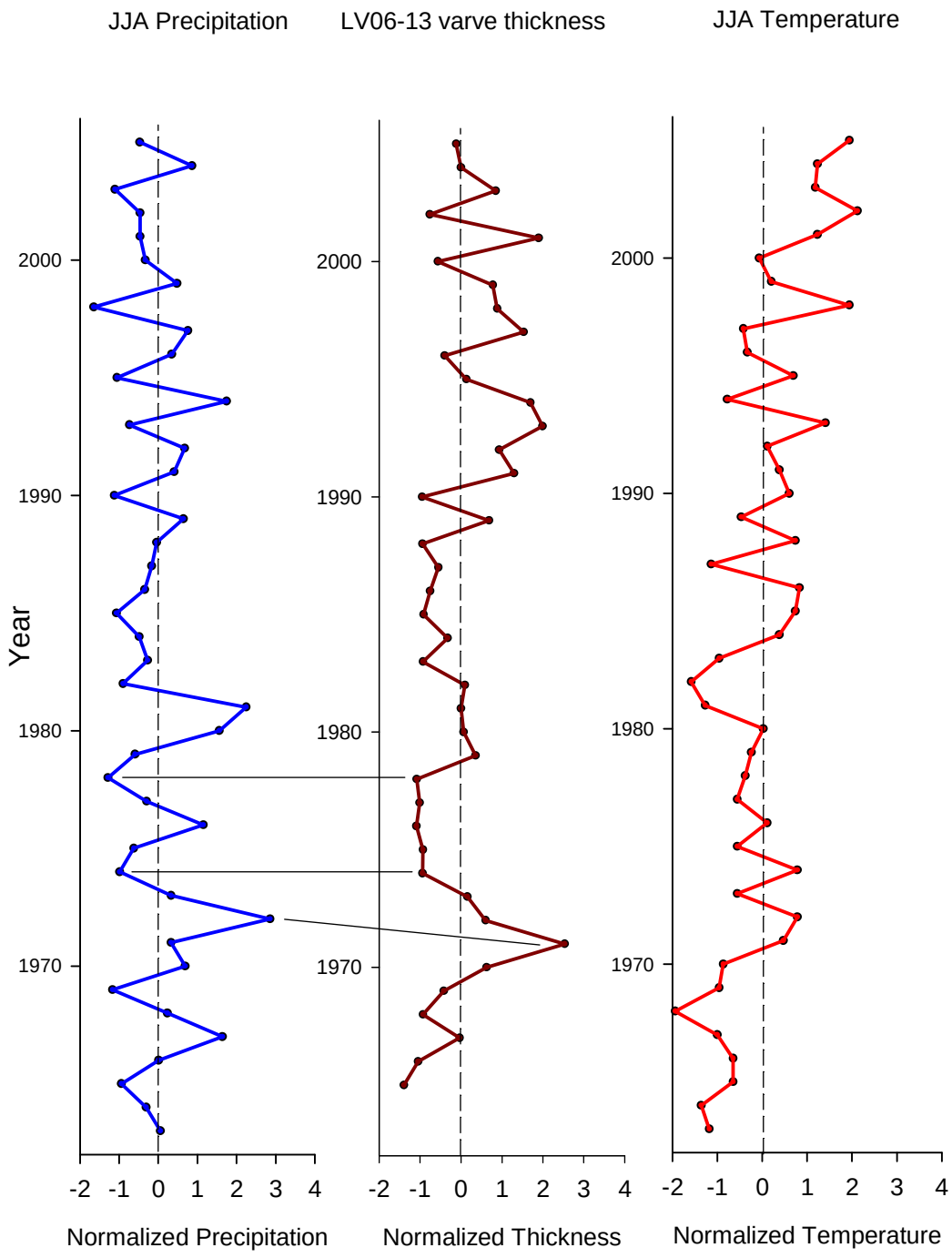

Figure 4.5: Varve thickness compared to June-July-August (JJA) precipitation and temperature with anomalies greater than 2 standard deviations from the mean removed. Normalized thickness is based on the average and standard deviation of the data set after anomalies were removed.

Analysis of correlations

There are numerous directions upon which to embark to analyze the relationship between the variables that control the sedimentation character of Linnévatnet and the varve stratigraphy. The following discussion includes a series of offshoots to examine the presented varve structure variability and preliminary comparison to weather records.

The climatological signal in the varve chronology is particularly complex in Linnévatnet and may be due to its glacial and nival fed character as well as its location by the sea. The west coast of Svalbard receives more precipitation in comparison with the regions around other high arctic lakes where clastic varve analyses have been correlated to arctic climate (Hardy et al., 1996; Retelle & Child, 1996; Lamoureux et al., 2001). This geographic factor may make the signal further complicated because the lake is not only glacial and nival fed, but receives a strong precipitation driven discharge as well.

Sediment transport driven by precipitation runoff, the nival melt, or melting of the glacier may all occur at different magnitudes which also may change in relationship to one another from year to year. Fluctuations in sediment transport are caused by changes in discharge on a diurnal scale due to higher daily temperatures causing more melting. The large volumes of sediment that can be transported in a short time span stresses the importance of frequent monitoring intervals as well as the importance to look at high resolution weather data.

Correlation to monthly average temperature and precipitation curves may be inconclusive if anomalous events are muted through the average. The daily records of temperature and precipitation are available and their analysis is a next possible approach to looking for a correlation.

Air temperature that controls glacial melting does not appear to have a close relationship to varve thickness. The extent of glaciation within the catchment must be relatively large for temperature to have a significant impact on the varve record (Leeman & Niessen, 1994). In Linnédalen, 6% of the catchment is glaciated whereas Leeman & Niessen (1994) suggest that 30% of the catchment should be glaciated for the varve record to be dominated by temperature related fluctuations in discharge.

The varve thickness may not correlate accurately to any one curve of temperature or precipitation, but anomalous events from the past forty years can be identified to explain thicker units. A multiple variable comparison may also be necessary.

Future progress

In future studies, it will be important to differentiate the varve structures as this study has done. When extending the varve count beyond the period of instrumental data, the thick homogenous units as well as regular variation should be interpreted together. A running average of varve thickness may even out the variability and improve comparison of longer term trends. One problem that is faced is that as one goes back in time, the environment under which the varves formed may have been different and the sediment sources may have changed.

Ultimately, the largest source of sediment for Linnévatnet is the glacier, Linnébreen. As the glacier retreats, as it has in the last seventy years, more sediment is released from the ice or exposed from its base and made available to erosion. Much of this sediment is washed into Linnévatnet, although large quantities of sediment are also deposited along the streambed and in a long mudflat between the glacier and the lake. Through the Holocene and Little Ice Age, glacial conditions have changed, thus altering the sedimentary processes through time (Svendsen & Mangerud, 1990; Werner, 1993; Mangerud & Svendsen, 1996; Snyder et al., 2000).

The Svalbard climate and thus the Linnévatnet varve stratigraphy may be particularly sensitive to changes in the sea surface temperature, or the patterns of the North Atlantic Drift. Gray et al. (2004) have demonstrated that sea surface temperatures have been consistent features of North Atlantic climate for the past five centuries. By reconstructing sea surface temperature, they created the Atlantic Multidecadal Oscillation (AMO) that shows a low frequency (60-100yr) cycle of sea surface temperature anomalies (SSTA). The AMO and SSTA contribute to a regional approach in understanding Svalbard's past climate. AMO and SSTA were plotted in Figure 4.3 in order to begin a comparison to other regional, low frequency climate approximations to the Linnévatnet varve record.

In future studies, a high resolution climate record could be produced once there is more data from monitoring modern processes, which depends heavily on performing fieldwork for the duration of the season from the nival freshet to the freezing of the lake. Once further years of monitoring are done in Linnédalen, upper varve stratigraphy may be compared to suspended sediment discharge from Linnéelva

and then also compared to sediment trap results to gauge how the sediment traps have predicted laminae deposition. This may be hindered by the lack of season-long monitoring from nival freshet to onset of winter as has been done at some stations in the Canadian Arctic (Bradley, 1996).

5. Conclusions

Conclusions

This thesis presented a well defined varve chronology from proglacial lake Linnévatnet from 1963 through 2004 using basin-wide correlations between a well constrained ^{137}Cs age and the core surface. Varve structures were identified and a detailed interpretation of depositional processes was discussed. Preliminary comparisons were made of the varve stratigraphy to instrumental weather records from Longyearbyen.

Lake inflow and mixing characteristics can vary significantly in the East Basin. Laminae were found to decrease in thickness with greater distance from the inlet and to change structure from proximal to distal sites. Annual laminae from proximal core sites were found to be primarily complex varves with multiple intra-annual laminae. Variation within complex varves often included overflow-interflow deposits as well as surge-type homogenites. Homogenites were interpreted to be deposited by continual underflow currents possibly caused by climatic or seasonal factors of weather or lake inflow conditions. No evidence was found for scouring of previously deposited laminae.

Distal cores contained more simple varve couplets and diffuse varves. Homogenite thickness decreased distally indicating that the underflows had less energy and transported less sediment farther from the inlet.

Tentative correlations with precipitation and temperature showed that the sedimentary processes are a complex system in Linnévatnet. High summer rainfall averages were found to correlate with many anomalously high varve thicknesses,

while periods of low precipitation correlated with low varve thickness. No clear relationships were found between varve thickness and temperature variations between 1963 and 2004. Although temperature controlled diurnal fluctuations of suspended sediment discharge have been monitored from Linnébreen, temperature was determined to be a minor factor in varve formation. Major factors of varve formation were interpreted to be the nival freshet and high summer precipitation. Care must be taken in using long term averages that may mute anomalous precipitation events that drive high discharge and sedimentation.

In order for future studies to extend an interpretation of past climatic conditions of Linnédalen to pre-instrumental laminae sedimentation, a closer relationship will be needed between the instrumental record and varve variation. The varve chronology of Linnévatnet has potential for interpreting late Holocene precipitation conditions on the west coast of Svalbard.

References

ACIA, 2004. Impacts of a Warming Arctic. Cambridge University Press: New York, NY. ed. S. J. Hassol. pp 139.

Bradley, R. S., M. J. Retelle, S.D. Ludlam, D. R. Hardy, B. Zolitchska, S. F. Lamoureux, & M. S. V. Douglas, 1996. The Taconite Inlet Project: a systems approach to paleoclimatic reconstruction. J. Paleolimnol. 16: 97-110.

DeGeer, G., 1912. A geochronologyof the last 12 000 years. Compte Rendu XI Session du Congres Geologique International, Stockholm 1910: 241-257.

Elverhøi, A., J. A. Dowdeswell, S. Funder, J. Mangerud, & R. Stein, 1998. Glacial and oceanic history of the polar North Atlantic margins: an overview. Quaternary Science Reviews. 17: 1-10.

Forman, S.L., D. H. Mann, &G. H. Miller, 1987. Late Weichselian and Holocene relative sea-level history of Broggerhalvoya, Spitsbergen. Quaternary Research. 27: 41-50.

Gray, S. T., L. J. Graumlich, J. L. Betancourt, & G. D. Pederson, 2004. A tree-ring based reconstruction of the Atlantic Multidecadal Oscillationsince 1567 A.D. Geophysical Research Letters, 31:L12205, doi:10.1029/2004GL019932.

Hardy, D. R., R. S. Bradley, B. Zolitchska, 1996. The climatic signal in varved sediments from Lake C2, northern Ellesmere Island, Canada. J. Paleolimnol. 16: 227-238.

Hjelle, A., Ø. Lauritzen, O. Salvegsen, T. S. Winsnes, 1986. Geological map. Svalbard 1:100,000. Sheet B10G Van Mijenfjorden. Nor. Polarinst. Temakart No. 2.

Humlum, O., 2002. Modelling late 20th-century precipitation in Nordenskiöld Land, Svalbard, by geomorphic means. Norwegian Journal of Geography. 56: 96-103.

Humlum, O. 2005. personal communication. University Centre on Svalbard.

Humlum, O. 2006. unpublished data. University Centre on Svalbard.

Ingólfsson, O., 2006. Outline of the Physical Geography and Geology of Svalbard. p. 10.

Jansen, E., Bleil, U., Heinrich, R., Kriststad, R., and Slettemark, B., 1987, Climatic changes in the Norwegian Sea during the last 2.8 Ma. Polar Research. 5: 329-332.

Jansson, P., G. Rosqvist, T. Schneider, 2005. Glacier fluctuations, suspended sediment flux and glacio-lacustrine sediments: Geografiska Annaler.Series A, Physical Geography, v. 87, p. 37-50.

Labconco®, 1998. A Guide to Freeze Drying for the Laboratory. Kansas City, MI.

Lamoureux, S.F., 1994. Embedding unfrozen lake sediments for thin section preparation. J. Paleolimnol. 10: 141-146.

Lamoureux, S. F., R. S. Bradley, 1996. A late Holocene varved sediment record of environmental change from northern Ellesmere Island, Canada. J. Paleolimnol. 16: 239-255.

Lamoureux, S.F., 1999. Catchment and lake controls over the formation of varves in monomictic Nicolay Lake, Cornwall Island, Nunavut. Canadian Journal of Earth Sciences = Revue Canadienne Des Sciences De La Terre 36: 1533-1546.

Lamoureux, S.F., J. H. England, M. J. Sharp, & A. B. J. Bush, 2001. A varve record of increased 'Little Ice Age' rainfall associated with volcanic activity, Arctic Archipelago, Canada. The Holocene 11: 243-249.

Larsson, S., 1982. Geomorphological Effects on the Slopes of Longyear Valley, Spitsbergen, After a Heavy Rainstorm in July 1972. Geografiska Annaler. 64 A: 105-125.

Leemann, A. & F. Niessen, 1994. Varve formation and the climatic record in an alpine proglacial lake; calibrating annually-laminated sediments against hydrological and meteorological data. The Holocene 4: 1-8.

Lewis, T., R. Gilbert, & S. F. Lamoureux, 2002. Spatial and Temporal Changes in Sedimentary Processes at Proglacial Bear Lake, Devon Island, Nunavut, Canada. Arctic, Antarctic, and Alpine Research 34: 119-129.

Lewis, T., C. Braun, D. R. Hardy, P. Francus, & R. Bradley, 2005. An Extreme Sediment Transfer Event in a Canadian High Arctic Stream. Arctic, Antartic, and Alpine Research. 37: 477-482.

Lotter, A.F., and Lemcke, G., 1999. Methods for preparing and counting biochemical varves: Boreas 28: 243-252.

Mangerud, J., J. I. Svendsen, 1990. Deglaciation chronology inferred from marine sediments in a proglacial lake basin, western Spitsbergen, Svalbard. Boreas 19: 249-272.

Mangerud, J., T. Dokken, D. Hebbeln, B. Heggen, Ó. Ingólfsson, J. Landvik, V. Mejdahl, J. I. Svendsen, T. O. Vorren, 1998. Fluctuations of the Svalbard-Barents sea ice sheet during the last 150000 years. Quaternary Science Reviews 17: 11-42.

Matell, N., 2006. unpublished BA thesis.

Motley, J. B., 2006. Sedimentation in Linnévatnet, Svalbard, during 2004-2005: a modern process study using sediment traps. [unpublished BS thesis]: Bates College, Lewiston, ME.

Overpeck, J., K. A. Hughen, D. Hardy, R. Bradley, R. Case, M. Douglas, B. Finney, K. Gajewski, G. Jacoby, A. Jennings, S. Lamoureux, A. Lasca, G. MacDonald, J. Moore, M. Retelle, S. Smith, A. Wolfe, & G. Zielinski, 1997. Arctic environmental change of the last four centuries: Science. 278: 1251-1256.

Pratt, E., 2006. Characterization and Calibration of Lamination Stratigraphy of Cores Recovered from Lake Linné, Svalbard, Norway. [unpublished BA degree]: Mt. Holyoke College, South Hadley, MA.

Retelle, M.J. & J.K. Child, 1996. Suspended sediment transport and deposition in a high arctic meromictic lake; Taconite Inlet Lakes Project: Journal of Paleolimnology, v. 16, p. 151-167.

Robbins, J., 2006. Environmental Radiotracers. National Oceanic and Atmospheric Association, Great Lakes Environmental Research Laboratory. URL: http://www.glerl.noaa.gov/res/Task_rpts/1980/bgrobbins08-1.html.

Saarnisto, M., 1986. Annually laminated lake sediments. Handbook of Holocene Palaeoecology and Palaeohydrology. John Wiley & Sons Ltd. ed. B. E. Berglund.

Shacketon, N. J., J. Backman, H. Zimmerman, D. V. Kent, M. A. Hall, D. G. Roberts, D. Schitker, J. G. Baldauf, A. Desprairies, R. Homrighausen, P. Huddlestun, J. B. Keene, A. J. Kaltenback, K. A. O. Krumsiek, A. C. Morton, J. W. Murray & J.

Westberg-Smith, 1984. Oxygen isotope calibration of the onset of ice-rafting and history of glaciation of the North Atlantic region. Nature 307: 620-623.

Smith, N. D., G. Ashley, 1985. Proglacial lacustrine environments. Ch. 4, in Glacial Sedimentary Environments, eds. G. Ashley., J. Shaw, & N. D. Smith; S.E.P.M. short course no. 16, p. 135-215.

Snyder, J. A., A. Werner, G. H. Miller, 2000. Holocene cirque glacier activity in western Spitsbergen, Svalbard: sediment records from proglacial Linnévatnet. The Holocene 10,5:555-563.

Sturm, M.M., 1979. Origin and composition of clastic varves. in Schluster, A. (ed.), Moraines and varves, Rotterdam, A. A. Balkema, p. 281-285.

Sturm, M., C. Siegentahler & R. A. Pickrill, 1995. Turbidites and 'homogenites'. A conceptual model of flood and slide deposits. Publ. IAS – 16th Regional Meeting Sedimentology, Paris 22: 140.

Svendsen, J.I., J. Mangerud, G. H. Miller, 1989. Denudation rates in the Arctic estimated from lake sediments on Spitsbergen, Svalbard: Palaeogeography, Palaeoclimatology, Palaeoecology 76: 153-168.

Svendsen, J.I., & J. Mangerud, 1997. Holocene glacial and climatic variations on Spitsbergen, Svalbard. The Holocene 7: 45-57.

Solheim, A., L. Russwurm, A. Elverhøi, & M. N. Berg, 1990. Glacial geomorphic features in the northern Barents Sea: direct evidence for grounded ice and implications for the pattern of deglaciation and late glacial sedimentation, *in* Dowdeswell, J. A. and Scourse, J. D., ed., Glacimarine environments: processes and sediments: Geological Society Special Publication, p. 253-268.

Werner, A., 1993. Holocene moraine chronology, Spitsbergen, Svalbard: lichenometric evidence for multiple Neoglacial advances in the Arctic. The Holocene. 3: 128-137.

Woo, M. K., 1983. Hydrology of a drainage basin in the Canadian High Arctic. Annals—Association of American Geographers 73: 577-596.

Zolitchska, B., 1996. Recent sedimentation in a high arctic lake, northern Ellesmere Island, Canada. J. Paleolimnol. 16: 169-186.

7. Appendices

Appendix A: Bulk Density Data. Wet and dry mass are equal to the density due to the 1cm^3 sampling volume. Not all digits are significant.

Sample number	Core #	Depth in core (cm)	Crucible mass (g)	Wet sed + crucible mass (g)	Dried sed + crucible mass (g)	Wet mass (g)	Dry mass (g)
1	LV06-19	1	18.6398	20.536	20.1108	1.8962	1.471
2	LV06-19	2	20.7876	22.7708	22.3309	1.9832	1.5433
3	LV06-19	3	20.7831	22.6788	22.2773	1.8957	1.4942
4	LV06-19	4	19.1501	21.0326	20.6168	1.8825	1.4667
5	LV06-19	5	21.2775	23.1021	22.6706	1.8246	1.3931
6	LV06-19	6	17.8402	19.7953	19.3451	1.9551	1.5049
7	LV06-19	7	19.85	21.7221	21.2863	1.8721	1.4363
8	LV06-19	8	20.2646	22.1093	21.6772	1.8447	1.4126
9	LV06-19	9	20.6996	22.6385	22.1812	1.9389	1.4816
10	LV06-19	10	18.5393	20.4152	19.9901	1.8759	1.4508
11	LV06-19	11	17.9748	19.8521	19.4392	1.8773	1.4644
12	LV06-19	12	16.6315	18.5013	18.0622	1.8698	1.4307
13	LV06-19	13	17.8219	19.7725	19.3311	1.9506	1.5092
14	LV06-19	14	21.5212	23.4148	22.965	1.8936	1.4438
15	LV06-19	15	21.3523	23.2666	22.799	1.9143	1.4467
16	LV06-19	16	19.2031	21.0542	20.6151	1.8511	1.412
17	LV06-19	17	18.7704	20.6329	20.1909	1.8625	1.4205
18	LV06-19	18	18.7731	20.6763	20.2162	1.9032	1.4431
19	LV06-19	19	15.2234	17.1322	16.697	1.9088	1.4736
20	LV06-19	20	20.4142	22.355	21.9087	1.9408	1.4945
21	LV06-19	21	18.1313	19.9958	19.5726	1.8645	1.4413
22	LV06-19	22	16.2011	18.1432	17.7258	1.9421	1.5247

Sample number	Core #	Depth in core (cm)	Crucible mass (g)	Wet sed + crucible mass (g)	Dried sed + crucible mass (g)	Wet mass (g)	Dry mass (g)
23	LV06-19	23	17.897	19.8188	19.377	1.9218	1.48
24	LV06-19	24	17.2441	19.1471	18.6992	1.903	1.4551
25	LV06-19	25	18.6573	20.5678	20.1162	1.9105	1.4589
26	LV06-19	26	18.3822	20.2914	19.8567	1.9092	1.4745
27	LV06-19	27	20.7456	22.6276	22.1963	1.882	1.4507
28	LV06-19	28	20.9549	22.8919	22.4674	1.937	1.5125
29	LV06-16	1	20.7411	22.6345	22.2084	1.8934	1.4673
30	LV06-16	2	18.5351	20.4762	20.0478	1.9411	1.5127
31	LV06-16	3	15.5777	17.535	17.1182	1.9573	1.5405
32	LV06-16	4	17.9041	19.8599	19.4273	1.9558	1.5232
33	LV06-16	5	21.1633	23.1023	22.7007	1.939	1.5374
34	LV06-16	6	19.6166	21.5494	21.0744	1.9328	1.4578
35	LV06-16	7	14.8026	16.7056	16.2377	1.903	1.4351
36	LV06-16	8	17.5534	19.514	19.0489	1.9606	1.4955
37	LV06-16	9	18.6728	20.618	20.1864	1.9452	1.5136
38	LV06-16	10	20.7247	22.6065	22.1679	1.8818	1.4432
39	LV06-16	11	20.5348	22.4457	22.0105	1.9109	1.4757
40	LV06-16	12	18.1638	19.9373	19.491	1.7735	1.3272
41	LV06-16	13	21.2294	23.1634	22.7057	1.934	1.4763
42	LV06-16	14	17.5403	19.4338	19.0199	1.8935	1.4796
43	LV06-16	15	15.7957	17.7068	17.2679	1.9111	1.4722
44	LV06-16	16	16.4234	18.3853	17.93	1.9619	1.5066
45	LV06-16	17	19.5597	21.4697	21.0458	1.91	1.4861
46	LV06-16	18	16.2296	18.047	17.6279	1.8174	1.3983
47	LV06-16	19	18.196	20.071	19.6287	1.875	1.4327

Sample number	Core #	Depth in core (cm)	Crucible mass (g)	Wet sed + crucible mass (g)	Dried sed + crucible mass (g)	Wet mass (g)	Dry mass (g)
48	LV06-16	20	18.2564	20.1772	19.727	1.9208	1.4706
49	LV06-16	21	21.8628	23.7815	23.3438	1.9187	1.481
50	LV06-16	22	19.9984	21.9276	21.4872	1.9292	1.4888
51	LV06-16	23	18.7547	20.6955	20.2583	1.9408	1.5036
52	LV06-13	1	17.7187	19.6154	19.1483	1.8967	1.4296
53	LV06-13	2	15.859	17.7677	17.3272	1.9087	1.4682
54	LV06-13	3	18.6415	20.6111	20.1563	1.9696	1.5148
55	LV06-13	4	19.2263	21.1343	20.6925	1.908	1.4662
56	LV06-13	5	19.7615	21.5964	21.13	1.8349	1.3685
57	LV06-13	6	18.5753	20.3858	19.9315	1.8105	1.3562
58	LV06-13	7	15.9262	17.871	17.3888	1.9448	1.4626
59	LV06-13	8	20.8137	22.6733	22.2188	1.8596	1.4051
60	LV06-13	9	17.4311	19.3488	18.8899	1.9177	1.4588
61	LV06-13	10	18.4135	20.3561	19.8589	1.9426	1.4454
62	LV06-13	11	18.684	20.5816	20.1494	1.8976	1.4654
63	LV06-13	12	17.1939	19.0466	18.6347	1.8527	1.4408
64	LV06-13	13	19.0748	21.0187	20.5517	1.9439	1.4769
65	LV06-13	14	16.8721	18.6876	18.284	1.8155	1.4119
66	LV06-13	15	20.139	22.0952	21.6201	1.9562	1.4811
67	LV06-13	16	18.5779	20.4064	19.9648	1.8285	1.3869
68	LV06-13	17	19.9378	21.8314	21.3708	1.8936	1.433
69	LV06-13	18	20.809	22.7617	22.3066	1.9527	1.4976
70	LV06-13	19	18.5206	20.3202	19.8873	1.7996	1.3667
71	LV06-13	20	18.6524	20.4689	20.0437	1.8165	1.3913
72	LV06-14	1	18.8954	20.846	20.3228	1.9506	1.4274

Sample number	Core #	Depth in core (cm)	Crucible mass (g)	Wet sed + crucible mass (g)	Dried sed + crucible mass (g)	Wet mass (g)	Dry mass (g)
73	LV06-14	2	20.2989	22.159	21.6886	1.8601	1.3897
74	LV06-14	3	20.1963	22.0374	21.5637	1.8411	1.3674
75	LV06-14	4	19.9535	21.8409	21.3649	1.8874	1.4114
76	LV06-14	5	18.7418	20.5858	20.0993	1.844	1.3575
77	LV06-14	6	21.7398	23.6941	23.2065	1.9543	1.4667
78	LV06-14	7	20.9521	22.7508	22.2609	1.7987	1.3088
79	LV06-14	8	18.4098	20.2634	19.7952	1.8536	1.3854
80	LV06-14	9	17.7853	19.6405	19.1736	1.8552	1.3883
81	LV06-14	10	16.111	18.0038	17.5196	1.8928	1.4086
82	LV06-14	11	16.5104	18.4076	17.9218	1.8972	1.4114
83	LV06-14	12	18.2377	20.1536	19.6684	1.9159	1.4307
84	LV06-14	13	21.2927	23.1649	22.7057	1.8722	1.413
85	LV06-14	14	18.8931	20.6773	20.2229	1.7842	1.3298
86	LV06-14	15	18.7234	20.7016	20.227	1.9782	1.5036
87	LV06-14	16	19.1975	21.0692	20.6147	1.8717	1.4172
88	LV06-14	17	18.1559	20.0242	19.5849	1.8683	1.429
89	LV06-14	18	18.3423	20.2344	19.7657	1.8921	1.4234
90	LV06-14	19	18.9722	20.9158	20.4352	1.9436	1.463
91	LV06-14	20	20.9553	22.756	22.3264	1.8007	1.3711
92	LV06-14	21	20.4628	22.4228	21.9503	1.96	1.4875
93	LV06-14	22	20.71	22.4974	22.0469	1.7874	1.3369
94	LV06-14	23	17.823	19.7166	19.2434	1.8936	1.4204

Appendix B: Lamination thickness measurements.

1. Thickness was measured using Sigma Scan Pro 5 software.
2. Season designates whether a laminae was interpreted as a summer or winter layer.
3. Year is the interpreted year of deposition (see text), although varve number can be counted down from the top of the core beginning with 1.
4. Couplet thickness is the thickness used for the annual layer or varve and is calculated by adding the summer and winter layer thicknesses for corresponding years.
5. Ratio of summer to winter thickness was calculated by dividing the thickness of the summer lamination by that of the winter lamination.
6. See text for how to calculate Normalized thickness.
7. Cumulative thickness adds the thickness of each varve downcore to those preceding it.
8. Averages are placed below the column for Couplet thickness.

Core	Thickness (mm)	Season	Year	Couplet thickness (w+s) (mm)	Ratio of Summer to Winter thickness	Normalized annual thickness	Cumulative thickness (mm)
LV06-19	2.04	s	2004	3.12	1.90	-0.60	3.12
LV06-19	2.76	s	2003	5.44	1.03	0.37	8.56
LV06-19	9.91	s	2002	13.40	2.84	3.71	21.95
LV06-19	3.02	s	2001	4.02	3.03	-0.22	25.97
LV06-19	1.28	s	2000	2.12	1.52	-1.01	28.09
LV06-19	3.57	s	1999	5.30	2.06	0.32	33.38
LV06-19	2.80	s	1998	3.71	3.10	-0.35	37.09
LV06-19	2.65	s	1997	4.08	1.85	-0.19	41.17
LV06-19	1.20	s	1996	2.94	0.69	-0.67	44.12
LV06-19	2.29	s	1995	3.78	1.53	-0.32	47.90
LV06-19	1.70	s	1994	3.13	1.18	-0.59	51.03
LV06-19	1.04	s	1993	2.35	0.80	-0.92	53.38
LV06-19	4.83	s	1992	6.40	3.07	0.78	59.79
LV06-19	2.73	s	1991	3.93	2.27	-0.26	63.71
LV06-19	2.65	s	1990	3.89	2.13	-0.27	67.61
LV06-19	5.87	s	1989	7.15	4.60	1.09	74.75
LV06-19	1.90	s	1988	2.74	2.26	-0.75	77.50

Core	Thickness (mm)	Season	Year	Couplet thickness (w+s) (mm)	Ratio of Summer to Winter thickness	Normalized annual thickness	Cumulative thickness (mm)
LV06-19	1.87	s	1987	3.21	1.40	-0.56	80.70
LV06-19	1.15	s	1986	2.17	1.14	-0.99	82.87
LV06-19	3.82	s	1985	4.92	3.45	0.16	87.79
LV06-19	1.34	s	1984	4.19	0.47	-0.15	91.98
LV06-19	3.36	s	1983	5.05	2.00	0.21	97.03
LV06-19	1.04	s	1982	2.24	0.87	-0.96	99.27
LV06-19	1.65	s	1981	2.82	1.41	-0.72	102.09
LV06-19	1.64	s	1980	2.91	1.28	-0.68	105.00
LV06-19	9.02	s	1979	11.15	4.23	2.77	116.16
LV06-19	1.99	s	1978	2.65	3.05	-0.79	118.80
LV06-19	3.27	s	1977	4.02	4.37	-0.22	122.82
LV06-19	1.68	s	1976	3.44	0.96	-0.46	126.27
LV06-19	1.40	s	1975	2.13	1.91	-1.01	128.40
LV06-19	7.21	s	1974	9.27	3.51	1.98	137.67
LV06-19	2.17	s	1973	5.53	0.64	0.41	143.20
LV06-19	2.80	s	1972	6.68	0.72	0.90	149.88
LV06-19	1.78	s	1971	4.08	0.77	-0.19	153.96
LV06-19	3.13	s	1970	4.39	2.48	-0.06	158.35
LV06-19	2.46	s	1969	3.68	2.03	-0.36	162.03
LV06-19	4.17	s	1968	5.64	2.85	0.46	167.67
LV06-19	5.59	s	1967	8.35	2.03	1.59	176.02
LV06-19	2.91	s	1966	3.82	3.22	-0.30	179.83
LV06-19	3.08	s	1965	4.27	2.61	-0.11	184.10
LV06-19	1.59	s	1964	3.07	1.07	-0.62	187.17
LV06-19	1.93	s	1963	3.58	1.17	-0.40	190.75

Core	Thickness (mm)	Season	Year	Couplet thickness (w+s) (mm)	Ratio of Summer to Winter thickness	Normalized annual thickness	Cumulative thickness (mm)
LV06-19	1.07	w	2004	AVERAGE:			
LV06-19	2.68	w	2003	4.54			
LV06-19	3.49	w	2002				
LV06-19	1.00	w	2001				
LV06-19	0.84	w	2000				
LV06-19	1.73	w	1999				
LV06-19	0.90	w	1998				
LV06-19	1.43	w	1997				
LV06-19	1.74	w	1996				
LV06-19	1.50	w	1995				
LV06-19	1.43	w	1994				
LV06-19	1.31	w	1993				
LV06-19	1.57	w	1992				
LV06-19	1.20	w	1991				
LV06-19	1.25	w	1990				
LV06-19	1.28	w	1989				
LV06-19	0.84	w	1988				
LV06-19	1.34	w	1987				
LV06-19	1.01	w	1986				
LV06-19	1.11	w	1985				
LV06-19	2.85	w	1984				
LV06-19	1.68	w	1983				
LV06-19	1.20	w	1982				
LV06-19	1.17	w	1981				
LV06-19	1.28	w	1980				

Core	Thickness (mm)	Season	Year	Couplet thickness (w+s) (mm)	Ratio of Summer to Winter thickness	Normalized annual thickness	Cumulative thickness (mm)
LV06-19	2.13	w	1979				
LV06-19	0.65	w	1978				
LV06-19	0.75	w	1977				
LV06-19	1.76	w	1976				
LV06-19	0.73	w	1975				
LV06-19	2.06	w	1974				
LV06-19	3.36	w	1973				
LV06-19	3.88	w	1972				
LV06-19	2.31	w	1971				
LV06-19	1.26	w	1970				
LV06-19	1.22	w	1969				
LV06-19	1.46	w	1968				
LV06-19	2.76	w	1967				
LV06-19	0.90	w	1966				
LV06-19	1.18	w	1965				
LV06-19	1.48	w	1964				
LV06-19	1.65	w	1963				
LV06-16	0.97	s	2004	1.82	1.15	-0.85	1.82
LV06-16	2.82	s	2003	6.76	0.71	0.58	8.58
LV06-16	15.49	s	2002	17.95	6.31	3.82	26.53
LV06-16	5.35	s	2001	6.10	7.13	0.39	32.63
LV06-16	1.96	s	2000	3.02	1.84	-0.50	35.65
LV06-16	3.19	s	1999	9.91	0.48	1.49	45.56
LV06-16	2.49	s	1998	3.79	1.92	-0.28	49.35
LV06-16	1.96	s	1997	5.98	0.49	0.35	55.33

Core	Thickness (mm)	Season	Year	Couplet thickness (w+s) (mm)	Ratio of Summer to Winter thickness	Normalized annual thickness	Cumulative thickness (mm)
LV06-16	0.86	s	1996	3.74	0.30	-0.30	59.07
LV06-16	2.64	s	1995	5.15	1.06	0.11	64.21
LV06-16	1.31	s	1994	3.35	0.65	-0.41	67.56
LV06-16	1.10	s	1993	2.94	0.59	-0.53	70.51
LV06-16	4.69	s	1992	7.75	1.54	0.87	78.25
LV06-16	7.09	s	1991	8.51	4.98	1.09	86.77
LV06-16	5.27	s	1990	6.21	5.62	0.42	92.98
LV06-16	5.29	s	1989	6.24	5.54	0.43	99.22
LV06-16	4.16	s	1988	5.10	4.43	0.10	104.32
LV06-16	4.99	s	1987	7.86	1.74	0.90	112.18
LV06-16	2.16	s	1986	3.82	1.30	-0.27	116.00
LV06-16	2.46	s	1985	4.07	1.52	-0.20	120.07
LV06-16	1.10	s	1984	3.51	0.45	-0.36	123.57
LV06-16	1.72	s	1983	3.62	0.91	-0.33	127.19
LV06-16	0.78	s	1982	2.02	0.63	-0.79	129.21
LV06-16	2.03	s	1981	2.68	3.17	-0.60	131.88
LV06-16	2.55	s	1980	4.16	1.58	-0.17	136.05
LV06-16	13.15	s	1979	16.68	3.72	3.46	152.73
LV06-16	1.63	s	1978	2.39	2.12	-0.69	155.12
LV06-16	1.25	s	1977	2.10	1.48	-0.77	157.22
LV06-16	0.88	s	1976	1.64	1.14	-0.90	158.86
LV06-16	1.14	s	1975	1.94	1.43	-0.82	160.80
LV06-16	2.11	s	1974	3.07	2.21	-0.49	163.87
LV06-16	2.39	s	1973	3.18	3.06	-0.46	167.05
LV06-16	1.69	s	1972	3.36	1.01	-0.40	170.41

Core	Thickness (mm)	Season	Year	Couplet thickness (w+s) (mm)	Ratio of Summer to Winter thickness	Normalized annual thickness	Cumulative thickness (mm)
LV06-16	3.26	s	1971	4.21	3.41	-0.16	174.62
LV06-16	1.78	s	1970	3.04	1.42	-0.50	177.66
LV06-16	1.94	s	1969	5.40	0.56	0.19	183.06
LV06-16	1.74	s	1968	2.50	2.27	-0.65	185.56
LV06-16	1.14	s	1967	2.43	0.89	-0.68	187.99
LV06-16	1.78	s	1966	2.66	2.04	-0.61	190.65
LV06-16	1.30	s	1965	3.93	0.49	-0.24	194.58
LV06-16	1.19	s	1964	2.32	1.06	-0.71	196.89
LV06-16	1.44	s	1963	2.97	0.94	-0.52	199.87
LV06-16	0.85	w	2004	AVERAGE:			
LV06-16	3.94	w	2003	4.76			
LV06-16	2.46	w	2002				
LV06-16	0.75	w	2001				
LV06-16	1.06	w	2000				
LV06-16	6.71	w	1999				
LV06-16	1.30	w	1998				
LV06-16	4.02	w	1997				
LV06-16	2.88	w	1996				
LV06-16	2.50	w	1995				
LV06-16	2.03	w	1994				
LV06-16	1.85	w	1993				
LV06-16	3.05	w	1992				
LV06-16	1.42	w	1991				
LV06-16	0.94	w	1990				
LV06-16	0.95	w	1989				

Core	Thickness (mm)	Season	Year	Couplet thickness (w+s) (mm)	Ratio of Summer to Winter thickness	Normalized annual thickness	Cumulative thickness (mm)
LV06-16	0.94	w	1988				
LV06-16	2.86	w	1987				
LV06-16	1.66	w	1986				
LV06-16	1.61	w	1985				
LV06-16	2.41	w	1984				
LV06-16	1.89	w	1983				
LV06-16	1.24	w	1982				
LV06-16	0.64	w	1981				
LV06-16	1.61	w	1980				
LV06-16	3.54	w	1979				
LV06-16	0.77	w	1978				
LV06-16	0.85	w	1977				
LV06-16	0.77	w	1976				
LV06-16	0.80	w	1975				
LV06-16	0.95	w	1974				
LV06-16	0.78	w	1973				
LV06-16	1.67	w	1972				
LV06-16	0.95	w	1971				
LV06-16	1.25	w	1970				
LV06-16	3.46	w	1969				
LV06-16	0.77	w	1968				
LV06-16	1.28	w	1967				
LV06-16	0.88	w	1966				
LV06-16	2.63	w	1965				
LV06-16	1.13	w	1964				

Core	Thickness (mm)	Season	Year	Couplet thickness (w+s) (mm)	Ratio of Summer to Winter thickness	Normalized annual thickness	Cumulative thickness (mm)
LV06-16	1.53	w	1963				
LV06-13	1.22	s	2004	1.78	2.17	-0.84	1.78
LV06-13	2.21	s	2003	3.07	2.56	-0.25	4.85
LV06-13	10.80	s	2002	11.94	9.45	3.84	16.79
LV06-13	3.63	s	2001	4.35	5.04	0.35	21.14
LV06-13	1.05	s	2000	2.21	0.91	-0.64	23.35
LV06-13	4.12	s	1999	5.74	2.53	0.99	29.09
LV06-13	1.46	s	1998	2.47	1.43	-0.52	31.56
LV06-13	1.31	s	1997	4.26	0.45	0.30	35.82
LV06-13	1.10	s	1996	4.40	0.33	0.37	40.22
LV06-13	2.32	s	1995	5.26	0.79	0.76	45.47
LV06-13	1.19	s	1994	2.69	0.79	-0.42	48.17
LV06-13	0.97	s	1993	3.40	0.40	-0.09	51.56
LV06-13	2.91	s	1992	5.48	1.13	0.87	57.04
LV06-13	3.19	s	1991	5.87	1.19	1.05	62.91
LV06-13	3.08	s	1990	4.46	2.24	0.40	67.37
LV06-13	3.10	s	1989	4.95	1.68	0.62	72.31
LV06-13	1.17	s	1988	1.96	1.50	-0.76	74.27
LV06-13	3.00	s	1987	4.13	2.67	0.24	78.40
LV06-13	0.86	s	1986	1.97	0.77	-0.75	80.37
LV06-13	1.55	s	1985	2.49	1.65	-0.51	82.86
LV06-13	1.08	s	1984	2.22	0.95	-0.63	85.08
LV06-13	1.11	s	1983	2.00	1.25	-0.74	87.09
LV06-13	1.46	s	1982	2.79	1.09	-0.38	89.87
LV06-13	1.24	s	1981	1.99	1.65	-0.74	91.86

Core	Thickness (mm)	Season	Year	Couplet thickness (w+s) (mm)	Ratio of Summer to Winter thickness	Normalized annual thickness	Cumulative thickness (mm)
LV06-13	1.75	s	1980	3.35	1.10	-0.12	95.21
LV06-13	8.48	s	1979	10.34	4.55	3.11	105.55
LV06-13	2.32	s	1978	3.30	2.35	-0.14	108.85
LV06-13	2.50	s	1977	3.69	2.11	0.04	112.55
LV06-13	1.00	s	1976	1.78	1.28	-0.84	114.33
LV06-13	1.17	s	1975	1.88	1.67	-0.79	116.21
LV06-13	1.08	s	1974	1.77	1.57	-0.84	117.98
LV06-13	0.64	s	1973	1.99	0.48	-0.74	119.97
LV06-13	1.35	s	1972	1.97	2.15	-0.75	121.94
LV06-13	2.99	s	1971	3.43	6.82	-0.08	125.37
LV06-13	1.75	s	1970	4.02	0.77	0.19	129.39
LV06-13	2.96	s	1969	6.59	0.81	1.38	135.98
LV06-13	2.85	s	1968	4.05	2.36	0.21	140.03
LV06-13	0.89	s	1967	2.66	0.50	-0.43	142.69
LV06-13	0.92	s	1966	1.99	0.87	-0.74	144.68
LV06-13	0.58	s	1965	3.18	0.22	-0.19	147.86
LV06-13	0.94	s	1964	1.83	1.05	-0.82	149.69
LV06-13	0.59	s	1963	1.36	0.78	-1.03	151.05
LV06-13	0.56	w	2004	AVERAGE:			
LV06-13	0.86	w	2003	3.60			
LV06-13	1.14	w	2002				
LV06-13	0.72	w	2001				
LV06-13	1.16	w	2000				
LV06-13	1.63	w	1999				
LV06-13	1.02	w	1998				

Core	Thickness (mm)	Season	Year	Couplet thickness (w+s) (mm)	Ratio of Summer to Winter thickness	Normalized annual thickness	Cumulative thickness (mm)
LV06-13	2.94	w	1997				
LV06-13	3.30	w	1996				
LV06-13	2.94	w	1995				
LV06-13	1.50	w	1994				
LV06-13	2.43	w	1993				
LV06-13	2.57	w	1992				
LV06-13	2.68	w	1991				
LV06-13	1.38	w	1990				
LV06-13	1.85	w	1989				
LV06-13	0.78	w	1988				
LV06-13	1.13	w	1987				
LV06-13	1.11	w	1986				
LV06-13	0.94	w	1985				
LV06-13	1.14	w	1984				
LV06-13	0.89	w	1983				
LV06-13	1.33	w	1982				
LV06-13	0.75	w	1981				
LV06-13	1.60	w	1980				
LV06-13	1.86	w	1979				
LV06-13	0.99	w	1978				
LV06-13	1.19	w	1977				
LV06-13	0.78	w	1976				
LV06-13	0.70	w	1975				
LV06-13	0.69	w	1974				
LV06-13	1.35	w	1973				

Core	Thickness (mm)	Season	Year	Couplet thickness (w+s) (mm)	Ratio of Summer to Winter thickness	Normalized annual thickness	Cumulative thickness (mm)
LV06-13	0.63	w	1972				
LV06-13	0.44	w	1971				
LV06-13	2.27	w	1970				
LV06-13	3.63	w	1969				
LV06-13	1.21	w	1968				
LV06-13	1.77	w	1967				
LV06-13	1.06	w	1966				
LV06-13	2.60	w	1965				
LV06-13	0.89	w	1964				
LV06-13	0.77	w	1963				
LV06-14	6.42	s	2002	7.22	8.06	3.71	7.22
LV06-14	2.06	s	2001	2.75	3.00	0.33	9.97
LV06-14	1.38	s	2000	2.28	1.52	-0.03	12.25
LV06-14	1.30	s	1999	3.11	0.72	0.60	15.36
LV06-14	1.03	s	1998	1.50	2.20	-0.62	16.86
LV06-14	0.80	s	1997	2.88	0.38	0.42	19.74
LV06-14	1.70	s	1996	3.58	0.91	0.95	23.31
LV06-14	1.77	s	1995	3.05	1.38	0.55	26.36
LV06-14	0.73	s	1994	1.73	0.73	-0.44	28.10
LV06-14	1.11	s	1993	2.78	0.66	0.35	30.88
LV06-14	1.08	s	1992	2.52	0.75	0.15	33.39
LV06-14	2.47	s	1991	3.73	1.95	1.07	37.13
LV06-14	1.47	s	1990	2.13	2.24	-0.15	39.25
LV06-14	3.39	s	1989	4.05	5.17	1.31	43.30
LV06-14	1.73	s	1988	2.31	3.00	-0.01	45.61

Core	Thickness (mm)	Season	Year	Couplet thickness (w+s) (mm)	Ratio of Summer to Winter thickness	Normalized annual thickness	Cumulative thickness (mm)
LV06-14	2.22	s	1987	2.83	3.64	0.38	48.44
LV06-14	0.70	s	1986	1.30	1.18	-0.78	49.74
LV06-14	0.89	s	1985	2.17	0.70	-0.11	51.91
LV06-14	0.58	s	1984	1.64	0.54	-0.51	53.55
LV06-14	0.77	s	1983	1.30	1.44	-0.78	54.85
LV06-14	0.81	s	1982	1.36	1.49	-0.73	56.20
LV06-14	0.47	s	1981	0.86	1.20	-1.11	57.06
LV06-14	3.61	s	1980	4.34	4.91	1.53	61.41
LV06-14	3.73	s	1979	4.39	5.69	1.57	65.80
LV06-14	0.66	s	1978	1.13	1.40	-0.91	66.92
LV06-14	1.05	s	1977	1.95	1.16	-0.28	68.88
LV06-14	0.42	s	1976	0.88	0.93	-1.09	69.75
LV06-14	0.34	s	1975	0.64	1.16	-1.27	70.39
LV06-14	0.50	s	1974	1.16	0.76	-0.88	71.55
LV06-14	0.64	s	1973	1.30	0.98	-0.78	72.85
LV06-14	0.89	s	1972	1.11	4.07	-0.92	73.95
LV06-14	1.22	s	1971	1.41	6.50	-0.69	75.36
LV06-14	1.50	s	1970	4.09	0.58	1.34	79.45
LV06-14	2.17	s	1969	2.86	3.16	0.41	82.31
LV06-14	0.77	s	1968	1.73	0.79	-0.44	84.05
LV06-14	0.89	s	1967	1.75	1.04	-0.43	85.80
LV06-14	0.44	s	1966	0.73	1.47	-1.20	86.53
LV06-14	2.47	s	1965	3.36	2.77	0.79	89.89
LV06-14	0.78	s	1964	1.38	1.32	-0.72	91.27
LV06-14	0.98	s	1963	1.39	2.42	-0.70	92.66

Core	Thickness (mm)	Season	Year	Couplet thickness (w+s) (mm)	Ratio of Summer to Winter thickness	Normalized annual thickness	Cumulative thickness (mm)
LV06-14	0.80	w	2002	AVERAGE:			
LV06-14	0.69	w	2001	2.32			
LV06-14	0.91	w	2000				
LV06-14	1.81	w	1999				
LV06-14	0.47	w	1998				
LV06-14	2.08	w	1997				
LV06-14	1.88	w	1996				
LV06-14	1.28	w	1995				
LV06-14	1.00	w	1994				
LV06-14	1.67	w	1993				
LV06-14	1.44	w	1992				
LV06-14	1.27	w	1991				
LV06-14	0.66	w	1990				
LV06-14	0.66	w	1989				
LV06-14	0.58	w	1988				
LV06-14	0.61	w	1987				
LV06-14	0.59	w	1986				
LV06-14	1.28	w	1985				
LV06-14	1.06	w	1984				
LV06-14	0.53	w	1983				
LV06-14	0.55	w	1982				
LV06-14	0.39	w	1981				
LV06-14	0.73	w	1980				
LV06-14	0.66	w	1979				
LV06-14	0.47	w	1978				

Core	Thickness (mm)	Season	Year	Couplet thickness (w+s) (mm)	Ratio of Summer to Winter thickness	Normalized annual thickness	Cumulative thickness (mm)
LV06-14	0.91	w	1977				
LV06-14	0.45	w	1976				
LV06-14	0.30	w	1975				
LV06-14	0.66	w	1974				
LV06-14	0.66	w	1973				
LV06-14	0.22	w	1972				
LV06-14	0.19	w	1971				
LV06-14	2.59	w	1970				
LV06-14	0.69	w	1969				
LV06-14	0.97	w	1968				
LV06-14	0.86	w	1967				
LV06-14	0.30	w	1966				
LV06-14	0.89	w	1965				
LV06-14	0.59	w	1964				
LV06-14	0.41	w	1963				